CATALYSIS FOR FORMATION OF BIO-DERIVED ESTERS AS PRODUCTS AND AS INTERMEDIATES TO EPOXIDES

 $\mathbf{B}\mathbf{y}$

Arati Santhanakrishnan

A DISSERTATION

Submitted to
Michigan State University
in partial fulfilment of the requirements
for the degree of

Chemical Engineering- Doctor of Philosophy

2016

ABSTRACT

CATALYSIS FOR FORMATION OF BIO-DERIVED ESTERS AS PRODUCTS AND AS INTERMEDIATES TO EPOXIDES

By

Arati Santhanakrishnan

The production of liquid fuels from renewable biomass resources will require multiple routes and feedstock sources beyond simple ethanol or biodiesel production. Esters are an important class of organic compounds that are used in several applications in the chemical industry as both end products and as intermediates to other value added products. Two reaction types have been studied in this dissertation that are very different in their chemistry, and thus their requirements, showing the range of processes involved in the design of bio-refineries. They are the liquid phase acid catalyzed parallel esterification reactions in batch reactor configurations, and vapor phase base catalyzed conversion of propylene glycol acetates to propylene oxide, a chemical with a fast growing global market, in a fixed bed reactor.

Four results should be highlighted in particular. The first is the development of a kinetic model for esterification that uses non ideal concentrations instead of conventional activity terms. The model enables the simulation of esterification occurring with feed streams of multiple alcohols and acids under a wide range of conditions. Second, a study of the structure-reactivity relationship of over eighty reactions from literature helps predict the rates for a number of simple esterification reactions with a number of catalysts.

Third, the reaction system involving acylation of propylene glycol with acetic acid has been successfully modeled to obtain rate constant parameters for esterification, transesterification and hydrolysis using the non-ideal concentration model. Fourth, a detailed reaction and catalyst properties study that optimized selectivity to nearly 90%, and establishes the chemical nature of the catalyst under reaction conditions.

These findings improve our understanding of chemical systems involving organic esters in a wide range of physical and chemical conditions, and will be useful in the design of complex processes for the production of esters and their use as intermediates.

ACKNOWLEDGEMENTS

I would like to thank Dr. Dennis J. Miller for being a patient teacher, role model and constant source of inspiration during the course of my dissertation work. I would like to express my gratitude to Dr. Carl T. Lira, Dr. James E. Jackson and Dr. David Hodge for serving on my committee, and for giving me their time and the benefit of their expertise and experience. I would also like to thank Dr. Lars Peereboom for training me in the art of experimental research, his patient explanations and all his help in the laboratory.

I would like to express my sincere thanks to the National Corn Growers Association and Michigan State University for funding my research. I would also like to specially thank Dr. Patrick B. Smith and Dr. Adina Dumitrascu from the Michigan Molecular Institute for their guidance on the propylene oxide study and for providing kinetic data on propylene glycol esterification with acetic acid.

I would like to thank Dr. Anne Lown, Dr. Alvaro Orjuelo, Dr. Xianfeng Ma, Dr. Xi Hong, Dr. Abu Hassan from whom I have learnt many useful things during the course of my research. I would also like to thank my family for being a constant source of support and encouragement.

TABLE OF CONTENTS

LIST OF TABLES	viii
LIST OF FIGURES	xi
LIST OF SCHEMES	xix
KEY TO SYMBOLS AND ABBREVIATIONS	XX
1 Introduction	
1.1 Esterification modeling	
1.2 Catalysis for propylene glycol epoxidation	2
2 Kinetics of mixed ethanol/ <i>n</i> -butanol esterification of butyric acid with Amberlyst 70 a	
para-toluene sulfonic acid	
2.1 Abstract	
2.2 Introduction	
2.3 Materials and Methods	
2.3.1 Materials	
2.3.2 Heterogeneous catalyst conditioning	
2.3.3 Kinetic experiments	
2.3.4 Analysis	
2.4 Results	
2.4.1 Mass transfer considerations	
2.4.2 Reaction equilibrium constants	
2.4.3 Kinetic Model Description	
2.4.4 Application of Kinetic Model to Single Alcohol Esterification	
2.4.5 Application of kinetic model to mixed alcohol esterification	
2.5 Conclusions	
Appendix A: Calibration plots for gas chromatography analysis	
Appendix B. Reaction profiles of Amberlyst 70 catalyzed reactions	
Appendix C: Reaction profiles of <i>p</i> -TSA catalyzed reactions	
REFERENCES	
KLI LIKLICED	
3 Unification of esterification rates using non-ideal concentration model	47
3.1 Abstract	
3.2 Introduction	47
3.3 Calculation procedure	50
3.4 Results	
3.4.1 Rate constants for straight chain alcohols with common acid and catalyst	
3.4.2 Rate constants for secondary alcohols with common acid and catalyst	
3.4.3 Different primary carboxylic acids esterified by common alcohol and catalyst	57

	3.4.4	Different branched carboxylic acids, same alcohol, same catalyst	. 58
	3.4.5	Ratio of rate constants of the same reaction with different catalysts	. 60
	3.5 Disc	cussion	. 63
	3.5.1	Taft equation	. 65
	3.6 Con	clusions	. 71
A	PPENDICE	S	. 72
	Appendix 1	D: Sample calculation of non-ideal concentration rate constant, k _{NIC}	. 73
	Appendix 1	E: Properties of alcohols, carboxylic acids and acid catalysts used in calculations	75
R)	EFERENCI	ES	. 78
4		of p-Touenesulfonic Acid-Catalyzed 1,2-Propylene Glycol Acetylation	
		tract	
		oduction	
		erials and Methods	
		ılts	
		Equilibrium constants	
		Kinetic modeling	
		clusions	
A			. 97
		F: Predicted and experimental mole fraction profiles of all experiments in PG	00
		on with acetic acid (Chapter 2)	. 98
		G. Raw data from propylene glycol esterification with acetic acid (conducted at	105
ъ.	_	Molecular Institute)	
K.	EFERENCI	ES	116
5	Catalytic	e epoxidation of propylene glycol and its acetates	118
J	-	tract	
		oduction	
		erials and Methods	
		Materials	
		Feed preparation.	
		Catalyst preparation	
		Fixed bed reactor and condensation system	
		Analysis	
		Catalyst characterization	
		ılts	
		Thermodynamic Analysis of Reaction Network	
		Control Reactions.	
		Cesium nitrate on silica gel.	
		Potassium salt catalysts	
	5.4.4.	· · · · · · · · · · · · · · · · · · ·	
	5.4.4.	•	
	5.4.4.		
	5.4.4.	1	
	5.4.4.	•	
	5.4.4.0		
	5.4.4.	; E	
	۶.┯.┽.	, Experimente with ixerie, ixees and ixeres based catalysis	101

5.4.4.8 FTIR and XPS analysis of catalysts	40
5.4.4.9 Monolayer coverage calculations and controlled pore glass catalysts 1	46
5 Conclusions and recommendations for future work	52
ENDICES	55
opendix H: List of all experiments with reaction conditions, conversion, selectivity and	
rbon recovery1	56
opendix I: Calibration plots for all components in reaction system	
opendix J: Mechanisms for major reactions in reaction system	
opendix K: Gibbs energy of reaction and equilibrium constants at reaction temperature 1	
opendix L: Weisz Prater calculation	
opendix M: TGA curve calculations, atomic concentrations from XPS and EDS analyses 1	
ERENCES	

LIST OF TABLES

Table 2.1: Summary of experiments and conditions
Table 2.2 : Estimated effectiveness factors for Amberlyst 70 catalyzed esterification reactions. 15
Table 2.3: UNIFAC groups and their counts in reaction components
Table 2.4: Group volume and surface area contributions
Table 2.5: UNIFAC group binary interaction parameters
Table 2.6: Optimized kinetic parameters with 95% confidence limits and equilibrium constants from experimental data (T in Kelvin)
Table 2.7: Absolute errors in model fits for each experiment
Table 3.1: Comparison of activity coefficient values estimated by NRTL-HOC and UNIFAC 51
Table 3.2: Summary of reactions and calculated non-ideal concentration-based rate constants at 60 °C
Table 3.3: Structures of branched carboxylic acids in Figure 3.6
Table 3.4: Ratio of rate constants at 60 °C based on non-ideal concentration model
Table 3.5: Es values for each alcohol in Figure 3.7
Table 3.6: H ⁺ concentrations of catalysts
Table 3.7:Densities of alcohols at 60 °C
Table 3.8: Densities of carboxylic acids at 60 °C
Table 4.1: Summary of reactions and experimental conditions
Table 4.2: UNIFAC groups and their counts in reaction components
Table 4.3: Group volume and surface area contributions
Table 4.4: UNIFAC group binary interaction parameters
Table 4.5 Optimized kinetic parameters with 95% confidence limits for PG acetylation with <i>p</i> -TSA catalyst
Table 4.6: Absolute residuals for each experiment

Table 4.7: Experiment 1
Table 4.8: Experiment 2
Table 4.9: Experiment 3
Table 4.10: Experiment 4
Table 4.11: Experiment 5
Table 4.12: Experiment 6
Table 4.13: Experiment 7
Table 4.14: Experiment 8
Table 4.15: Experiment 9
Table 4.16: Experiment 10
Table 4.17: Experiment 11
Table 4.18: Experiment 12
Table 4.19: Experiment 13
Table 4.20: Experiment 14
Table 4.21: Experiment 15
Table 4.22: Experiment 16
Table 4.23: Experiment 17
Table 5.1: List of reactions run with 1.5 mmol/g CsNO3 on silica gel catalyst with space velocity =1.7 g feed/g catalyst/h
Table 5.2: List of experiments with KOH on silica gel
Table 5.3: Surface areas of KOH on silica gel catalysts and supports determined by N_2 adsorption (BET method)
Table 5.4: Experiments conducted with KOAc at temperature of 400C and WHSV = 3.4 g feed/g cat/h
Table 5.5: Experiments conducted with 1.25 mmol K ₂ CO ₃ /g catalyst at 400 °C 140
Table 5.6: Binding energy peaks from XPS spectra for calcined support silica gel, neat K ₂ O:SiO ₂ and neat K ₂ CO ₃

Table 5.7: Binding energy peaks from XPS spectra for 2.5 mmol K^+/g catalyst made from KOH, KOAC and K_2CO_3 .
Table 5.8: Binding energy peaks from XPS spectra for lower loadings of KOH on silica gel (0.5 and 1.5 mmol/g)
Table 5.9: Potassium silicate on silica gel at 400 °C
Table 5.10: Surface areas of catalysts and supports determined by N ₂ adsorption (BET method)
Table 5.11: Experiments done to determine the effect of surface area with 1.25 mmol/g K ₂ CO ₃
Table 5.12: Binding energy peaks from XPS spectra for K_2CO_3 on CPG before and after use . 150
Table 5.13: Monolayer coverage calculations
Table 5.14: List of all experiments with reaction conditions, conversion, selectivity and carbon recovery
Table 5.15: Gibbs energy polynomial function values and Gibbs energy of formation at standard conditions (298 K) and at reaction temperature (673 K)
Table 5.16: Equilibrium constants estimated from Gibbs energy of reaction calculations at reaction temperature of 673 K
Table 5.17: Atomic concentrations from XPS spectra for 2.5 mmol K^+/g catalyst made from KOH, KOAC and K_2CO_3
Table 5.18: XPS spectra for lower loadings of KOH on silica gel (0.5 and 1.5 mmol/g) 169
Table 5.19: Atomic concentrations from XPS spectra for K ₂ CO ₃ on CPG before and after use 169
Table 5.20: Atomic concentrations from EDS spectra for 2.5 mmol K ⁺ /g catalyst made from KOH, KOAC and K ₂ CO ₃

LIST OF FIGURES

Figure 2.1: Van't Hoff plot of mole fraction- (gray) and activity- (black) based esterification equilibrium constants from experimental data. $(\blacksquare, \blacksquare) - Ethanol, (+, +) - n\text{-}butanol$
Figure 2.2: Experimental and predicted concentration profiles of ethanol and n -butanol individual esterification in the presence of 1 wt.% Amberlyst 70: a) Run 2 (Ethanol, T = 80 °C); b) Run 5 (n -Butanol, T = 60 °C). (——) — Mole fraction based fits; (——) — Activity based fits. (\bullet) — butyric acid; (\blacksquare) —ethanol; (\blacktriangle) —ethyl butyrate; (\times) —water; (\circ) — n -butanol; (\bullet)- n -butyl butyrate
Figure 2.3: Experimental and predicted concentration profiles of ethanol and n -butanol individual esterification in the presence of 0.1 wt.% p -TSA: a) Run 20 (Ethanol, T = 100 °C); b) Run 23 (n -Butanol, T = 80 °C). (——) — Mole -fraction based fits; (——) — Activity based fits. (\blacklozenge) — butyric acid; (\blacksquare) —ethanol; (\blacktriangle) —ethyl butyrate; (\times) —water; (\circ) — n -butanol; (\bullet)- n -butyl butyrate.
Figure 2.4: Experimental and predicted concentration profiles of mixed alcohol esterification in the presence of 1 wt.% Amberlyst 70. a) Run 13 (Ethanol: n -Butanol = 1.15:1, T=80°C); b) Run 11 (Ethanol: n -Butanol = 0.21:1, T = 60 °C); c) Run 9 (Ethanol: n -Butanol = 1:1, T = 60°C). (——) -mole fraction based fits; (——) -activity based fits. (•) - butyric acid; (•) -ethanol; (•) - n -butyl butyrate; (×) -water; (°) - n -butanol; (•)- n -butyl butyrate
Figure 2.5: Experimental and predicted concentration profiles of mixed alcohol esterification in the presence of 0.1 wt.% p -TSA. a) Run 31 (Ethanol: n -Butanol = 4.1:1 , T = 80°C); b) Run 29 (Ethanol: n -Butanol = 0.18:1,T = 80 °C); c) Run 30 (Ethanol: n -Butanol = 1:1,T =80°C). (——) —nole fraction based fits; (——) —activity based fits. (\blacklozenge) — butyric acid; (\blacksquare) —ethanol; (\blacktriangle) — ethyl butyrate; (\times) —water; (\circ) — n -butanol; (\blacklozenge) — n -butyl butyrate
Figure 2.6: Plot of area ratio vs weight ratio of ethanol over internal standard ethyl caprylate 30
Figure 2.7: Plot of area ratio vs weight ratio of ethyl butyrate over internal standard ethyl caprylate
Figure 2.8: Plot of area ratio vs weight ratio of water over internal standard ethyl caprylate 31
Figure 2.9: Plot of area ratio vs weight ratio of butanol over internal standard ethyl caprylate 31
Figure 2.10: Plot of area ratio vs weight ratio of butyl butyrate over internal standard ethyl caprylate

Figure 2.11: Plot of area ratio vs weight ratio of butyric acid over internal standard ethyl caprylate
Figure 2.12: Experimental and predicted concentration profiles of ethanol individual esterification in the presence of 1 wt.% Amberlyst 70: Run 1, T = 60 °C (——) – Mole -fraction based fits; (——) – Activity based fits. (♦) – butyric acid; (■) –ethanol; (▲) –ethyl butyrate; (×) –water
Figure 2.13: Experimental and predicted concentration profiles of ethanol individual esterification in the presence of 1 wt.% Amberlyst 70: Run 3, T = 100 °C (——) – Mole -fraction based fits; (— —) – Activity based fits. (♦) – butyric acid; (■) –ethanol; (▲) –ethyl butyrate; (×) –water
Figure 2.14: Experimental and predicted concentration profiles of ethanol individual esterification in the presence of 1 wt.% Amberlyst 70: Run 4, T = 120 °C (——) – Mole -fraction based fits; (——) – Activity based fits. (♦) – butyric acid; (■) –ethanol; (▲) –ethyl butyrate; (×) –water ————————————————————————————————————
Figure 2.15: Experimental and predicted concentration profiles of <i>n</i> -butanol individual esterification in the presence of 1 wt.% Amberlyst 70: Run 6, T = 80 °C (——) – Mole -fraction based fits; (——) – Activity based fits. (\bullet) – butyric acid; (\circ) – <i>n</i> -butanol; (\bullet)- <i>n</i> -butyl butyrate; (\times) –water ——34
Figure 2.16: Experimental and predicted concentration profiles of n -butanol individual esterification in the presence of 1 wt.% Amberlyst 70: Run 7, T = 100 °C (——) – Mole -fraction based fits; (— —) – Activity based fits. (\bullet) – butyric acid; (\circ) – n -butanol; (\bullet)- n -butyl butyrate; (\times) –water ——35
Figure 2.17: Experimental and predicted concentration profiles of <i>n</i> -butanol individual esterification in the presence of 1 wt.% Amberlyst 70: Run 8, $T = 120 ^{\circ}\text{C}$ (——) – Mole -fraction based fits; (——) – Activity based fits. (\bullet) – butyric acid; (\circ) – <i>n</i> -butanol; (\bullet)- <i>n</i> -butyl butyrate; (\times) –water ——35
Figure 2.18: Experimental and predicted concentration profiles of mixed alcohol esterification in the presence of 1 wt.% Amberlyst 70. Run 10 (Ethanol: n -Butanol =1:1, T=80°C) (——) –mole fraction based fits; (——) –activity based fits. (\blacklozenge) – butyric acid; (\blacksquare) –ethanol; (\blacktriangle) –ethyl butyrate; (\times) –water; (\circ) – n -butanol; (\blacklozenge)- n -butyl butyrate
Figure 2.19: Experimental and predicted concentration profiles of mixed alcohol esterification in the presence of 0.5 wt.% Amberlyst 70. Run 12 (Ethanol: n -Butanol = 0.88:1, T=80°C) (——) – mole fraction based fits; (— —) –activity based fits. (\blacklozenge) – butyric acid; (\blacksquare) –ethanol; (\blacktriangle) –ethyl butyrate; (\times) –water; (\circ) – n -butanol; (\bullet)- n -butyl butyrate

Figure 2.20: Experimental and predicted concentration profiles of mixed alcohol esterification in the presence of 0.75 wt.% Amberlyst 70. Run 14 (Ethanol: n -Butanol = 1.05:1, T=80°C) (——) — mole fraction based fits; (——) —activity based fits. (\blacklozenge) — butyric acid; (\blacksquare) —ethanol; (\blacktriangle) —ethyl butyrate; (\times) —water; (\circ) — n -butanol; (\blacklozenge) — n -butyl butyrate
Figure 2.21: Experimental and predicted concentration profiles of mixed alcohol esterification in the presence of 1 wt.% Amberlyst 70. Run 15 (Ethanol: n -Butanol = 0.21:1, T=80°C) (——) — mole fraction based fits; (——) —activity based fits. (\blacklozenge) — butyric acid; (\blacksquare) —ethanol; (\blacktriangle) —ethyl butyrate; (\times) —water; (\circ) — n -butanol; (\blacklozenge)— n -butyl butyrate
Figure 2.22: Experimental and predicted concentration profiles of mixed alcohol esterification in the presence of 2 wt.% Amberlyst 70. Run 16 (Ethanol: n -Butanol = 0.86:1, T=80°C) (——) — mole fraction based fits; (——) —activity based fits. (\blacklozenge) — butyric acid; (\blacksquare) —ethanol; (\blacktriangle) —ethyl butyrate; (\times) —water; (\circ) — n -butanol; (\blacklozenge) — n -butyl butyrate
Figure 2.23: Experimental and predicted concentration profiles of mixed alcohol esterification in the presence of 1 wt.% Amberlyst 70. Run 17 (Ethanol: n -Butanol = 0.2:1, T=80°C) (——) — mole fraction based fits; (——) —activity based fits. (\blacklozenge) — butyric acid; (\blacksquare) —ethanol; (\blacktriangle) —ethyl butyrate; (\times) —water; (\circ) — n -butanol; (\blacklozenge) — n -butyl butyrate
Figure 2.24: Experimental and predicted concentration profiles of ethanol individual esterification in the presence of 0.1 wt.% p -TSA: Run 18, T = 60 °C (——) – Mole -fraction based fits; (— —) – Activity based fits. (\blacklozenge) – butyric acid; (\blacksquare) –ethanol; (\blacktriangle) –ethyl butyrate; (\times) –water ——39
Figure 2.25: Experimental and predicted concentration profiles of ethanol individual esterification in the presence of 0.1 wt.% p -TSA: Run 19, T = 80 °C (——) – Mole -fraction based fits; (——) – Activity based fits. (\blacklozenge) – butyric acid; (\blacksquare) –ethanol; (\blacktriangle) –ethyl butyrate; (\times) –water.
Figure 2.26: Experimental and predicted concentration profiles of ethanol individual esterification in the presence of 0.1 wt.% p -TSA: Run 21, T = 120 °C (——) – Mole -fraction based fits; (— —) – Activity based fits. (\blacklozenge) – butyric acid; (\blacksquare) –ethanol; (\blacktriangle) –ethyl butyrate; (\times) –water.
Figure 2.27: Experimental and predicted concentration profiles of n -butanol individual esterification in the presence of 0.1 wt.% p -TSA: Run 22, T=60 °C (——) — Mole -fraction based fits; (— —) — Activity based fits. (\bullet) — butyric acid; (\circ) — n -butanol; (\bullet) — n -butyl butyrate; (\times) — water ————————————————————————————————————
Figure 2.28: Experimental and predicted concentration profiles of n -butanol individual esterification in the presence of 0.1 wt.% p -TSA: Run 24, T=100 °C (——) – Mole -fraction

based fits; $()$ – Activity based fits. (\bullet) – butyric acid; (\circ) – <i>n</i> -butanol; (\bullet) - <i>n</i> -butyl butyrate; (\times) –water
Figure 2.29: Experimental and predicted concentration profiles of n -butanol individual esterification in the presence of 0.1 wt.% p -TSA: Run 25, T=120 °C (——) — Mole -fraction based fits; (— —) — Activity based fits. (\bullet) — butyric acid; (\circ) — n -butanol; (\bullet) — n -butyl butyrate; (\times) —water ————————————————————————————————————
Figure 2.30: Experimental and predicted concentration profiles of mixed alcohol esterification in the presence of 0.1 wt.% p -TSA. Run 26 (Ethanol: n -Butanol = 0.22:1, T=60°C) (——) —mole fraction based fits; (— —) —activity based fits. (\blacklozenge) — butyric acid; (\blacksquare) —ethanol; (\blacktriangle) —ethyl butyrate; (\times) —water; (\circ) — n -butanol; (\blacklozenge)— n -butyl butyrate
Figure 2.31: Experimental and predicted concentration profiles of mixed alcohol esterification in the presence of 0.1 wt.% p -TSA. Run 27 (Ethanol: n -Butanol = 1:1, T=60°C) (——) —mole fraction based fits; (— —) —activity based fits. (\blacklozenge) — butyric acid; (\blacksquare) —ethanol; (\blacktriangle) —ethyl butyrate; (\times) —water; (\circ) — n -butanol; (\blacklozenge) — n -butyl butyrate
Figure 2.32: Experimental and predicted concentration profiles of mixed alcohol esterification in the presence of 0.1 wt.% p -TSA. Run 28 (Ethanol: n -Butanol = 5:1, T=60°C) (——) –mole fraction based fits; (— —) –activity based fits. (\blacklozenge) – butyric acid; (\blacksquare) –ethanol; (\blacktriangle) –ethyl butyrate; (\times) –water; (\circ) – n -butanol; (\blacklozenge)- n -butyl butyrate
Figure 3.1: Non ideal rate constants at 60 °C for reaction families with differing number of carbons in primary alcohol chain with common carboxylic acid and catalyst. (●)-Butyric acid, Amberlyst 70 (▲)-Butyric acid, Amberlyst 15 (×)- Butyric acid, Amberlyst 36 (○)-Propionic acid, Dowex W50×4
Figure 3.2: Non ideal rate constants at 60 °C for families of reactions with differing number of carbons in primary alcohol chain with common carboxylic acid and catalyst. (●)-Acetic acid, Smopex-101 (▲)-Propionic acid, Smopex-101 (■)- Pentanoic acid, Smopex-101
Figure 3.3: Non ideal rate constants at 60 °C for reaction families with branched alcohols with common carboxylic acid and catalyst. ()- Propionic acid, Dowex W4 ()-Butyric acid, Amberlyst 70 ()-Propionic acid, Smopex-101
Figure 3.4: Non ideal rate constants at 60 °C for reaction families with differing number of carbons in primary carboxylic acid chain with common alcohol and catalyst. (▲)-Methanol, SAC-13, (■)-2-Propanol, Smopex-101
Figure 3.5: Non ideal rate constants at 60 °C for reaction families with differing number of carbons in primary carboxylic acid chain with common alcohol and catalyst. (▲)-Methanol, Sulfuric acid (■)- Methanol, Hydrochloric acid

Figure 3.6: Non ideal rate constants at 60 °C for reaction families with differing number of carbons in branched carboxylic acid chain with methanol and hydrochloric acid catalyst
Figure 3.7: Taft equation applied to a candidate family of reactions (Reactions based on study by Erdem and Cebe) ³⁴ . Concentration based rate constant ratios (■), and non-ideal concentration based rate constant ratios of methanol (●), primary alcohols (♦), and branched alcohols (▲) are plotted. 69
Figure 4.1: Van't Hoff plot of experimental activity-based equilibrium constants for the acetylation of PG and PGMA $(\bullet) - K_{a1}$; $(\blacksquare) - K_{a2}$
Figure 4.2: Experimental and predicted concentration profiles of PG acetylation (Experiment 3: 63 °C, 0.008 kg cat/kg soln, initial molar ratio PG:AA = 1:2) (——) – UNIFAC activity based model prediction; (♦) – acetic acid; (■) – propylene glycol monoacetate; (▲) – propylene glycol diacetate; (×) –propylene glycol; (○) – water. ——93
Figure 4.3: Experimental and predicted concentration profiles of PGDA hydrolysis (Experiment 13: 75 °C, 0.010 kg cat/kg soln, initial molar ratio PGDA:water = 3:1) (——) – UNIFAC activity based model prediction; (♦) – acetic acid; (■) – propylene glycol monoacetate; (▲) – propylene glycol diacetate; (×) –propylene glycol; (○) – water
Figure 4.4:Experimental and predicted concentration profiles of PG-PGDA transacetylation (Experiment 15: 85 °C, 0.007 kg cat/kg soln, initial molar ratio PGDA:PG = 1:1) (——) — UNIFAC activity based model prediction; (♦) — acetic acid; (■) — propylene glycol monoacetate; (▲) — propylene glycol diacetate; (×) —propylene glycol; (○) — water
Figure 4.5: Parity plot of kinetic model fit for PGMA mole fractions in experiments
Figure 4.6: Experimental and predicted concentration profiles of PG acetylation (Experiment 1: 63 °C, 0.012 kg cat/kg soln, initial molar ratio PG:AA=1:1) (——) – UNIFAC activity based model prediction; (♦) – acetic acid; (■) – propylene glycol monoacetate; (▲) – propylene glycol diacetate; (×) –propylene glycol; (○) – water
Figure 4.7: Experimental and predicted concentration profiles of PG acetylation (Experiment 2: 63 °C, 0.016 kg cat/kg soln, initial molar ratio PG:AA=2:1) (——) – UNIFAC activity based model prediction; (♦) – acetic acid; (■) – propylene glycol monoacetate; (▲) – propylene glycol diacetate; (×) –propylene glycol; (○) – water
Figure 4.8: Experimental and predicted concentration profiles of PG acetylation (Experiment 4: 75 °C, 0.008 kg cat/kg soln, initial molar ratio PG:AA=1:2) (———) – UNIFAC activity based model prediction; (♦) – acetic acid; (■) – propylene glycol monoacetate; (▲) – propylene glycol diacetate: (×) –propylene glycol: (○) – water ————————————————————————————————————

Figure 4.9: Experimental and predicted concentration profiles of PG acetylation (Experiment 5: 75 °C, 0.012 kg cat/kg soln, initial molar ratio PG:AA=1:1) (——) – UNIFAC activity based model prediction; (♦) – acetic acid; (■) – propylene glycol monoacetate; (▲) – propylene glycol diacetate; (×) –propylene glycol; (○) – water
Figure 4.10: Experimental and predicted concentration profiles of PG acetylation (Experiment 6: 75 °C, 0.006 kg cat/kg soln, initial molar ratio PG:AA=1:1) (——) – UNIFAC activity based model prediction; (♦) – acetic acid; (■) – propylene glycol monoacetate; (▲) – propylene glycol diacetate; (×) – propylene glycol; (○) – water
Figure 4.11: Experimental and predicted concentration profiles of PG acetylation (Experiment 7: 75 °C, 0.025 kg cat/kg soln, initial molar ratio PG:AA=1:1) (——) – UNIFAC activity based model prediction; (♦) – acetic acid; (■) – propylene glycol monoacetate; (▲) – propylene glycol diacetate; (×) – propylene glycol; (○) – water
Figure 4.12: Experimental and predicted concentration profiles of PG acetylation (Experiment 8: 75 °C, 0.063 kg cat/kg soln, initial molar ratio PG:AA= 1:1) (——) – UNIFAC activity based model prediction; (♦) – acetic acid; (■) – propylene glycol monoacetate; (▲) – propylene glycol diacetate; (×) – propylene glycol; (○) – water
Figure 4.13: Experimental and predicted concentration profiles of PG acetylation (Experiment 9: 86 °C, 0.012 kg cat/kg soln, initial molar ratio PG:AA=1:1) (——) – UNIFAC activity based model prediction; (♦) – acetic acid; (■) – propylene glycol monoacetate; (▲) – propylene glycol diacetate; (×) – propylene glycol; (○) – water
Figure 4.14: Experimental and predicted concentration profiles of PG acetylation (Experiment 10: 86 °C, 0.016 kg cat/kg soln, initial molar ratio PG:AA=2:1) (——) – UNIFAC activity based model prediction; (♦) – acetic acid; (■) – propylene glycol monoacetate; (▲) – propylene glycol diacetate; (×) – propylene glycol; (○) – water
Figure 4.15: Experimental and predicted concentration profiles of PG acetylation (Experiment 11: 86 °C, 0.008 kg cat/kg soln, initial molar ratio PG:AA= 1:2) (——) – UNIFAC activity based model prediction; (♦) – acetic acid; (■) – propylene glycol monoacetate; (▲) – propylene glycol diacetate; (×) – propylene glycol; (○) – water
Figure 4.16: Experimental and predicted concentration profiles of PGDA hydrolysis (Experiment 12: 63 °C, 0.013 kg cat/kg soln, initial molar ratio PGDA:water = 3:1) (——) – UNIFAC activity based model prediction; (♠) – acetic acid; (■) – propylene glycol monoacetate; (▲) – propylene glycol diacetate; (×) – propylene glycol; (○) – water
Figure 4.17: Experimental and predicted concentration profiles of PGDA hydrolysis (Experiment 14: 86 °C, 0.010 kg cat/kg soln, initial molar ratio PGDA:water = 3:1) (——) – UNIFAC activity

based model prediction; (♦) – acetic acid; (■) – propylene glycol monoacetate; (▲) – propylene glycol diacetate; (×) – propylene glycol; (○) – water
Figure 4.18: Experimental and predicted concentration profiles of PG transacetylation (Experiment 16: 75 °C, 0.004 kg cat/kg soln, initial molar ratio PGDA:PG=3:1) (——) − UNIFAC activity based model prediction; (♦) − acetic acid; (■) − propylene glycol monoacetate; (▲) − propylene glycol diacetate; (×) −propylene glycol; (○) − water
Figure 4.19: Experimental and predicted concentration profiles of PG transacetylation (Experiment 17: 65 °C, 0.007 kg cat/kg soln, initial molar ratio PGDA:PG=1:3) (——) − UNIFAC activity based model prediction; (♦) − acetic acid; (■) − propylene glycol monoacetate; (▲) − propylene glycol diacetate; (×) −propylene glycol; (○) − water
Figure 5.1: Conversion (\square), PO selectivity (Δ) vs weight hour space velocity. (T= 400 °C, 0.5 mmol/g of KOH in catalyst
Figure 5.2: Rate constant vs contact time for a first order reaction A straight line through the origin fits the data with an R ² value of 0.94
Figure 5.3: Conversion (\square), PO selectivity(Δ), temperature. (WHSV= 1.7 g feed/g cat/ h), loading = 2.5 mmol/g of KOH in catalyst) (R14 – R18)
Figure 5.4: Arrhenius plot of composite reaction of PGA to products (R14-R18)
Figure 5.5: Conversion (\square), PO selectivity (Δ) vs catalyst loading. (T= 400 °C, WHSV = 1.7 g feed/g cat/h)
Figure 5.6:Thermogravimetric analyses 1. (——) KOAc on silica, 2. (——) silica gel, 3. (——) neat KOAc
Figure 5.7: Absorbance FTIR analyses of fresh and used catalyst samples. (1: 1.25 mmol/g K ₂ CO ₃ on silica, 2: post reaction 2.5 mmol KOAc/g on silica, 3: post reaction 2.5 mmol/g KOH on silica, 4: unused 2.5 mmol/g KOH on silica)
Figure 5.8: Absorbance FTIR analyses of fresh and used catalyst samples. (1: silica gel support, 2: calcined fresh 1.5 mmol KOH/g on silica, 3: post reaction 1.5 mmol/g KOH on silica, 4: unused 1.25 mmol/g K ₂ SiO ₃ on silica, 5: neat K ₂ SiO ₃)
Figure 5.9: Absorbance FTIR analyses of fresh and used catalyst samples. (1: K ₂ SiO ₃ on silica gel, 2:1.25 mmol/g K ₂ CO ₃ on CPG post reaction, 3: 1.25 mmol/g K ₂ CO ₃ on CPG calcined, unused, 4: K ₂ SiO ₃ , neat)
Figure 5.10: Conversion on silica gel catalysts (\square), PO selectivity on silica gel catalysts (Δ), conversion on CPG catalyst (\circ), PO selectivity on CPG catalyst (\diamond) vs percentage coverage of potassium base salt on silica surface. (T= 400 °C, WHSV = 3.4 g feed/g cat/h). Percentage

coverage >100% if surface is fully saturated, and more than one layer of potassium salt is present
Figure 5.11: Plot of area ratio vs weight ratio of PO over internal standard decanol
Figure 5.12: Plot of area ratio vs weight ratio of propanal over internal standard decanol 158
Figure 5.13: Plot of area ratio vs weight ratio of water over internal standard decanol
Figure 5.14: Plot of area ratio vs weight ratio of allyl alcohol over internal standard decanol 159
Figure 5.15: Plot of area ratio vs weight ratio of propylene glycol over internal standard decanol
Figure 5.16: Plot of area ratio vs weight ratio of acetone over internal standard decanol 160
Figure 5.17: Plot of area ratio vs weight ratio of acetic acid over internal standard decanol 160
Figure 5.18: Plot of area ratio vs weight ratio of propylene glycol diacetate over internal standard decanol
Figure 5.19: Plot of area ratio vs weight ratio of allyl acetate over internal standard decanol 161
Figure 5.20: Plot of area ratio vs weight ratio of 2-ethyl,4-methyl,1,3-dioxolane over internal standard decanol
Figure 5.21: XPS C 1s spectra of 1.5 mmol/g KOH on silica gel post reaction
Figure 5.22: XPS O 1s spectra of 1.25 mmol/g K ₂ CO ₃ on CPG post reaction
Figure 5.23: SEM image of post reaction 2.5 mmol/g KOH on silica gel
Figure 5.24: SEM image of post reaction 2.5 mmol/g KOAc on silica gel
Figure 5.25: SEM image of post reaction 1.25 mmol/g K ₂ CO ₃ on silica gel

LIST OF SCHEMES

Scheme 2.1: Esterification of butyric acid with ethanol and <i>n</i> -butanol	8
Scheme 3.1: Rate limiting step of esterification reaction mechanism	67
Scheme 4.1: Glycol-carboxylic acid system reactions	83
Scheme 4.2: Acetylation of 1,2 - propylene glycol with acetic acid.	84
Scheme 4.3: Simplified reaction scheme for kinetic model	86
Scheme 5.1: Chlorohydrin process	119
Scheme 5.2: tert-Butyl peroxide process	119
Scheme 5.3: Routes from propylene glycol to propylene oxide	120
Scheme 5.4: Propylene glycol acetates deacetoxylation system	127
Scheme 5.5: Formation of potassium carbonate on surface of catalyst during reaction	137
Scheme 5.6: Mechanisms for formation of PO and its isomers	162

KEY TO SYMBOLS AND ABBREVIATIONS

Nomenclature and Units

C_{BA} = concentration of butyric acid in liquid phase, kmol m⁻³

 C_T = total molar density of the reacting fluid, kmol m⁻³

 D_{eff} = effective diffusivity of butyric acid, m^2 s⁻¹

D_{BA} = bulk diffusivity of butyric acid in alcohol, m² s⁻¹

 d_p = swelled diameter of catalyst in reaction conditions, m

 $E_{a,m} = \mbox{the activation energy of the rate constant for the reaction } m, \, kJ \, kmol^{-1}$

 F_{min} = square root of mean of squared absolute residues

 $K_{a,m}$ = activity based equilibrium constant for reaction m

 $K_{x,m}$ = mole fraction based equilibrium constant for reaction m

 $k_{0,m}$ = the pre-exponential factor of reaction m, kg soln \circ m³(kg catalyst)⁻¹s⁻¹kmol⁻¹

 N_C = number of components in reaction

 N_T = total number of moles in the reactor, kmol

 $r_m = \text{rate of reaction m per unit volume, kmol s}^{-1} \text{ m}^{-3}$

 r^*_{obs} = observed rate of reaction per weight of catalyst, mol s⁻¹ kg⁻¹

 $V = reaction volume, m^3$

 $V_{p,swollen}$ = volume of swollen catalyst, m^3

 $V_{p,dry} = dry \text{ volume of catalyst, } m^3$

w_{CAT} = catalyst loading in the reaction mixture, kg catalyst/ kg solution

 x_i = mole fraction of component i in the reaction mixture at equilibrium

 x_i = mole fraction of component i in the liquid mixture

 a_i = activity of species i in solution

 C_T = total molar density of the reacting fluid, kmol/m³

E_{a,m} =activation energy for reaction m, kJ/kmol

F_{min} =objective function for kinetic parameter fitting

 $k_m = \text{rate constant for reaction m, m}^3 \, \text{soln} \cdot \text{kg soln/kg cat/kmol/s}$

k-m = reverse rate constant for reaction m, m³ soln·kg soln/kg cat/kmol/s

 $K_{a,m}$ = activity based equilibrium constant for reaction m

 $k_{0,m}$ = pre-exponential factor for reaction m, m³ soln·kg soln/kg cat/kmol/s

n = number of samples taken in an experiment

 N_c = number of reacting species in experiment

 N_T = total number of moles in the reactor, kmol

 r_m = rate of reaction m per unit volume, kmol/s/m³

 $V = volume of reacting phase, m^3$

 w_{CAT} = catalyst loading in the reaction mixture, kg cat/kg soln)

 $k_{0,AC}$ = activity based rate constant, (m³ soln/(kmole soln) · (kg cat) · s)

 $k_{0,NIC}$ = non ideal concentration model based rate constant, (m 6 soln/(kmole soln) \cdot (kmole $H^+) \cdot s)$

 k_1 = concentration based rate constants of the reaction of interest

 k_{Ref} = concentration based rate constants of reference reaction

 E_S = steric effect of substituents

 C_{TS} = concentration of the transition state, kmole/m³

 K^{TS} = Equilibrium constant for formation of transition state from reactants

k_B Boltzmann constant

T = temperature

h = Planck's constant

 ΔG^{TS} = Gibbs free energy of reaction of reactants to form transition state, J/mole

C_{PGA} = concentration of propylene glycol acetates in liquid phase, mole m⁻³

Greek

 γ_i = activity coefficient of component i in the reaction mixture at equilibrium

 ε = particle porosity

 η = intraparticle effectiveness factor

 ϕ_w = Thiele modulus

 ρ_{CAT} = density of catalyst, kg m⁻³

 $\theta_{i,m}$ = ratio of stoichiometric coefficient of component i with respect to the reference component in reaction m

 v_i = stoichiometric coefficient of component i in the reaction mixture at equilibrium

 ∂ = sensitivity of the reaction to steric effects of the substituent relative to the corresponding reaction that involves the reference reactant

 μ_b = frequency of the transition state crossing the activation barrier (s⁻¹)

 $\theta_{i,m}$ =ratio of stoichiometric coefficients of component i with respect to the reference component in reaction m

 τ = contact time, s

Abbreviations

FTIR = Fourier transform infrared spectroscopy

XPS = X-ray photoelectron spectroscopy

EDS = energy-dispersive X-ray spectroscopy

A-70 = Amberlyst 70

p-TSA = para-toluene sulfonic acid

EQ = equilibrium

UNIFAC = UNIversal Functional Activity Coefficient

EB = ethyl butyrate

BA = butyric acid

Eth = ethanol

W = water

NRTL = Non-random two liquid model

AA = acetic acid

PG = propylene glycol

PGDA = propylene glycol diacetate

PGMA = propylene glycol monoacetate (1: primary, 2: secondary)

PO = propylene oxide

Conv. = Conversion

Temp = Temperature

CPG = Controlled Pore Glass

1 Introduction

The production of fuels and specialty chemicals from renewable biomass sources will require multiple economic and environmentally friendly routes and feedstock sources. Side products of several bio-refinery processes such as ethanol and biodiesel production present opportunities for further processing to produce value added products. Esters are one such important class of organic compounds used in a variety of applications in the chemical industry. This dissertation focuses on esters in particular as both end products and as intermediates to other products.

1.1 Esterification modeling

In bio-refinery processes, streams with multiple carboxylic acids and multiple alcohols are frequently encountered, for instance the Guerbet reaction of ethanol to higher alcohols, and fermentation to succinic acid along with acetic acid as a side product. The possibility of converting such mixed streams to ester mixtures for value addition and for easy separation by process integrated techniques such as reactive distillation is attractive, but hinges on answering certain questions. Does the presence of one alcohol inhibit the rate of another? Can we develop kinetic models that can predict the rate of reactions in a mixture using information from individual reactions?

In Chapter 2, as a case study, a detailed investigation was conducted of the kinetics of acylation of ethanol-butanol mixtures with butyric acid in both homogeneous and heterogeneous catalysis conditions with the conventionally used mole fraction and activity based models, followed by attempts to fit the mixed reactions to them. There were large deviations from

experiment using both models, especially in comparing kinetic rates of different alcohol systems. It was also observed that purely activity based models do not predict reactions with varying initial molar ratios of reactants well irrespective of the activity coefficient model used. Therefore, both non ideality (e.g. activity) and differences in molar densities (e.g. absolute concentrations) were incorporated into a single kinetic model that fit the mixed simultaneous acylation of multiple alcohols.

In Chapter 3, it was observed that when normalizing rates to the molar densities, the rates of many esterification reactions simplified to a single turn over number value for a specific catalyst. The implications of this are that essentially most alcohols and acids react at the same rate for a specific catalyst, and that this single value may be used to predict most esterification reactions, including parallel reactions with any initial composition. The condensation of kinetic information for so many reactions also allows the study of structure-reactivity relationships of similar esterification families. The comparatively higher rates for methanol and acetic acid shows that after an initial decrease in rate with addition of carbons, the length of the carbon chain is not an important factor for rate of reaction until it starts to inhibit the formation of a single phase. Trends have been studied of linear and branched alcohols and carboxylic acids, and with different homogeneous and heterogeneous catalysts and the results documented provide a useful database for estimating the rate of future reactions of interest.

1.2 Catalysis for propylene glycol epoxidation

Propylene oxide is a useful intermediate chemical for many everyday products such as defoamers, anti-freeze, and lubricants in the form of polyglycols, polyurethanes and polyglycol ethers. Current commercial technologies rely on the use of propylene from petrochemical sources.

In the interest of reducing our reliance on fossil sources and shifting to more environmentally friendly processes, alternate routes to make propylene oxide are being investigated. Processes to convert sorbitol and glycerol to propylene glycol have been commercialized. Instead of the traditional pathway to propylene glycol from propylene derived propylene oxide, the pathway to propylene oxide from bio-glycerol derived propylene glycol becomes an attractive option. A number of catalyst screening studies are available in literature, but in order to design an economically viable process, the reaction pathways need to be understood, and the catalyst needs to be characterized.

In Chapter 4, the acylation of propylene glycol with acetic acid to give propylene glycol mono acetates and propylene glycol diacetate is modeled using the non-ideal concentration based model. The results align with the esterification model developed in Chapter 2. The rates of esterification are the expected value predicted by findings in Chapter 1 and 2.

In Chapter 5, several candidate catalysts were chosen, and experiments were conducted to understand their activity in depth. Initial runs with pure propylene glycol show a large amount of di-propylene glycol formation, which was much reduced when a feed mixture of propylene glycol and its acetates were used instead. The effect of various reaction parameters such as temperature, catalyst loading, contact time, and feed concentration has been evaluated in a gas phase fixed bed reactor configuration. The optimum conditions for the best propylene oxide yield have been found to be at 400 °C, with a short contact time and mid ranged loading of alkali metal salt on silica. Extremely short contact times and low concentrations did not in effect increase selectivity above 90% by mole.

It is also important to understand the chemical nature of the basic salt on the surface of the catalyst to see how it participates in the reaction. Alkali metal salts on silica can react to form the respective silicates or remain unchanged depending on a number of factors including temperature, basicity and loading of alkali metal, and type of support used. For this reason, the unused and post reaction catalysts were characterized by a number of techniques such as FTIR, XPS and EDS.

The work in this dissertation expands the possibilities of esters as intermediates as well as products of bio-refineries. A more thorough understanding of the basics of esterification reaction kinetics is achieved, which in turn is useful for flexible process design.

Included in the following chapter is a copy of the paper: Kinetics of Mixed Ethanol/n-Butanol Esterification of Butyric Acid with Amberlyst 70 and p-Toluene Sulfonic Acid, by Arati Santhanakrishnan , Abigail Shannon , Lars Peereboom , Carl T. Lira , and Dennis J. Miller

Department of Chemical Engineering and Materials Science, Michigan State University, 2527 Engineering Building, East Lansing, Michigan 48824-1226, United States

Reprinted with permission from Ind. Eng. Chem. Res., 2013, 52 (5), pp 1845–1853

Copyright © 2013 American Chemical Society

2 Kinetics of mixed ethanol/n-butanol esterification of butyric acid with Amberlyst 70 and para-toluene sulfonic acid

2.1 Abstract

Esterification of butyric acid with ethanol, *n*-butanol and ethanol/*n*-butanol mixtures was studied using Amberlyst 70 cation exchange resin and homogeneous *para*-toluene sulfonic acid as catalysts. The kinetics of individual alcohol acylation were first examined in batch reactions at different temperatures and catalyst loadings, and then esterification in ethanol-*n*-butanol mixtures of varying concentration ratios was characterized. Both non-ideal solution and ideal solution kinetic models were developed. These models accurately predict the esterification of butyric acid by the individual alcohols, and a simple additive combination of the individual kinetic models provides a good description of mixed alcohol esterification. Using non-ideal concentration as the measure of species activity, ethanol and *n*-butanol esterification kinetics are described by a common rate constant that is postulated to be universal for any normal alcohol esterification of butyric acid over a given catalyst. The kinetic models thus have broad application such as in simulating reactive distillation processes for mixed alcohol esterification.

2.2 Introduction

The growing need to reduce dependence on fossil sources for fuels and chemicals has led to the exploration of pathways for their manufacture from renewable sources. Esters of higher alcohols (alcohols with more than two carbons) are one such industrially important class of compounds, and economically viable processes for making them need to be designed. Blends of esters are being considered as attractive solvents or as additives to biofuels because of their high energy density and favorable fuel properties. The most common route for producing esters is the

direct esterification of carboxylic acids with alcohols¹ using either homogeneous acid catalysts such as sulfuric acid or para-toluene sulfonic acid (p-TSA) or solid heterogeneous acid catalysts such as cationic exchange resins.

Mixed alcohol streams from biomass can be obtained in several ways: from condensation of lower alcohols to higher alcohols via the Guerbet reaction,^{2–4} via Fischer-Tropsch synthesis of alcohols from synthesis gas^{5–8}, or from fusel alcohols⁹ produced in ethanol fermentation. Esterification for biofuel or solvent applications is an attractive use of these mixed alcohol streams, as it would lead to value-added products without the need for separation into individual components. Simultaneous esterification with multiple alcohols is described in the patent literature.^{10–13}

Since esterification reactions are thermodynamically limited, reactive distillation is a viable option for mixed alcohol processing. ^{14,15} In simulations of reactive distillation, esterification of a mixture of amyl alcohol and *n*-butanol with acetic acid has been examined to compare separation-first and reaction-first schemes. ¹⁶ Reaction first schemes were determined to be more economical. The design of such reactive distillation schemes for mixed alcohols requires a good understanding of the kinetics of the reaction system, as it is generally not known whether the presence of one alcohol accelerates or inhibits the rate of reaction of another, or if the formation of mixed esters leads to transesterification that could overcomplicate the recovery process.

Recent advances in producing butyric acid via fermentation of biomass carbohydrates has sparked interest in using butyric acid as a building block via esterification and other reactions. Apart from their potential as biofuel components, ethyl butyrate and n-butyl butyrate serve as food flavoring agents and green solvents 18. The kinetics of n-butyl butyrate formation using Dowex 19

as an esterification catalyst has been previously studied and modeled using quasi-homogeneous, Eley-Rideal, and Langmuir-Hinshelwood rate models. The kinetics of ethyl butyrate formation have not been previously reported.

In this study, the kinetic behavior of butyric acid esterification with mixed ethanol and *n*-butanol (Scheme 2.1) is investigated using homogeneous (*p*-TSA) and heterogeneous (Amberlyst 70 ion exchange resin) catalysts. Kinetics of individual ethanol and *n*-butanol esterification reactions are first presented and then reaction kinetics for mixtures of varying ethanol and *n*-butanol compositions are reported. The kinetic model fitted to experimental data is useful in designing and characterizing reactive distillation columns for mixed alcohol esterification reactions.

Scheme 2.1: Esterification of butyric acid with ethanol and *n*-butanol

2.3 Materials and Methods

2.3.1 Materials

Reagent grade ethanol (200 Proof, Decon Labs, Inc., King of Prussia, Pennsylvania), *n*-butanol (99.9%, Sigma Aldrich Corp., St. Louis, Missouri), *n*-butyl butyrate (>98%, Sigma Aldrich Corp., St. Louis, Missouri) ethyl butyrate (>99%, Sigma Aldrich Corp., St. Louis, Missouri), water (HPLC solvent, JT Baker Reagent Chemicals. Phillipsburg, New Jersey), *p*-

toluene sulfonic acid monohydrate (Spectrum Quality Products, Inc., Gardena, California), butyric acid (>99%, natural, Sigma Aldrich Corp., St. Louis, Missouri), acetonitrile (HPLC grade, Emanuel Merck Damstadt Chemicals, Philadelphia, Pennsylvania), methanol (Sigma Aldrich Corp., St. Louis, Missouri) and ethyl octanoate (Sigma Aldrich Corp., St. Louis, Missouri) were used without further purification. Gas chromatographic (GC) analysis of the aforementioned chemicals showed no significant presence of impurities except for trace amounts of water. Hydranal-coulomat E solution (Riedel-de Haën, Seelze, Germany) was used in Karl-Fisher titrations. Helium (99.995%, AirGas, USA) was used as carrier gas for GC. The properties of the heterogeneous cation exchange resin catalyst Amberlyst 70® (Dow Chemical Company, Midland, Michigan) are reported in the literature.²⁰

2.3.2 Heterogeneous catalyst conditioning

As-received Amberlyst 70 (A-70) was sieved in a series of US-standard sieves (Dual Manufacturing Company, Chicago, Illinois) and the -45 +60 mesh (0.25 – 0.35 mm diameter) fraction was used in kinetic experiments. The resin was washed with methanol multiple times until the supernatant liquid was colorless, and then filtered to remove excess methanol. The resin was then dried in an oven at 373 K for 2 days. The dried resin was stored in a sealed container in a desiccator and removed in required amounts for reactions. Fresh catalyst was used for each experiment.

To find the ion exchange capacity of the catalyst, a known quantity of dry A-70 was submerged in ethanol for 4-5 hours and then titrated with NaOH. The average ion exchange capacity was found to be 2.35 ± 0.1 equivalents H⁺/kg, in reasonable agreement with the value of reported by the manufacturer.²⁰

2.3.3 Kinetic experiments

Isothermal kinetic experiments were carried out in 75 ml batch reactors in a Parr 5000 Multireactor system (Parr Instrument Co., Moline, Illinois). The reactor system is equipped with temperature and stirring speed control, and with a dip tube on each reactor to collect liquid samples during reaction. The end of the dip tube is fitted with a 2 µm stainless steel filter to avoid withdrawing solid catalyst along with liquid sample.

To begin an experiment, ethanol and n-butanol were weighed out alone or in predetermined molar ratios and added to the reactor with a known amount of catalyst (Amberlyst 70 for heterogeneous catalysis and p-toluene sulfonic acid for homogeneous catalysis). The reactor was sealed and heated until it stabilized at the desired reaction temperature. Stirring was set to 800 rpm unless otherwise specified. Once the desired temperature was reached, a specified amount of butyric acid was added to the reactor through the sample port in a single shot; the moment of addition was taken as time zero of the reaction. Total reactant weight came up to approximately 0.040 kg per reaction. Samples of 0.5 - 1 mL were withdrawn at specified time intervals during the kinetic regime (0 - 6 hr) using a 3 mL Luer-lok tip syringes (Becton Dickson and Co., Franklin Lakes, NJ) and stored in hermetically sealed vials in a standard refrigerator at 277 K. Samples to characterize reaction equilibrium were taken 24-36 hours after the start of the reaction.

2.3.4 Analysis

The initial water concentration in the reactants was determined by Karl Fischer titration in an Aquacounter coulometric titrator AQ-2100[®] (JM Science Inc., Grand Island, NY) and taken into account for calculations.

Analysis of reaction samples was carried out in a Varian 450 gas chromatograph outfitted with a thermal conductivity detector (Varian Medical Systems Inc., Palo Alto, CA). Reaction samples were diluted 10-fold in acetonitrile containing 11.11 wt.% ethyl octanoate as an internal standard. Separation was done on a 0.53mm ID Aquawax-DA 30 m capillary column with 1.0µm film thickness. Helium carrier gas flow rate was set to 10 mL min⁻¹. The following temperature program was used: initial column temperature 313 K for 2 min, ramp at 10 K min⁻¹ to 423 K, ramp at 30 K min⁻¹ to 503 K, hold 2 min. The detector temperature was held at 513 K. Standards of known composition in the range of interest were prepared and run in the chromatograph before and after reaction samples to calibrate the response factor of each component of the reaction.

2.4 Results

A list of all experiments conducted, along with their conditions (temperature, initial reactant molar ratio, weight fraction of catalyst) is given in Table 2.1. Control experiments to investigate autocatalysis of the reaction showed negligible rates over the temperature range studied. Although etherification side reactions have been observed in other studies involving the acylation of n-butanol^{7,13} and ethanol⁸ at temperatures above 386 K, no ethers (di-n-butyl ether, diethyl ether or ethyl n-butyl ether) were observed in the reaction samples in this study. This is because low loadings of catalyst (\sim 0.1 wt.% p-TSA and 1 wt.% A-70), low ratios of alcohol to acid (\sim 3:1-5:1), and relatively low temperatures were used in the experiments.

Table 2.1: Summary of experiments and conditions

No.	Temperature	Catalyst	Molar feed ratios		Solution Density	Catalyst loading	Figure No.
	(°C)		ethanol:	<i>n</i> -butanol:	(C _T)	(kg cat / kg	_
			acid	acid	(kmol m ⁻³)	soln)	
1	60	A-70	4.3		14.9	0.01	2.12
2	80	A-70	2.8		15.0	0.01	2.2
3	100	A-70	8.7		15.0	0.0075	2.13
4	120	A-70	6.6		14.9	0.0099	2.14
5	60	A-70		3.7	10.9	0.0096	2.2
6	80	A-70		4.4	10.9	0.0101	2.15
7	100	A-70		4.5	10.9	0.0101	2.16
8	120	A-70		3.3	10.9	0.0115	2.17
9	60	A-70	0.5	4.7	14.9	0.0109	2.4
10	60	A-70	2.6	2.6	12.8	0.0085	2.18
11	60	A-70	0.9	4.2	11.5	0.0099	2.4
12	80	A-70	1.5	1.7	12.6	0.005	2.19
13	80	A-70	4.5	3.9	12.9	0.0105	2.4
14	80	A-70	2.0	1.9	12.6	0.0077	2.20
15	80	A-70	0.8	3.8	11.5	0.0093	2.21
16	80	A-70	1.9	2.2	12.6	0.0196	2.22
17	80	A-70	0.6	3.0	11.5	0.0097	2.23
18	60	p-TSA	2.9		14.8	0.0012	2.24
19	80	p-TSA	2.8		14.9	0.0013	2.25
20	100	p-TSA	3.7		15.0	0.0012	2.3
21	120	p-TSA	3.7		15.0	0.0013	2.26
22	60	p-TSA		2.0	10.9	0.0013	2.27
23	80	p-TSA		3.0	10.9	0.0013	2.3
24	100	p-TSA		2.8	10.9	0.0014	2.28
25	120	p-TSA		3.7	10.9	0.0013	2.29
26	60	p-TSA	0.4	1.8	11.4	0.0012	2.30

Table 2.1 (cont'd)									
27	60	p-TSA	3.6	3.3	13.0	0.0013	2.31		
28	60	p-TSA	5.0	1.0	14.4	0.0013	2.32		
29	80	p-TSA	0.5	2.7	11.4	0.0013	2.5		
30	80	p-TSA	1.9	1.9	12.6	0.0014	2.5		
31	80	p-TSA	3.7	0.9	14.0	0.0014	2.5		

2.4.1 Mass transfer considerations

Accurate characterization of reaction kinetics requires that the experiments be conducted in the kinetic regime; i.e. at conditions where external and internal mass transfer resistances do not affect reaction rate. Preliminary experiments at varying stirring speeds showed that conversion rates were unaffected above 600 rpm, implying that the external mass transfer resistances are negligible at a stirring speed of 800 rpm. To estimate the influence of intra-particular mass transfer resistance in this heterogeneous catalyst reaction, the Weisz-Prater criterion was used.²¹ The observable modulus was first calculated (Eq. 2.1).

$$\phi_{w} = \frac{(r_{obs}^{*})\rho_{CAT}}{D_{eff}C_{BA}} \left(\frac{d_{p}}{6}\right)^{2}$$
 (2.1)

where r^*_{obs} is the observed rate of reaction per weight of catalyst, ρ_{CAT} is density of catalyst (assumed to be 1000 kg m⁻³), C_{BA} is the liquid phase concentration of butyric acid, d_p is swelled diameter of catalyst at reaction conditions (Eq. 2.2)

$$d_p = d_{p,dry} \times \sqrt[3]{\frac{V_{p,swollen}}{V_{p,dry}}}$$
 (2.2)

where d_p is 0.30 mm and $V_{p,swollen}/V_{p,dry}$ is determined from a simple measurement to be 2.0 for both alcohols. The effective diffusivity D_{eff} of butyric acid in alcohol is estimated (Eq. 2.3), where pore tortuosity τ is assumed to be equal to the inverse of particle porosity ε , and D_{BA} is bulk diffusivity of butyric acid in alcohol estimated from the Wilke-Chang equation.²²

$$D_{eff} = D_{BA} \left(\frac{\varepsilon}{\tau}\right) = D_{BA} \varepsilon^2 \tag{2.3}$$

The Thiele modulus (φ) and effectiveness factor (η) for butyric acid esterification are calculated from the observable modulus $\phi_w = \eta \varphi^2$ assuming the reaction is pseudo first order in butyric acid (i.e. excess alcohol) and thus $\eta = \frac{\tanh(\varphi)}{\varphi}$. Values of η were evaluated for butyric acid in each of the alcohols (Table 2.2) and were found to be ~0.93 and ~0.96 for ethanol and n-butanol esterification, respectively. These values of η indicate that intra-particular resistances can be neglected.

Table 2.2 : Estimated effectiveness factors for Amberlyst 70 catalyzed esterification reactions

Run	Temperature (°C)	Molar fe	ad ratio	η
	(C)	ethanol: acid	n- butanol: acid	
1	60	4.3		0.94
2	80	2.8		0.94
3	100	8.7		0.96
4	120	6.6		0.89
5	60		3.7	0.97
6	80		4.4	0.92
7	100		4.5	0.94

2.4.2 Reaction equilibrium constants

Equilibrium constants were determined for each reaction by sampling the reactor contents after 24 to 48 hours of reaction. The activity-based equilibrium constant $K_{a,m}$ for reaction m is given in Eq. 2.4.

$$K_{a,m} = K_{x,m} K_{\gamma,m} = \prod_{i=1}^{Nc} (x_i \gamma_i)_{EQ}^{\nu_i}$$
 (2.4)

Here x_i , y_i , and v_i represent the mole fraction, activity coefficient, and stoichiometric coefficient of component i in the reaction mixture at equilibrium. The ratio of activity coefficients ($K_{\gamma,m}$) accounts for deviations from ideal behavior; values of activity coefficients were estimated using UNIFAC (UNIversal Functional Activity Coefficient).²³ The group type counts for each component in the reaction system, the group surface area and volume contributions, and the group binary interaction parameters are recorded in Table 2.3, Table 2.4, and Table 2.5, respectively.

Table 2.3: UNIFAC groups and their counts in reaction components

Component name	Group	Count
butyric acid	СНЗ	1
	CH2	2
	СООН	1
ethanol	CH3	1
	CH2	1
	ОН	1
ethyl butyrate	CH3	2
	CH2	2
	CH2COO	1
water	H2O	1
<i>n</i> -butanol	CH3	1
	CH2	2
	ОН	1
butyl butyrate	CH3	2
	CH2	4
	CH2COO	1

Table 2.4: Group volume and surface area contributions

Group	Rk	Qk	
CH3	0.9011	0.848	
CH2	0.6754	0.54	
COOH	1.3013	1.224	
CH2COO	1.6764	1.42	
H2O	0.92	1.4	
ОН	1	1.2	

Table 2.5: UNIFAC group binary interaction parameters

Name	CH2	ОН	H2O	CH2COO	СООН
CH2	0	986.5	1318	232.1	663.5
ОН	156.4	0	353.5	101.1	199
H2O	300	-229.1	0	72.87	-14.09
CH2COO	114.8	245.4	200.8	0	660.2
СООН	315.3	-151	-66.17	-256.3	0

The mole-fraction based equilibrium constants ($K_{x,m}$) were calculated from the composition of the reaction mixture. The experimental mole fraction-based and activity-based equilibrium constants for butyric acid with ethanol and n-butanol are presented in Figure 2.1. The enthalpy of reaction (ΔH_r), obtained from the slope of the trend line in Figure 2.1, is 17 kJ/mole for ethanol and 19 kJ/mole for n-butanol esterification of butyric acid. Although previous studies have reported temperature independent values of equilibrium constants in kinetic models 19 here the data in Figure 2.1 were used to calculate temperature-dependent equilibrium constants in the kinetic model described below.

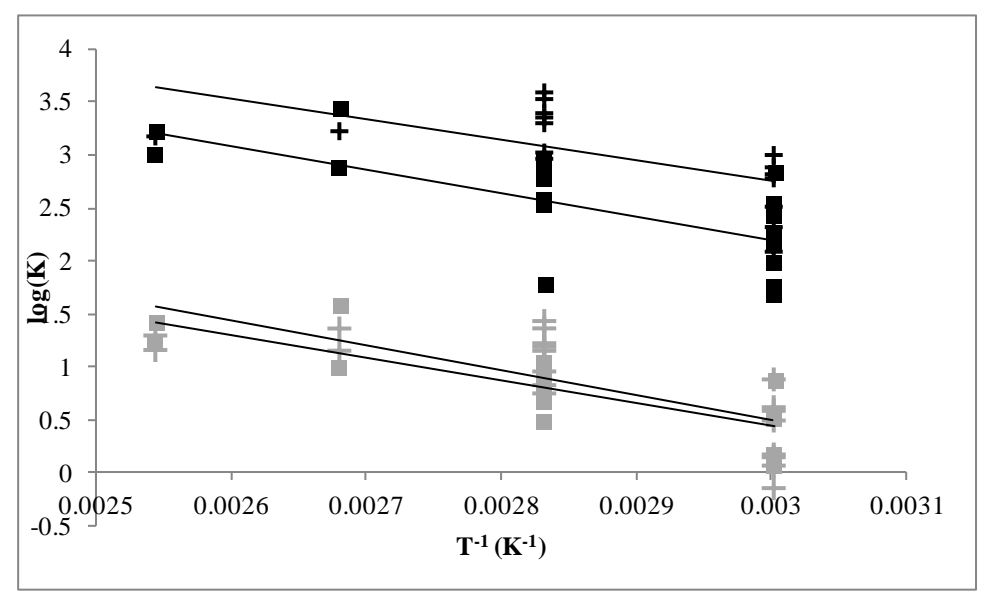


Figure 2.1: Van't Hoff plot of mole fraction- (gray) and activity- (black) based esterification equilibrium constants from experimental data. (\blacksquare , \blacksquare) – *Ethanol*, (+, +) – *n-butanol*

2.4.3 Kinetic Model Description

In a batch reactor, the change in number of moles N_i of component i participating in M reactions can be expressed as

$$\frac{dN_i}{dt} = N_T \frac{dx_i}{dt} = \left(\sum_{1}^{M} \theta_{i,m} r_m\right) V \tag{2.5}$$

where N_T is the total number of moles in the reactor, M is the number of reactions in the system, V is the reaction volume, r_m is the rate of reaction m per unit volume, and x_i is the mole fraction of component i in the liquid mixture. The parameter $\theta_{i,m}$ is the ratio of stoichiometric coefficients of component i with respect to the reference component in reaction m.

For this esterification system, Eq. 2.5 can be expressed in terms of total molar density of the liquid phase ($C_T = N_T/V$) because the total number of moles is conserved and reaction volume is thus assumed constant during reaction.

$$\frac{dx_i}{dt} = \frac{1}{C_T} \left(\sum_{m=1}^m \theta_{i,m} r_m \right) \tag{2.6}$$

With a neat mixture (e.g., no solvent) of reactants that constitute a non-ideal liquid phase, the rate of formation of ester in reaction m, r_m , is based on the law of mass action (e.g. a "power law" model) with an non-ideal concentration equal to $C_T x_i \gamma_i$ (kmol/m³) representing the activity of each species in the rate expression. This non-ideal concentration has been previously defined and used for liquid phase reactions. ^{24,25} Its use is required here in order to compare butyric acid esterification rates in neat mixtures of different alcohols, because the usual form of thermodynamic

activity ($a_i = x_i \gamma_i$) does not account for differences in the overall solution density (C_T , Table 2.1) and thus differences in the absolute concentration of each species in the mixture for different alcohol species. The rate of formation of ethyl butyrate (EB) in the batch reaction can thus be expressed in terms of the mole fractions and activity coefficients of butyric acid (BA), ethanol (Eth), ethyl butyrate, and water (W); w_{CAT} , the catalyst loading in the reaction mixture; C_T , the total molar density of the reacting fluid; $k_{0,1}$, the pre-exponential factor, and $E_{a,1}$, the activation energy of the rate constant for the reaction.

$$r_{EB} = w_{CAT} C_T^2 k_{0,1} \exp\left(-\frac{E_{a,1}}{RT}\right) \left[x_{BA} \gamma_{BA} x_{Eth} \gamma_{Eth} - \frac{x_{EB} \gamma_{EB} x_W \gamma_W}{K_{a,1}}\right]$$
(2.7)

A similar expression is derived for the formation of n-butyl butyrate (BB) by esterification with n-butanol (But).

$$r_{BB} = w_{CAT} C_T^2 k_{0,2} \exp\left(-\frac{E_{a,2}}{RT}\right) \left[x_{BA} \gamma_{BA} x_{But} \gamma_{But} - \frac{x_{BB} \gamma_{BB} x_W \gamma_W}{K_{a,2}} \right]$$
(2.8)

Using the rate expressions (Eq. 2.7 and 2.8), Eq. 2.6 can be written for every species in the reaction mixture to give six ordinary differential equations describing the esterification system.

2.4.4 Application of Kinetic Model to Single Alcohol Esterification

Data from individual esterification reactions involving only one alcoholic species were first fit to obtain reliable kinetic models to describe their behavior, and then parameters obtained from individual esterification reactions were used to predict mixed alcohol esterification behavior. The set of ordinary differential equations (Eq. 2.6) for each species in the reaction mixture were integrated numerically using the functions nlinfit and ode23 from the optimization toolbox in Matlab 7.12.0. Both non-ideal concentration (herein "activity-based") and ideal concentration

(herein "mole fraction-based" with all activity coefficients defined as unity) models were regressed. Optimization was done by minimizing F_{min} (Eq. 2.9) defined as the sum of squared differences between calculated (x_{i-calc}) and experimental (x_{i-exp}) species mole fractions for all species in all esterification reactions conducted.

$$F_{min}^{2} = \frac{1}{n} \sum_{samples} \sum_{i=1}^{N_C} (x_{i-exp} - x_{i-calc})^{2}$$
 (2.9)

In Eq. 2.9, n is the number of experimental samples withdrawn in the experiments regressed, and N_c is the number of reacting components in those experiments.

Optimized kinetic parameters with 95% confidence limits are reported in Table 2.6 for both A-70 and p-TSA catalysts. Activation energies are in the expected range of values (45 \pm 10 kJ mol⁻¹) for esterification of small aliphatic carboxylic acids with aliphatic alcohols. Absolute errors for each experiment were calculated (Eq. 2.10) and are presented in Table 2.7.

$$f_{ABS} = \frac{1}{n} \sum_{i=1}^{N_C} |x_{i-exp} - x_{i-calc}|$$
 (2.10)

Table 2.6: Optimized kinetic parameters with 95% confidence limits and equilibrium constants from experimental data (T in Kelvin)

Constants from experin	nental data (T in Kelvin)	<u></u>			
	Mole fraction				
Alcohol (Catalyst)		Activity model			
	model				
Ethanol (A-70)	Ethanol (A-70)				
k_{O}	4.1.0.7.103	62.16.103			
(leg golm a m ³ (leg gotolyst)-lg-llem ol-l)	$4.1\pm0.5\times10^{3}$	$6.2\pm1.6\times10^3$			
$(kg soln \circ m^3(kg catalyst)^{-1}s^{-1}kmol^{-1})$					
E_a (kJ kmol ⁻¹)	45900±3400	47300±6100			
K_1	$\exp(-2119/T + 6.80)$	$\exp(-2219/T + 8.83)$			
Rate constant value at 60 °C	2.6±3.5×10 ⁻⁴	2.4±7.8×10 ⁻⁴			
Raie Considii value di 60°C	2.0±3.3×10	2.4±7.0×10			
n-Butanol (A-70)					
k_0 (kg soln \circ m ³ (kg catalyst) ⁻¹ s ⁻¹ kmol ⁻¹)	$6.8\pm1.4\times10^3$	$11.9 \pm 0.5 \times 10^3$			
E_a (kJ kmol ⁻¹)	46800±290	48300±155			
$L_a(\mathbf{K}\mathbf{J} \mathbf{K}\mathbf{H}\mathbf{O}\mathbf{I}')$	+0000±270	+0300±133			
K_2	$\exp(-2339/T + 7.5)$	$\exp(-1921/T + 8.8)$			
		1			
Rate constant value at 60 °C	3.1±0.3×10 ⁻⁴	3.2±0.04×10 ⁻⁴			
Ethanol (p-TSA)					
k_0 (kg soln \circ m ³ (kg catalyst) ⁻¹ s ⁻¹ kmol ⁻¹)	$22.9 \pm 1.4 \times 10^3$	$26.2\pm1.7\times10^3$			
	44000 : 100	45000 : 100			
E_a (kJ kmol ⁻¹)	44900±182	45200±192			
Rate constant value at 60 °C	2.1±0.1×10 ⁻³	2.1±0.1×10 ⁻³			
n-Butanol (p-TSA)					
k_0 (kg soln \circ m ³ (kg catalyst) ⁻¹ s ⁻¹ kmol ⁻¹)	$21.3 \pm 2.6 \times 10^3$	$71.8 \pm 6.8 \times 10^3$			
λυ (kg som · m (kg catalyst) s killol)	∠1.3 ±∠.0 × 10	/1.0 ± 0.0× 10			
E_a (kJ kmol ⁻¹)	44900±375	48300±300			
Rate constant value at 60 °C	1.9±0.2×10 ⁻³	$1.9\pm0.3\times10^{-3}$			

Table 2.7: Absolute errors in model fits for each experiment

Run	Temperature	Catalyst	Absolute Error	
	(°C)		Mole	Activity
			fraction	
			F _{abs}	F_{abs}
1	60	A-70	0.043	0.051
2	80	A-70	0.045	0.045
3	100	A-70	0.049	0.046
4	120	A-70	0.051	0.053
5	60	A-70	0.019	0.024
6	80	A-70	0.031	0.060
7	100	A-70	0.040	0.063
8	120	A-70	0.077	0.11
9	60	A-70	0.058	0.051
10	60	A-70	0.044	0.045
11	60	A-70	0.051	0.062
12	80	A-70	0.071	0.082
13	80	A-70	0.068	0.069
14	80	A-70	0.072	0.087
15	80	A-70	0.098	0.099
16	80	A-70	0.028	0.036
17	80	A-70	0.042	0.048
18	60	p-TSA	0.048	0.048
19	80	p-TSA	0.065	0.065
20	100	p-TSA	0.083	0.083
21	120	p-TSA	0.046	0.046
22	60	p-TSA	0.055	0.095
23	80	p-TSA	0.107	0.069
24	100	p-TSA	0.117	0.084
25	120	p-TSA	0.134	0.080
26	60	p-TSA	0.052	0.188
27	60	p-TSA	0.029	0.035
28	60	p-TSA	0.074	0.069
29	80	p-TSA	0.033	0.100
30	80	p-TSA	0.018	0.054
31	80	p-TSA	0.013	0.029

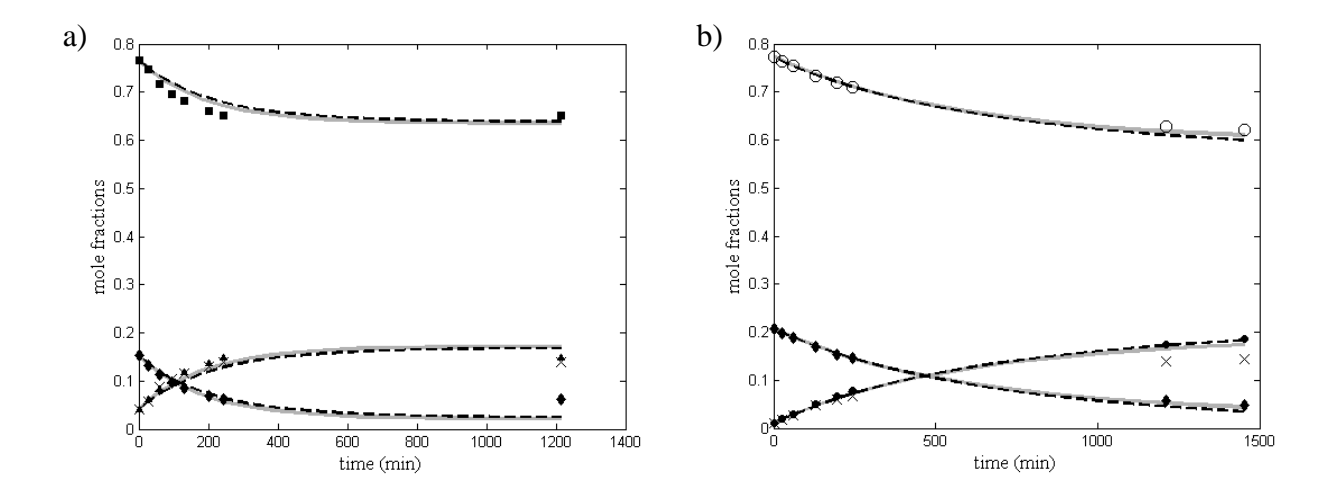


Figure 2.2: Experimental and predicted concentration profiles of ethanol and n-butanol individual esterification in the presence of 1 wt.% Amberlyst 70: a) Run 2 (Ethanol, T = 80 °C); b) Run 5 (n-Butanol, T = 60 °C). (——) — Mole fraction based fits; (——) — Activity based fits. (\bullet) — butyric acid; (\blacksquare) —ethanol; (\blacktriangle) —ethyl butyrate; (\times) —water; (\circ) —n-butanol; (\bullet)- n-butyl butyrate.

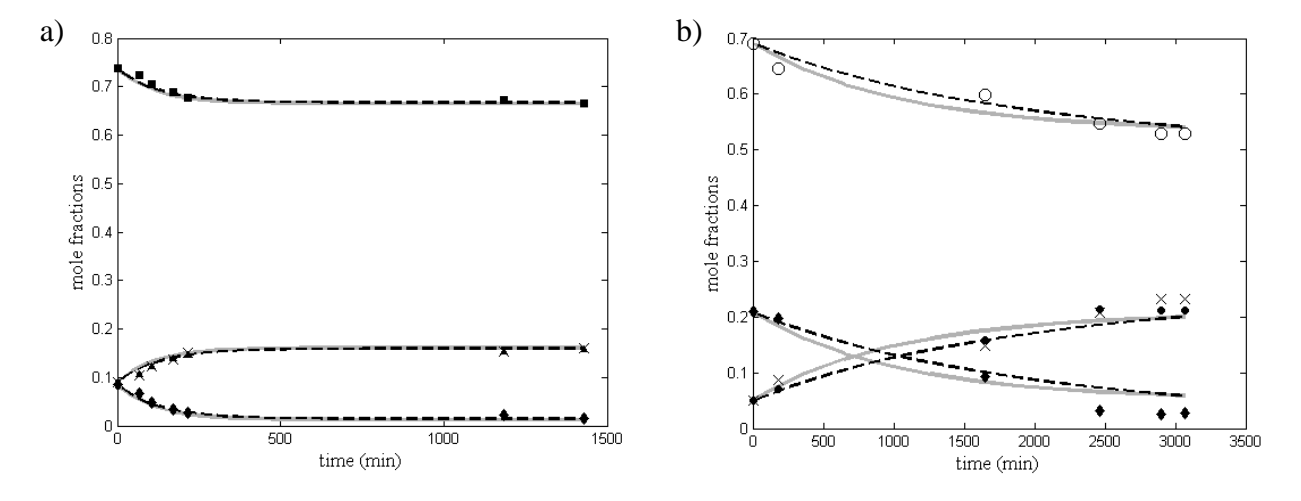


Figure 2.3: Experimental and predicted concentration profiles of ethanol and n-butanol individual esterification in the presence of 0.1 wt.% p-TSA: a) Run 20 (Ethanol, T = 100 °C); b) Run 23 (n-Butanol, T = 80 °C). (——) — Mole -fraction based fits; (——) — Activity based fits. (\bullet) — butyric acid; (\blacksquare) —ethanol; (\blacktriangle) —ethyl butyrate; (\times) —water; (\circ) —n-butanol; (\bullet) - n-butyl butyrate.

Select mole fraction profiles of activity-based and mole fraction based models fits with experimental data for individual ethanol and *n*-butanol esterification experiments are shown in

Figure 2.2 for A-70 catalyst and in Figure 2.3 for *p*-TSA. All remaining mole fraction profiles for both catalysts are shown in Figure 2.12 through Figure 2.32 in Appendix B and C. These plots indicate that the models fit experimental data reasonably well.

The rate of esterification with homogeneous p-TSA catalyst is substantially higher than with heterogeneous A-70 resin. Using catalyst loadings, the A-70 acid site density of 2.35 eq H⁺/kg, and initial concentrations, the initial turn over number (TON, kmol BA/kmol H⁺/hr) for ethanol on p-TSA is 70.8 and on A-70 is 16.8. For butanol, the initial TON is 40.7 on p-TSA and 11.3 on A-70. The ratio of TON for the two catalysts is approximately four for both alcohols. We attribute the lower TON in A-70 not to mass transport effects (see Table 2.2) but to steric effects associated with limited access of acid and alcohol to an anchored acid site in the porous solid catalyst versus the unhindered access acid and alcohol have to free acid in solution. The similarity in activation energies over the two catalysts supports this postulate and that the reaction mechanism is the same on homogeneous p-TSA and heterogeneous A-70.

The absolute rate of butyric acid esterification (kmol/m³/sec) in ethanol is higher than in n-butanol for both catalysts. This is expected because the absolute concentration (kmol/m³) of ethanol in solution is higher than n-butanol, and thus the hydroxyl group concentration is higher. However, in the rate expression using non-ideal concentration ($C_Tx_i\gamma_i$) for each of the catalysts, the rate constants for ethanol and butanol esterification (Table 2.6) have the same value within experimental uncertainty. The values given in Table 2.6 are thus "universal" rate constants for butyric acid esterification with alcohols over the respective catalysts, provided non-ideal concentration is used as the measure of species activity. This result is consistent with earlier results obtained in a broader study in our laboratory, where a common rate constant for C2 to C8

alcohols was observed over A-70 catalyst. Interestingly, methanol showed a substantially higher rate constant on the same basis.

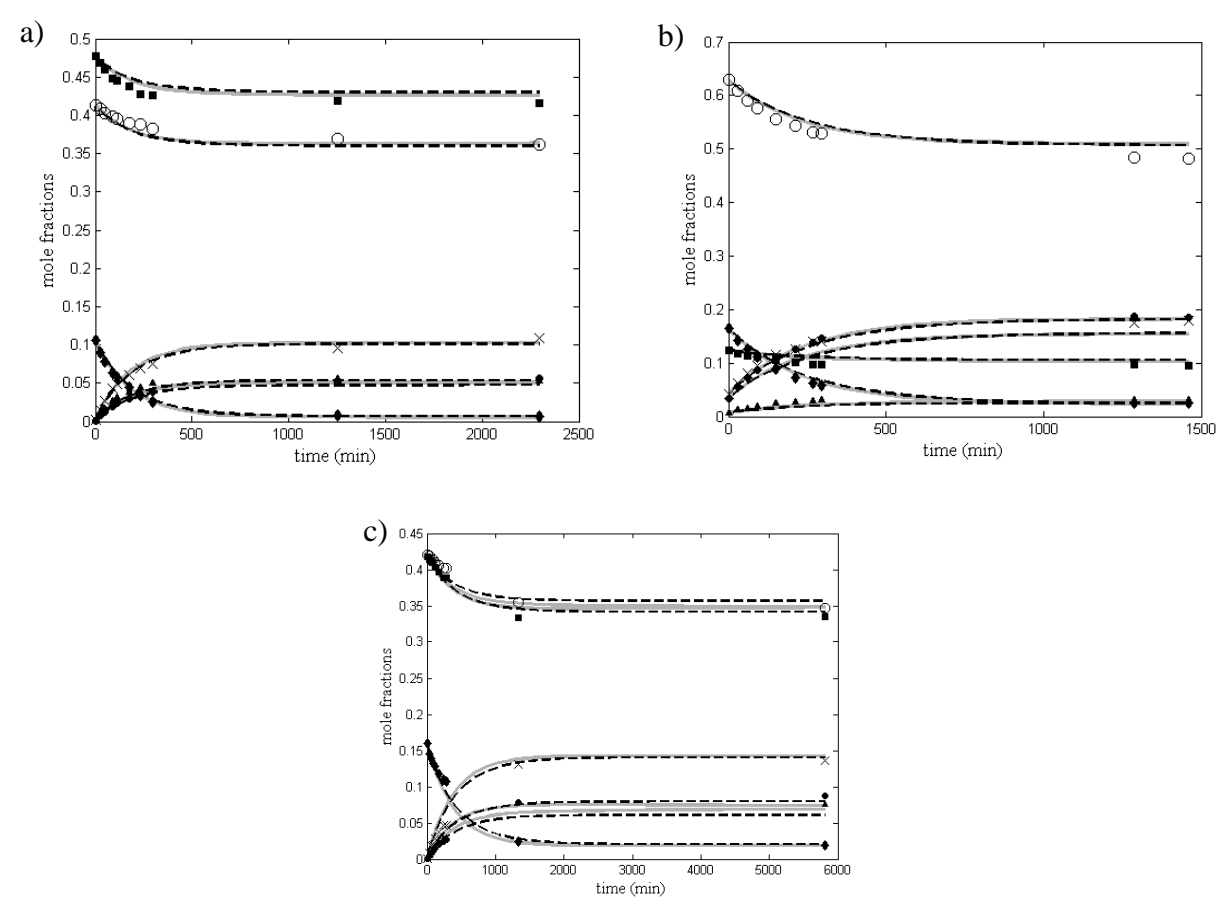


Figure 2.4: Experimental and predicted concentration profiles of mixed alcohol esterification in the presence of 1 wt.% Amberlyst 70. a) Run 13 (Ethanol:*n*-Butanol = 1.15:1, T=80°C); b) Run 11 (Ethanol:*n*-Butanol = 0.21:1, T = 60 °C); c) Run 9 (Ethanol: *n*-Butanol = 1:1, T = 60°C). (——) −mole fraction based fits; (——) −activity based fits. (♦) − butyric acid; (■) − ethanol; (▲) −ethyl butyrate; (×) −water; (○) −*n*-butanol; (●)- *n*-butyl butyrate.

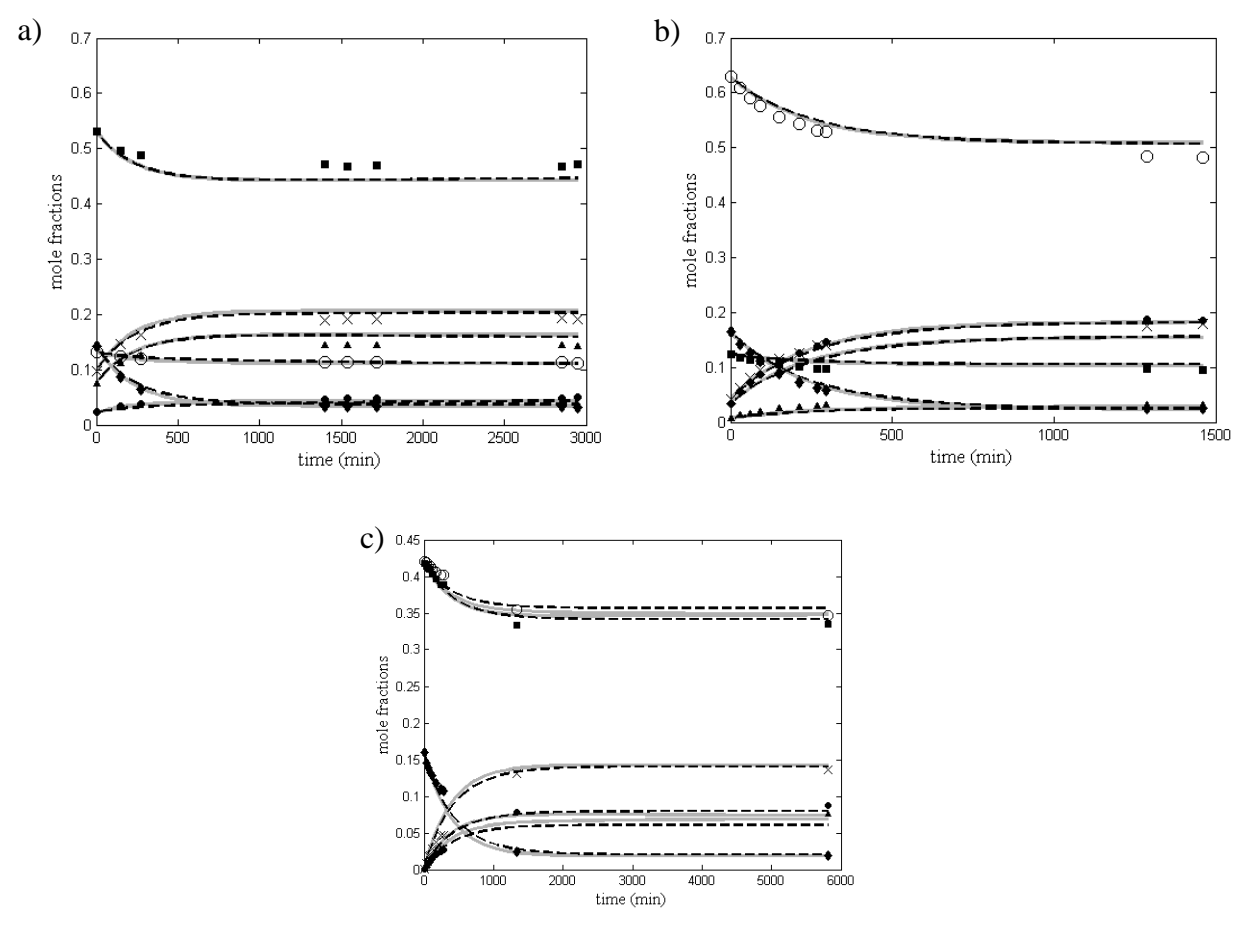


Figure 2.5: Experimental and predicted concentration profiles of mixed alcohol esterification in the presence of 0.1 wt.% \underline{p} -TSA. a) Run 31 (Ethanol:n-Butanol = 4.1:1 , T = 80°C); b) Run 29 (Ethanol:n-Butanol = 0.18:1,T = 80°C); c) Run 30 (Ethanol:n-Butanol = 1:1,T =80°C). (——) -mole fraction based fits; (——) -activity based fits. (\blacklozenge) - butyric acid; (\blacksquare) -ethanol; (\blacktriangle) -ethyl butyrate; (\times) -water; (\circ) -n-butanol; (\bullet)- n-butyl butyrate.

2.4.5 Application of kinetic model to mixed alcohol esterification

The parameters from the activity and mole fraction based models from the two individual esterification studies were used to predict mixed alcohol behavior in initially ethanol rich, n-butanol rich and equimolar reactant mixtures. Figure 2.4 compares the prediction of the two models with experimental data from mixed alcohol esterification runs for A-70. Figure 2.5 does the same for p-TSA catalyzed mixed alcohol reactions. The additive combination of individual alcohol esterification rate models predicts the mixed ethanol/n-butanol esterification system well

for both catalysts. This result, observed over a wide range of alcohol molar ratios and supported by the common value of rate constant, is strong evidence that the alcohols are not competing to adsorb on the acid catalyst sites in either solid Amberlyst 70 or in solution with *p*-toluenesulfonic acid. Rather, the alcohols behave similarly, and the rate determining step for esterification must be related to formation of an intermediate from butyric acid, or must take place apart from the active catalyst site.

To the best of our knowledge, there have been no previous experimental kinetic studies on mixed alcohol esterification using homogeneous or heterogeneous catalysis. However, a similar study examining mixed acid esterification found that the additive combination of both esterification reactions also predicted the kinetics of the mixed acid system well.²⁷ The ability to predict mixed alcohol or acid esterification rates based on individual species rates, along with the commonality of rate constants for analogous species, greatly simplifies the characterization of complex esterification systems likely to be encountered in the bio-refinery, where either or both mixed alcohols and mixed acids are present.

2.5 Conclusions

The kinetics of ethanol and *n*-butanol esterification of butyric acid in the presence of homogeneous *p*-toluene sulfonic acid and heterogeneous ion exchange resin catalyst Amberlyst 70 have been accurately described by ideal (mole fraction-based) and non-ideal (activity-based) models. Mixed alcohol esterification kinetics are accurately predicted from an additive combination of esterification rates of the individual alcohols, Further, by using non-ideal concentration as the measure of species activity, ethanol and *n*-butanol esterification kinetics are described with a single rate constant, which serves as a "universal" rate constant for butyric acid esterification over a given catalyst. The additivity of rates and common rate constant greatly

simplify the simulation of actual biorefinery processes where multiple alcohol species are forming
esters.

APPENDICES

Appendix A: Calibration plots for gas chromatography analysis

The following plots (Figure 2.6 through Figure 2.11) show calibrations of standards prepared to determine response factors of each component in the reaction system, determined by the slope of area ratio over weight ratio of component over internal standard ethyl caprylate.

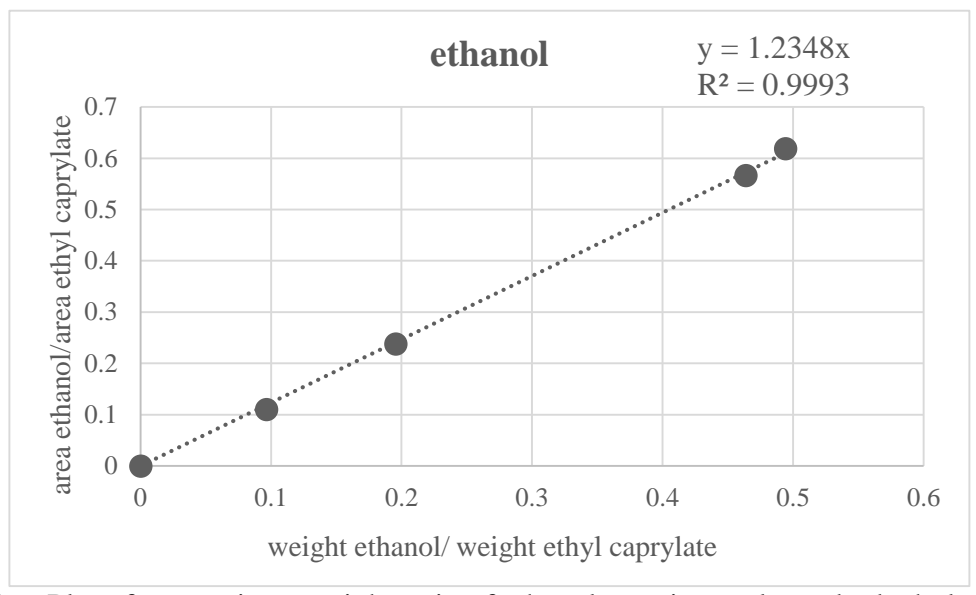


Figure 2.6: Plot of area ratio vs weight ratio of ethanol over internal standard ethyl caprylate

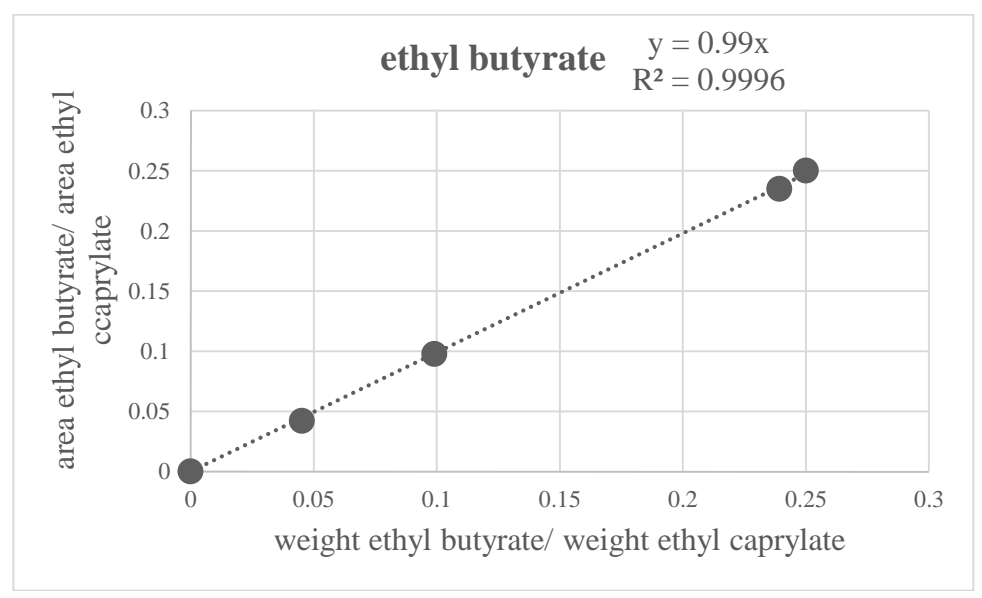


Figure 2.7: Plot of area ratio vs weight ratio of ethyl butyrate over internal standard ethyl caprylate

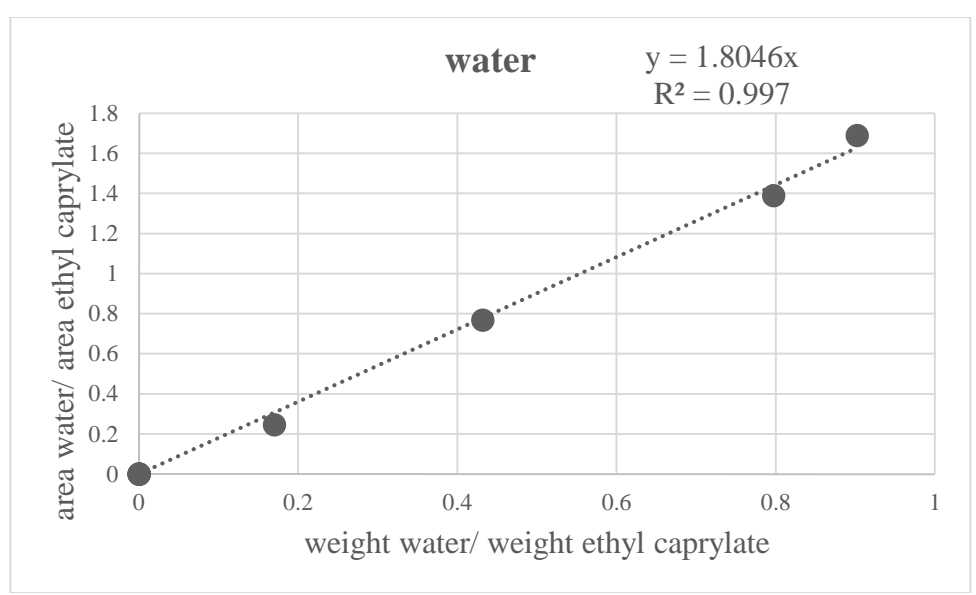


Figure 2.8: Plot of area ratio vs weight ratio of water over internal standard ethyl caprylate

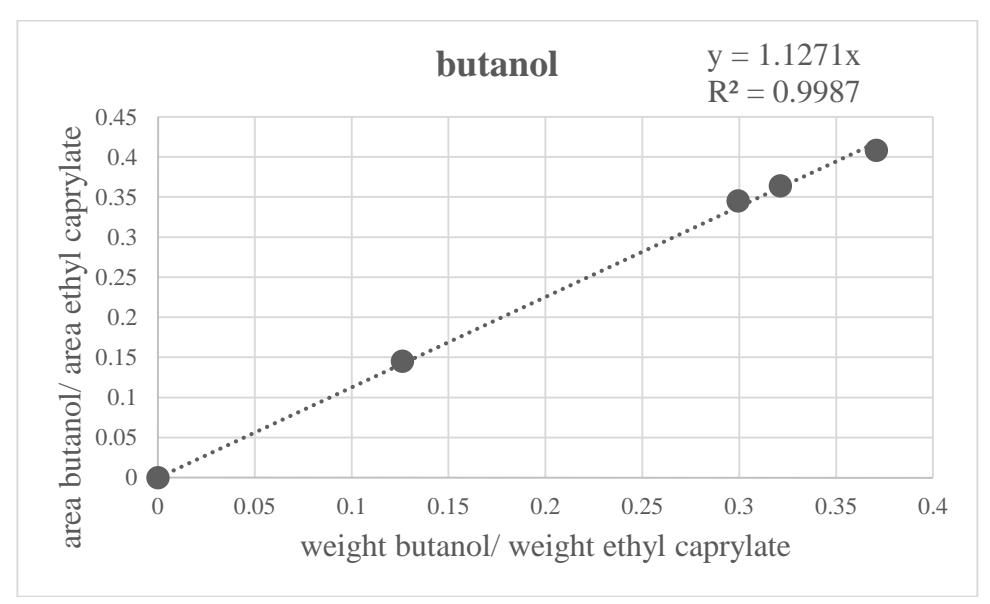


Figure 2.9: Plot of area ratio vs weight ratio of butanol over internal standard ethyl caprylate

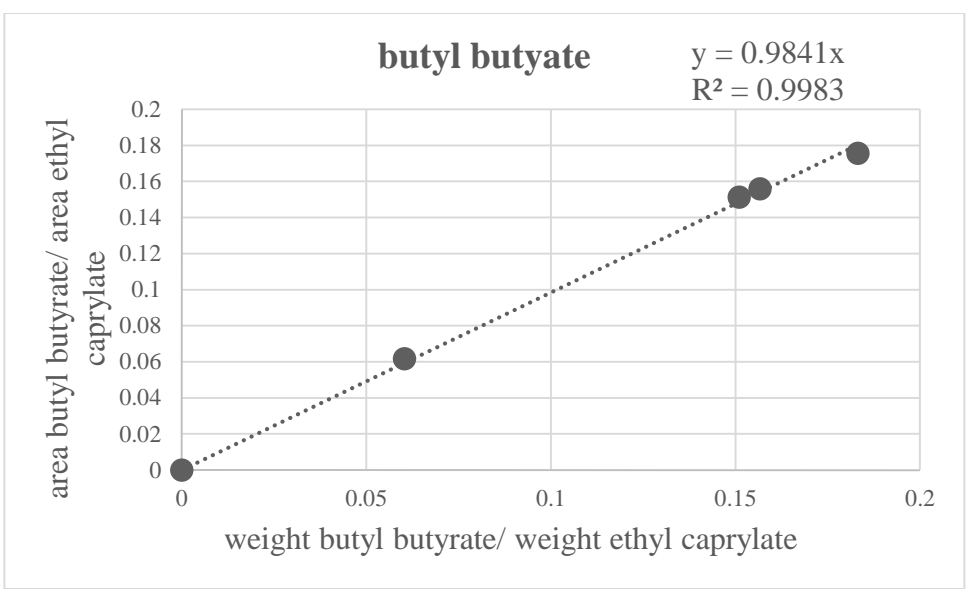


Figure 2.10: Plot of area ratio vs weight ratio of butyl butyrate over internal standard ethyl caprylate

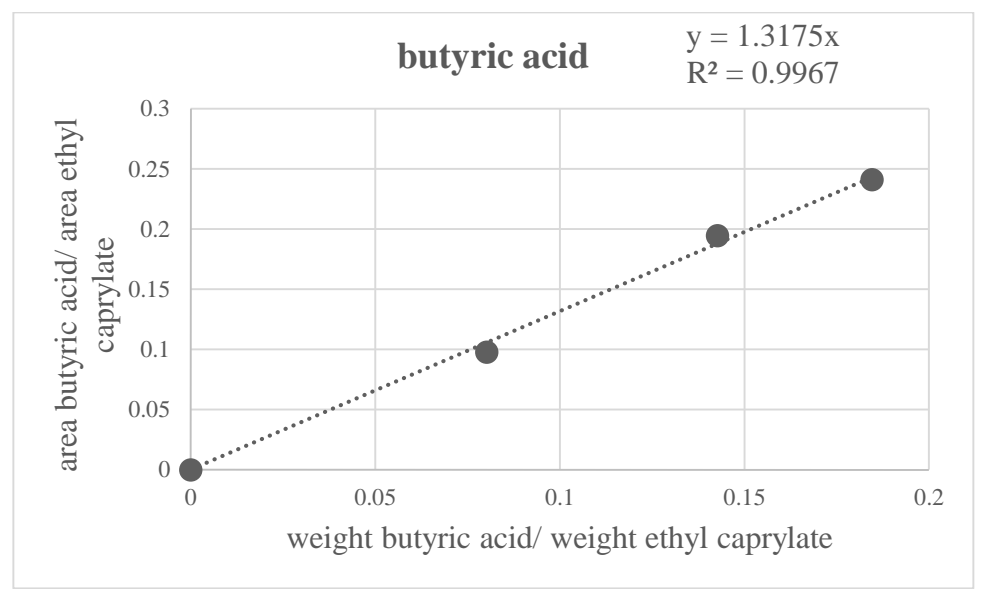


Figure 2.11: Plot of area ratio vs weight ratio of butyric acid over internal standard ethyl caprylate

Appendix B. Reaction profiles of Amberlyst 70 catalyzed reactions

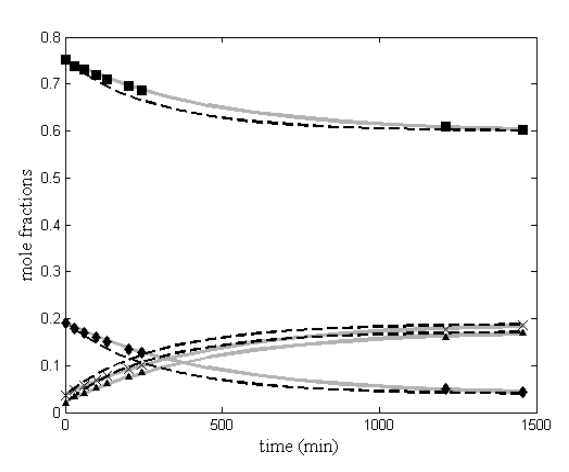


Figure 2.12: Experimental and predicted concentration profiles of ethanol individual esterification in the presence of 1 wt.% Amberlyst 70: Run 1, $T = 60 \,^{\circ}\text{C}$ (——) – Mole - fraction based fits; (— —) – Activity based fits. (\blacklozenge) – butyric acid; (\blacksquare) –ethanol; (\blacktriangle) –ethyl butyrate; (\times) –water

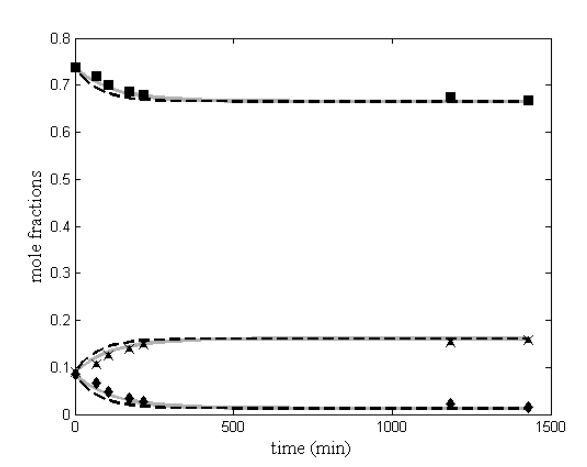


Figure 2.13: Experimental and predicted concentration profiles of ethanol individual esterification in the presence of 1 wt.% Amberlyst 70: Run 3, $T = 100 \,^{\circ}\text{C}$ (——) – Mole - fraction based fits; (— —) – Activity based fits. (\blacklozenge) – butyric acid; (\blacksquare) –ethanol; (\blacktriangle) –ethyl butyrate; (\times) –water

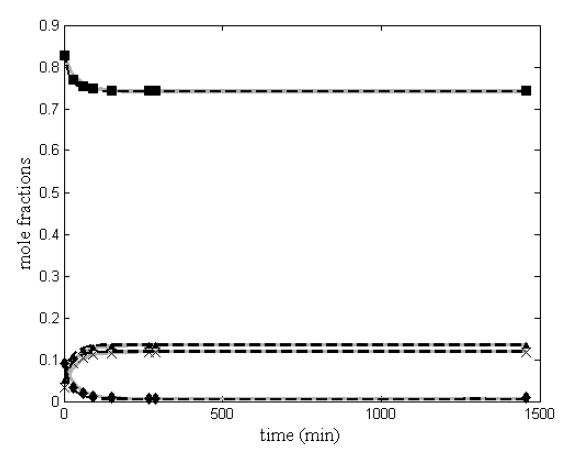


Figure 2.14: Experimental and predicted concentration profiles of ethanol individual esterification in the presence of 1 wt.% Amberlyst 70: Run 4, $T = 120 \,^{\circ}\text{C}$ (——) – Mole - fraction based fits; (— —) – Activity based fits. (\bullet) – butyric acid; (\blacksquare) –ethanol; (\blacktriangle) –ethyl butyrate; (\times) –water

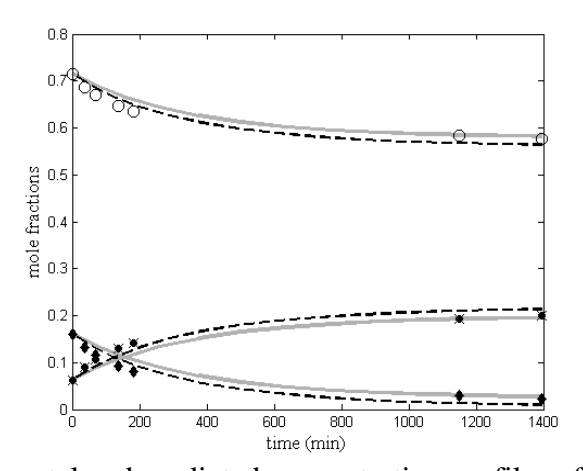


Figure 2.15: Experimental and predicted concentration profiles of *n*-butanol individual esterification in the presence of 1 wt.% Amberlyst 70: Run 6, T = 80 °C (——) – Mole - fraction based fits; (— —) – Activity based fits. (\bullet) – butyric acid; (\circ) –*n*-butanol; (\bullet)- *n*-butyl butyrate; (\times) –water

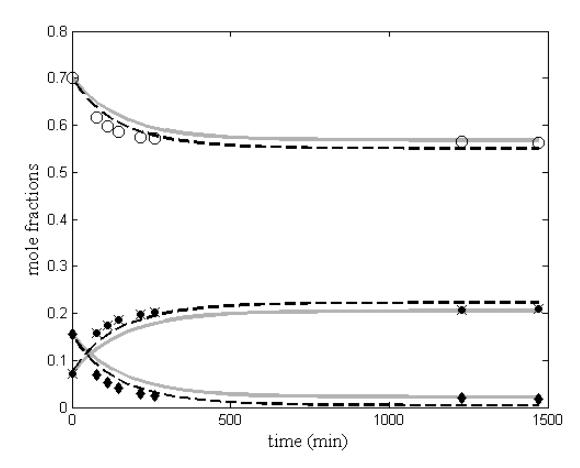


Figure 2.16: Experimental and predicted concentration profiles of *n*-butanol individual esterification in the presence of 1 wt.% Amberlyst 70: Run 7, $T = 100 \,^{\circ}\text{C}$ (——) – Mole - fraction based fits; (— —) – Activity based fits. (\bullet) – butyric acid; (\circ) –*n*-butanol; (\bullet)- *n*-butyl butyrate; (\times) –water

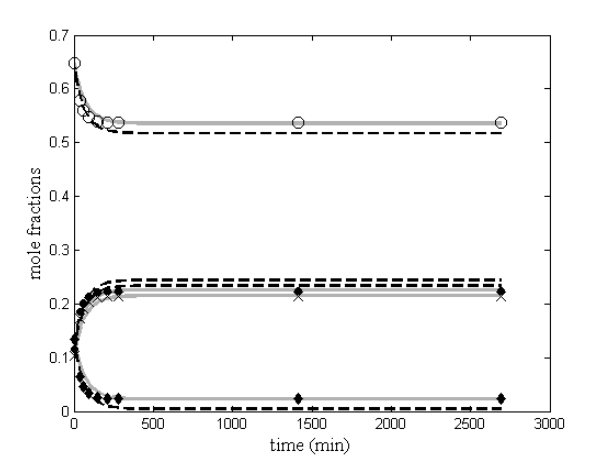


Figure 2.17: Experimental and predicted concentration profiles of *n*-butanol individual esterification in the presence of 1 wt.% Amberlyst 70: Run 8, $T = 120 \,^{\circ}\text{C}$ (——) – Mole - fraction based fits; (— —) – Activity based fits. (\bullet) – butyric acid; (\circ) –*n*-butanol; (\bullet)- *n*-butyric butyrate; (\times) –water

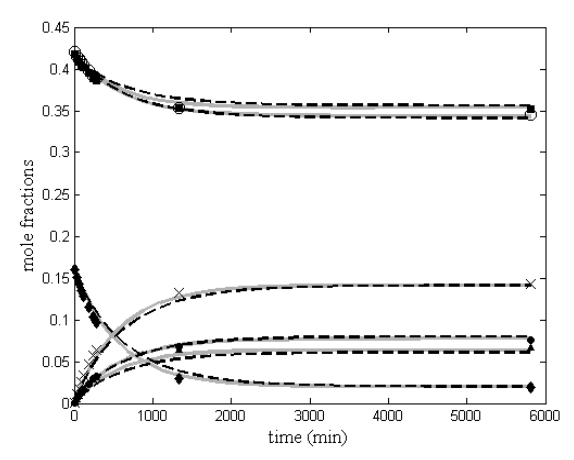


Figure 2.18: Experimental and predicted concentration profiles of mixed alcohol esterification in the presence of 1 wt.% Amberlyst 70. Run 10 (Ethanol:n-Butanol =1:1, T=80°C) (——) — mole fraction based fits; (— —) —activity based fits. (\blacklozenge) — butyric acid; (\blacksquare) —ethanol; (\blacktriangle) — ethyl butyrate; (\times) —water; (\circ) —n-butanol; (\blacklozenge) —n-butyl butyrate

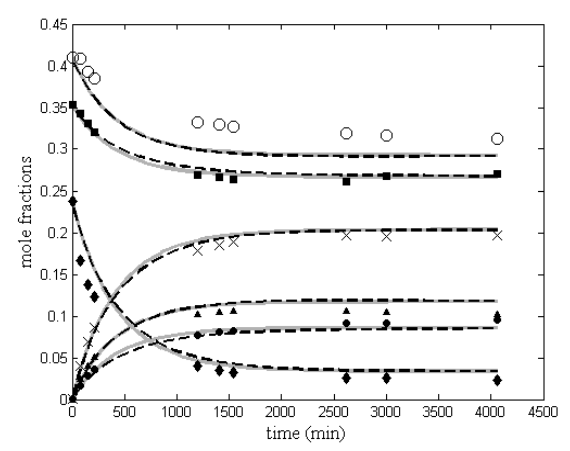


Figure 2.19: Experimental and predicted concentration profiles of mixed alcohol esterification in the presence of 0.5 wt.% Amberlyst 70. Run 12 (Ethanol:*n*-Butanol = 0.88:1, T=80°C)

(——) –mole fraction based fits; (— —) –activity based fits. (♦) – butyric acid; (■) –ethanol; (△) –ethyl butyrate; (×) –water; (∘) –*n*-butanol; (●)- *n*-butyl butyrate

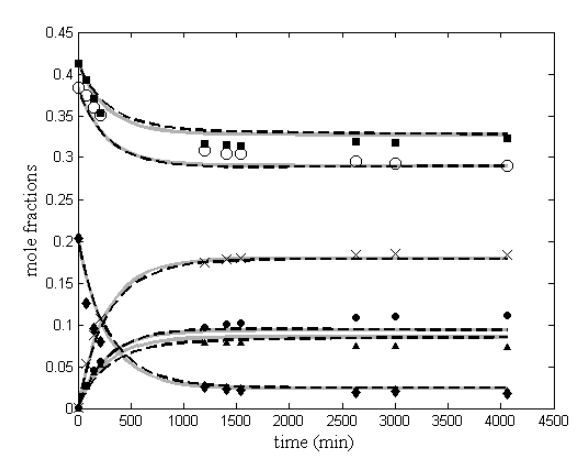


Figure 2.20: Experimental and predicted concentration profiles of mixed alcohol esterification in the presence of 0.75 wt.% Amberlyst 70. Run 14 (Ethanol:*n*-Butanol = 1.05:1, T=80°C)

(——) –mole fraction based fits; (— —) –activity based fits. (♦) – butyric acid; (■) –ethanol; (△) –ethyl butyrate; (×) –water; (○) –*n*-butanol; (●)- *n*-butyl butyrate

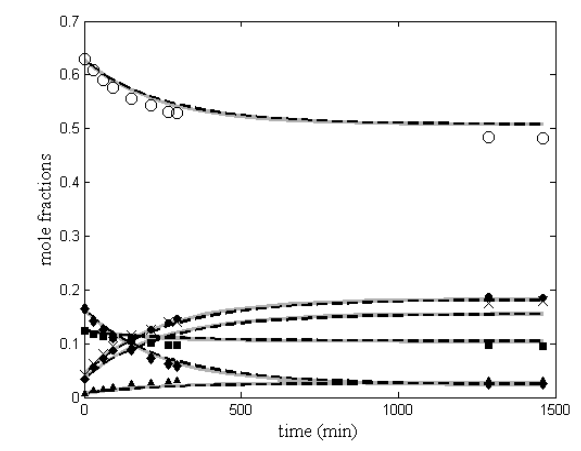


Figure 2.21: Experimental and predicted concentration profiles of mixed alcohol esterification in the presence of 1 wt.% Amberlyst 70. Run 15 (Ethanol:n-Butanol = 0.21:1, T=80°C) (——) —nole fraction based fits; (——) —activity based fits. (\blacklozenge) — butyric acid; (\blacksquare) —ethanol; (\blacktriangle) — ethyl butyrate; (\times) —water; (\circ) —n-butanol; (\blacklozenge)—n-butyl butyrate

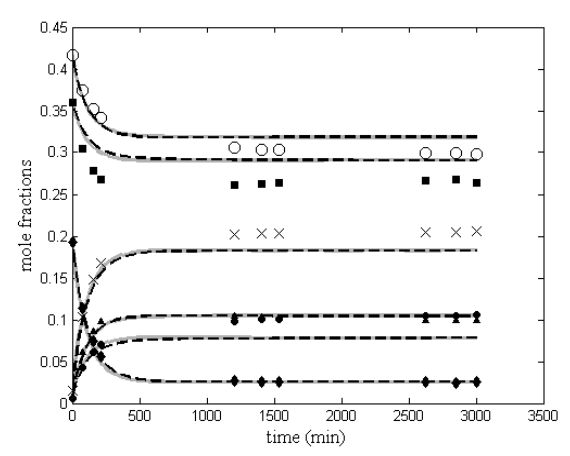


Figure 2.22: Experimental and predicted concentration profiles of mixed alcohol esterification in the presence of 2 wt.% Amberlyst 70. Run 16 (Ethanol:n-Butanol = 0.86:1, T=80°C) (——) — mole fraction based fits; (— —) —activity based fits. (\blacklozenge) — butyric acid; (\blacksquare) —ethanol; (\blacktriangle) — ethyl butyrate; (\times) —water; (\circ) —n-butanol; (\blacklozenge) —n-butyl butyrate

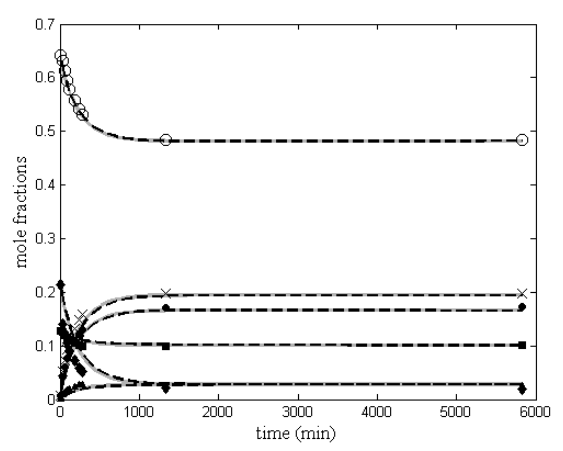


Figure 2.23: Experimental and predicted concentration profiles of mixed alcohol esterification in the presence of 1 wt.% Amberlyst 70. Run 17 (Ethanol:n-Butanol = 0.2:1, T=80°C) (——) – mole fraction based fits; (— —) –activity based fits. (\blacklozenge) – butyric acid; (\blacksquare) –ethanol; (\blacktriangle) – ethyl butyrate; (\times) –water; (\circ) –n-butanol; (\blacklozenge)- n-butyl butyrate

Appendix C: Reaction profiles of *p***-TSA catalyzed reactions**

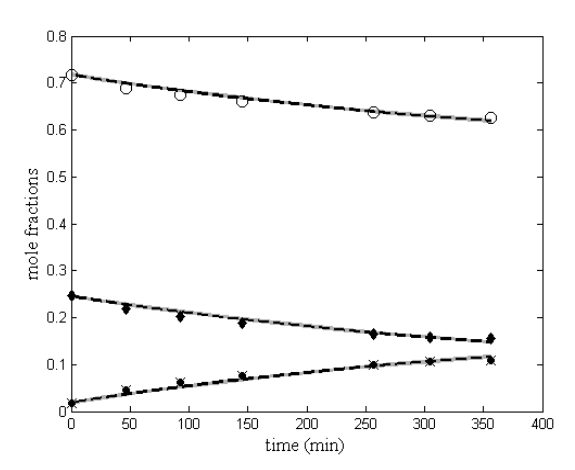


Figure 2.24: Experimental and predicted concentration profiles of ethanol individual esterification in the presence of 0.1 wt.% p-TSA: Run 18, T = 60 °C (——) – Mole -fraction based fits; (——) – Activity based fits. (\blacklozenge) – butyric acid; (\blacksquare) –ethanol; (\blacktriangle) –ethyl butyrate; (\times) –water

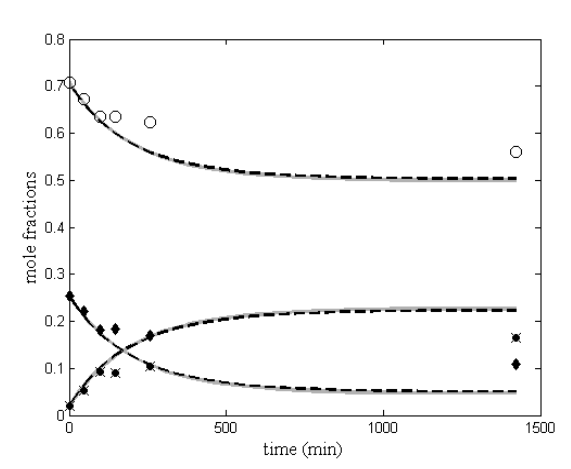


Figure 2.25: Experimental and predicted concentration profiles of ethanol individual esterification in the presence of 0.1 wt.% p-TSA: Run 19, T = 80 °C (——) – Mole -fraction based fits; (——) – Activity based fits. (\blacklozenge) – butyric acid; (\blacksquare) –ethanol; (\blacktriangle) –ethyl butyrate; (\times) –water

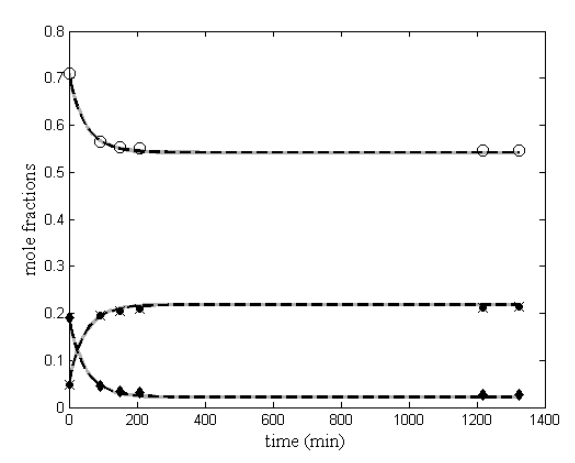


Figure 2.26: Experimental and predicted concentration profiles of ethanol individual esterification in the presence of 0.1 wt.% p-TSA: Run 21, T = 120 °C (——) – Mole -fraction based fits; (— —) – Activity based fits. (\blacklozenge) – butyric acid; (\blacksquare) –ethanol; (\blacktriangle) –ethyl butyrate; (\times) –water

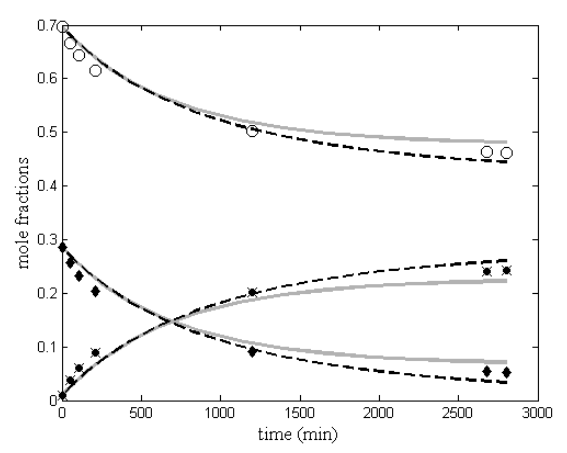


Figure 2.27: Experimental and predicted concentration profiles of n-butanol individual esterification in the presence of 0.1 wt.% p-TSA: Run 22, T=60 °C (——) — Mole -fraction based fits; (— —) — Activity based fits. (\bullet) — butyric acid; (\circ) —n-butanol; (\bullet) —n-butyl butyrate; (\times) —water

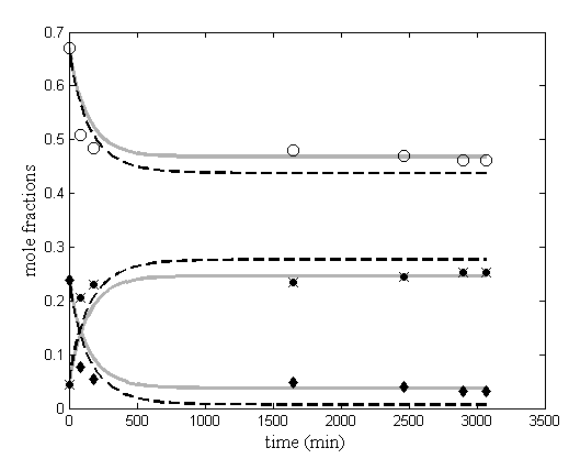


Figure 2.28: Experimental and predicted concentration profiles of *n*-butanol individual esterification in the presence of 0.1 wt.% *p*-TSA: Run 24, T=100 °C (——) – Mole -fraction based fits; (— —) – Activity based fits. (\bullet) – butyric acid; (\circ) –*n*-butanol; (\bullet)- *n*-butyl butyrate; (\times) –water

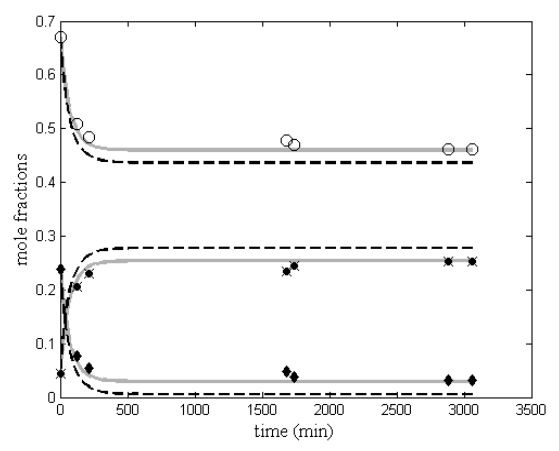


Figure 2.29: Experimental and predicted concentration profiles of *n*-butanol individual esterification in the presence of 0.1 wt.% *p*-TSA: Run 25, T=120 °C (——) – Mole -fraction based fits; (— —) – Activity based fits. (\bullet) – butyric acid; (\circ) –*n*-butanol; (\bullet)- *n*-butyl butyrate; (\times) –water

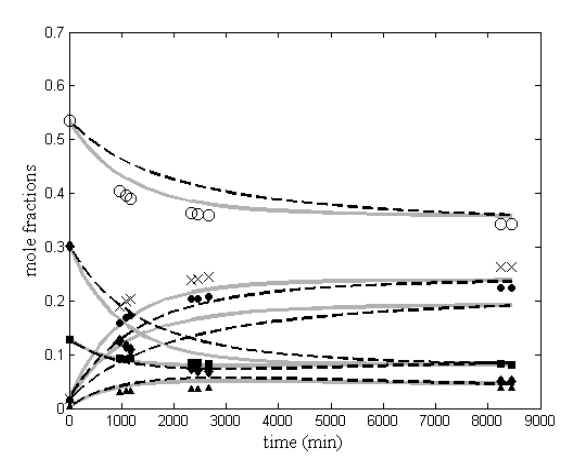


Figure 2.30: Experimental and predicted concentration profiles of mixed alcohol esterification in the presence of 0.1 wt.% *p*-TSA. Run 26 (Ethanol:*n*-Butanol = 0.22:1, T=60°C) (——) – mole fraction based fits; (— —) –activity based fits. (\blacklozenge) – butyric acid; (\blacksquare) –ethanol; (\blacktriangle) – ethyl butyrate; (\times) –water; (\circ) –*n*-butanol; (\blacklozenge) – *n*-butyl butyrate

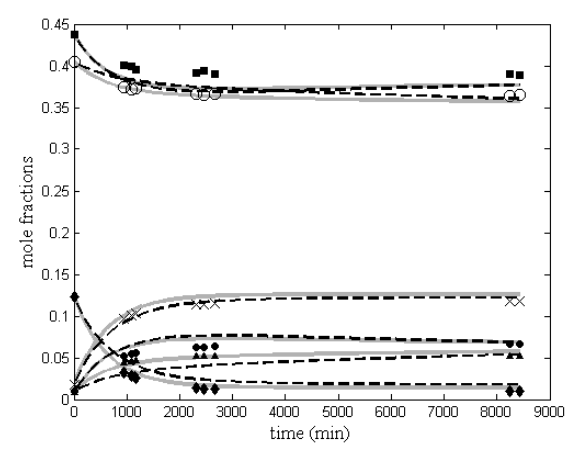


Figure 2.31: Experimental and predicted concentration profiles of mixed alcohol esterification in the presence of 0.1 wt.% p-TSA. Run 27 (Ethanol:n-Butanol = 1:1, T=60°C) (——) —mole fraction based fits; (— —) —activity based fits. (\blacklozenge) — butyric acid; (\blacksquare) —ethanol; (\blacktriangle) —ethyl butyrate; (\times) —water; (\circ) —n-butanol; (\blacklozenge) —n-butyl butyrate

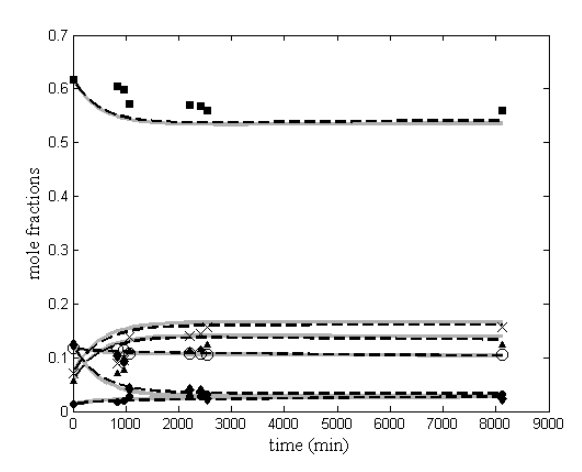


Figure 2.32: Experimental and predicted concentration profiles of mixed alcohol esterification in the presence of 0.1 wt.% p-TSA. Run 28 (Ethanol:n-Butanol = 5:1, T=60°C) (——) —mole fraction based fits; (— —) —activity based fits. (\blacklozenge) — butyric acid; (\blacksquare) —ethanol; (\blacktriangle) —ethyl butyrate; (\times) —water; (\circ) —n-butanol; (\blacklozenge) —n-butyl butyrate

REFERENCES

REFERENCES

- (1) Iwasaki, T.; Maegawa, Y.; Ohshima, T.; Mashima, K. In *Kirk-Othmer Encyclopedia of Chemical Technology*; John Wiley & Sons, Inc., 2000.
- (2) Ueda, W.; Ohshida, T.; Kuwabara, T.; Morikawa, Y. Catal. Lett. 1992, 12, 97–104.
- (3) Carlini, C.; Girolamo, M. D.; Macinai, A.; Marchionna, M.; Noviello, M.; Galletti, A. M. R.; Sbrana, G. J. Mol. Catal. Chem. 2003, 204–205, 721–728.
- (4) Carlini, C.; Macinai, A.; Raspolli Galletti, A. M.; Sbrana, G. J. Mol. Catal. Chem. 2004, 212, 65–70.
- (5) Mazanec, T. J. J. Catal. **1986**, 98, 115–125.
- (6) Mills, G. A. Fuel **1994**, 73, 1243–1279.
- (7) Xiang, M.; Li, D.; Xiao, H.; Zhang, J.; Qi, H.; Li, W.; Zhong, B.; Sun, Y. Fuel **2008**, 87, 599–603.
- (8) Dry, M. E. Catal. Today **2002**, 71, 227–241.
- (9) Peralta-Yahya, P. P.; Keasling, J. D. *Biotechnol. J.* **2010**, *5*, 147–162.
- (10) Schulz, E.; Bauer, H.; Merscher, K. D. Coupled production of two esters. US7115773 B2, October 3, 2006.
- (11) Thurman, L. R.; Harris, J. B.; Mcatee, M. R. Coproduction of low molecular weight esters of alkanols. EP0260572 A1, March 23, 1988.
- (12) Warner, R. J.; Murphy, C. D.; Grajales, G. A. R.; Santiago, F. J. S.; Solorzano, F. A.; Torres, J. A. Process for the simultaneous coproduction and purification of ethyl acetate and isopropyl acetate. US6765110 B2, July 20, 2004.
- (13) Acker, P. E. van; Mathieu, O.; Milner, R. J.; Pacynko, W. F. Ester co-production. US6093845 A, July 25, 2000.
- (14) Harmsen, G. J. Chem. Eng. Process. Process Intensif. 2007, 46, 774–780.
- (15) Stankiewicz, A. Chem. Eng. Process. Process Intensif. 2003, 42, 137–144.
- (16) Lee, H.-Y.; Yen, L.-T.; Chien, I.-L.; Huang, H.-P. *Ind. Eng. Chem. Res.* **2009**, *48*, 7186–7204.
- (17) Zhang, C.; Yang, H.; Yang, F.; Ma, Y. Curr. Microbiol. **2009**, *59*, 656–663.
- (18) Armstrong, D. W.; Yamazaki, H. *Trends Biotechnol.* **1986**, *4*, 264–268.
- (19) Ju, I. B.; Lim, H.-W.; Jeon, W.; Suh, D. J.; Park, M.-J.; Suh, Y.-W. *Chem. Eng. J.* **2011**, *168*, 293–302.

- (20) Amberlyst 70 product data sheet, 2005.
- (21) Weisz, P. B.; Hicks, J. S. Chem. Eng. Sci. 1995, 50, 3951–3958.
- (22) Wilke, C. R.; Chang, P. AIChE J. 1955, 1, 264–270.
- (23) Hansen, H. K.; Rasmussen, P.; Fredenslund, A.; Schiller, M.; Gmehling, J. *Ind. Eng. Chem. Res.* **1991**, *30*, 2352–2355.
- (24) Eckert, C. A.; Hsieh, C. K.; McCabe, J. R. AIChE J. 1974, 20, 20–36.
- (25) Eckert, C. A. Ind. Eng. Chem. 1967, 59, 20–32.
- (26) Pappu, V. K. S.; Kanyi, V.; Santhanakrishnan, A.; Lira, C. T.; Miller, D. J. *Bioresour. Technol.* **2013**, *130*, 793–797.
- (27) Orjuela, A.; Yanez, A. J.; Santhanakrishnan, A.; Lira, C. T.; Miller, D. J. *Chem. Eng. J.* **2012**, *188*, 98–107.

3 Unification of esterification rates using non-ideal concentration model

3.1 Abstract

A number of liquid phase esterification systems from the literature with different carboxylic acids, alcohols and acid catalysts (homogeneous and heterogeneous) have been considered in the framework of a non-ideal concentration model to ascertain if an estimate of most esterification reaction rates is possible from the data already available. Trends observed from comparing the non-ideal concentration model-based rate constants of five different types of reaction families are reported. Different primary alcohols of varying carbon chain lengths were found to have similar rate constants. The same was observed for different primary carboxylic acids. For branched alcohols and carboxylic acids, the rates were lower than the rates of their primary counterparts, but within a level of branching, a group of reactants have comparable rate constants. Rate constants of reactions involving the same reactants but different acid catalysts, homogeneous and heterogeneous, were also examined. It was found that the ratios of the rate constants of reactions of two different catalysts is the same for multiple reaction sets involving the same reactants. This could be an effective test for similarity of mechanisms between two catalysts and offers the possibility of estimating the rate of one catalyst provided the rate of another and properties of both. The Taft equation is related to non-ideal concentration based rates.

3.2 Introduction

There is a preponderance of literature on acid catalyzed esterification reactions. As an increasing number of esters are becoming commercially important chemicals¹, the possibility of manufacturing multiple esters with product distributions depending on market needs is being

explored.^{2–7} Carboxylic acids and alcohols form a significant portion of biomass derived esters for use as biofuel additives, green solvents, and food flavoring agents. There is therefore a need to gain a deeper understanding of the factors that affect the rate of reaction to facilitate flexible process design. Multiple attempts have been made to determine commonalities in rates of similar reaction systems, whether from investigating structure-reactivity relationships^{8–18} or by examining the surface reaction mechanism involved¹⁹.

Conventionally, kinetics of heterogeneously catalyzed esterification reactions are reported as either concentration or activity based models, sometimes with modifications for local sorption equilibria at the surface of the catalyst due to swelling, ^{20,21} and for adsorption and desorption at the surface, such as Eley-Rideal and Langmuir Hinshelwood mechanisms. ²² Activity based models are usually found to predict kinetic behavior as well as or better than purely concentration based models, as they account for deviations from ideality of the reaction mixture. Activity based rate expressions for pseudo-homogeneous models typically take the form:

$$r_{ester} = W_{CAT} k_{0,AC} \exp\left(-\frac{E_a}{RT}\right) \left[a_{Acid} a_{Alc} - \frac{a_{ester} a_W}{K_a}\right]$$
(3.1)

Activities here are calculated based on mole fractions and activity coefficients estimated by a suitable model ($a_i = x_i \gamma_i$). In designing processes where similar initial compositions will be used as those used in the kinetic study, such as when reactant ratios are limited to those involving a large excess of alcohol due to solubility limitations, this expression has worked well.^{23,24} This is because the total solution density does not vary appreciably and a composite rate constant may be used without error.

Ideally, kinetic parameters reported should work for any composition, temperature and catalyst concentration. To overcome the limitation of kinetic rate expressions such as that described in Eq. 3.1, we use the concept of "non-ideal" concentration (Eq. 3.2 below) that accounts for both non-ideality and variations in initial molar concentrations for a wide range of initial compositions of its reactants. The non-ideal concentration model reflects the reduced number of moles per volume of higher molecular weight reactants for the same molar reaction mixture composition, and enables us to make some observations on structure-reactivity relationships as well as on reaction mechanisms. The inclusion of solution density makes the rate dependent on the absolute concentration of the alcoholic and carboxylic species (-OH and -COOH) in the solution. The need for this became more noticeable in a previous work conducted to study the behavior of two alcohols, ethanol and butanol, reacting simultaneously with butyric acid, where it became important to also distinguish between cases where the ratio of alcohol to acid was the same but the ratio of the individual alcohols was different (2 moles of ethanol and 1 mole of butanol vs 1 mole of ethanol and 2 moles of butanol). With the non-ideal concentration model, both ethanol and nbutanol were found to have the same rate constant within experimental uncertainty. This has prompted a more expansive study to look at other esterification systems in the literature.

Rather than deal with a rigorous derivation of activities from molarities instead of mole fractions, which would involve calculation of excess volume dependency on composition, one can still empirically represent varying initial effective functional group concentrations by an expression of the form in Eq. 3.2:

$$r_{ester} = w_{CAT} C_T^2 k_{0,NIC} \exp\left(-\frac{E_a}{RT}\right) \left[x_{Acid} \gamma_{Acid} x_{Alc} \gamma_{Alc} - \frac{x_{ester} \gamma_{ester} x_W \gamma_W}{K_a}\right]$$
(3.2)

It should be noted that, fortuitously, this empirical modification works for reactions in which the total number of moles on the reactant and product sides is the same (in this case, two). If this were not the case, it would not be possible to factorize out C_T , leading to less elegant expressions, with the value of C_T changing through the course of the experiment. Equilibrium constants would have to be defined in terms of effective molarities. Nevertheless, this expression accounts for both non ideality and variations in concentrations, and has been used before. Catalyst weight fraction w_{CAT} is converted to molar hydronium concentration [H⁺] to enable comparisons between different reactions.

3.3 Calculation procedure

A total of 86 esterification systems from our laboratories and from the literature consisting of various alcohols, acids and catalysts have been considered. The vast majority of the kinetic studies surveyed did not consider changes in (actual species or functional group concentrations), leading to reported values being a composite of the reactant ratios used in each individual study. Calculations of non-ideal rate constants were therefore done from initial stages of reaction. A reference experiment at 60°C was chosen for each reaction system. Initial rates were calculated based on a first or second order fit of the first several data points extrapolated to time=0 from available information (graphs of conversion or reaction profile data). Confidence intervals were calculated based on the fits using MATLAB R2013a and are reported (Table 3.1 in Section 3.4). NRTL-HOC was used to find the activity coefficients of the acid and alcohol where binary interaction parameters were available from literature (accessed via ASPEN v8.7); in the absence of binary interaction parameters, UNIFAC was used to estimate activity coefficients. Activity coefficients for both models were calculated using a MATLAB program developed by Dr. Carl T.

Lira of the department of Chemical Engineering and Materials Science at Michigan State University. The method used for calculating activity coefficients is reported (Table 3.1 in Section 3.4). NRTL-HOC is a modification of the conventional NRTL model that is recommended for systems that include carboxylic acids, and accounts for dimerization of carboxylic acids in the vapor phase. A comparison of activity coefficient values calculated by NRTL-HOC and UNIFAC at 60 °C for several reaction systems is reported (Table 3.x). It should be noted that only reaction systems which have data available for both NRTL-HOC and UNIFAC are included. The difference in activity coefficients of alcohols between the two models ranges from 1% to 15%. The average difference for propanol is much higher than for ethanol and butanol. In the case of carboxylic acids, the average difference between the two models varies by 8-10%. More data is required to ascertain the suitability of UNIFAC for carboxylic acids with non-linear structures.

Table 3.1: Comparison of activity coefficient values estimated by NRTL-HOC and UNIFAC

			NRTL-HOC activity			
Reaction system:		coefficients		UNIFAC		
				Carboxylic		Carboxylic
Alcohol	Carboxylic acid	Catalyst	Alcohol	acid	Alcohol	acid
			Yalcohol	Yacid	Yalcohol	Yacid
Methanol	Butyric Acid	Amberlyst 70	0.9902	1.0193	0.9890	1.0980
Methanol	Butyric Acid	Amberlyst 15	0.9902	1.0193	0.9890	1.0980
Methanol	Butyric Acid	Amberlyst 36	0.9902	1.0193	0.9890	1.0980
Methanol	Acetic Acid	Amberlyst 15	0.9524	0.9894	0.9561	0.9506
Methanol	Acetic Acid	HI	0.9621	0.9780	0.9680	0.9374
Butanol	Acetic Acid	Smopex-101	0.9805	1.0233	0.9888	1.0302
Ethanol	Acetic Acid	Smopex-101	0.9944	1.0054	0.9348	0.9509
Methanol	Acetic Acid	Smopex-101	0.9530	0.9888	0.9568	0.9499
Ethanol	Acetic Acid	Amberlyst 15	0.9944	1.0054	0.9348	0.9509

Table 3.1 (Table 3.1 (cont'd)					
Methanol	Propionic Acid	Smopex-101	0.9652	1.0087	0.9074	1.0340
Ethanol	Propionic Acid	Smopex-101	0.9970	0.9977	0.9956	1.0060
Propanol	Acetic Acid	Smopex-101	0.9867	1.0127	0.9373	0.9524
Propanol	Propionic Acid	Smopex-101	0.9833	0.9933	0.8317	0.8895
Methanol	Propionic Acid	Dowex 50Wx8- 400	0.9652	1.0087	0.9074	1.0340
Ethanol	Propionic Acid	Dowex 50Wx8- 400	0.9970	0.9977	0.9947	0.9962
Propanol	Propionic Acid	Dowex 50Wx8- 400	0.9833	0.9933	0.8317	0.8895
Methanol	Acetic Acid	SAC-13	0.9757	0.9562	0.9816	0.9166
Methanol	Propionic Acid	SAC-13	0.9783	0.9890	0.9538	0.9632
Methanol	Butyric Acid	SAC-13	0.9873	1.0270	0.9833	1.1137
Methanol	Acetic Acid	sulfuric Acid	0.9757	0.9562	0.9816	0.9166
Methanol	Propionic Acid	sulfuric Acid	0.9783	0.9890	0.9538	0.9632
Methanol	Butyric Acid	sulfuric Acid	0.9873	1.0270	0.9833	1.1137
Methanol	Acetic Acid	HCl	0.9999	0.8480	0.9999	0.8431
Methanol	Propionic Acid	HCl	0.9998	0.8792	0.9998	0.7734
Methanol	Butyric Acid	HCl	0.9998	0.9448	0.9999	1.0197
Butanol	Acetic Acid	Amberlyst 15	0.9805	1.0233	0.9888	1.0302
Methanol	Propionic Acid	Amberlyst 15	0.9652	1.0087	0.9074	1.0340
Methanol	Propionic Acid	Smopex-101	0.9652	1.0087	0.9074	1.0340

Densities and van der Waal volumes of compounds were obtained from DIPPR. A sample calculation is shown for the system 2-propanol-acetic acid in presence of Amberlyst 36 in Appendix D.¹⁹

3.4 Results

The results of non-ideal concentration rate analysis for several reactions computed from literature data are reported (Table 3.2). Families of reactions where one component was varied

while keeping the other two constant (alcohol, carboxylic acid, acid catalyst) were used to study the trends of rate constants to shed light on structure-reactivity relationships after accounting for differences in solution density and non-ideal behavior.

Table 3.2: Summary of reactions and calculated non-ideal concentration-based rate constants at 60 °C

	constants at 60 °C				
No.	Alcohol	Carboxylic acid	Catalyst	Rate constant k_{NIC} (m6 soln/(kmole soln) · (kmole $H+)\cdot s$)	Ref.
1	Methanol	Acetic Acid	Amberlyst 15	2.74±1.9E-04	20
2	2-Butanol	Butyric Acid	Amberlyst 70	6.09±0.20E-05	29
3	2-Butanol	Propionic Acid	Dowex 50W-4	7.72±1.10E-05	34
4	2-Butanol	Propionic Acid	Smopex-101	2.69±0.32E-05	34
5	2-Ethyl Hexanol	Butyric Acid	Amberlyst 70	1.32±0.16E-04	29
6	2-Propanol	Acetic Acid	Amberlite IRA 120	6.09±0.60E-05	19
7	2-Propanol	Acetic Acid	Amberlyst 15	6.22±0.20E-05	19
8	2-Propanol	Acetic Acid	Dowex 50Wx8-400	1.36±0.80E-04	19
9	2-Propanol	Propionic Acid	Dowex 50W-4	1.00±0.09E-04	34
10	2-Propanol	Acetic Acid	Smopex-101	5.62±0.20E-05	33
11	2-Propanol	Pentanoic Acid	Smopex-101	1.74±0.33E-05	33
12	2-Propanol	Propionic Acid	Smopex-101	2.45±0.31E-05	33
13	4-Heptanol	Butyric Acid	Amberlyst 70	1.09±0.51E-04	29
14	4-Heptanol	Butyric Acid	p-TSA	5.88±2.79E-04	29
15	Amyl Alcohol	Acetic Acid	Amberlite IRA 120	1.41±0.07E-05	32
16	Amyl Alcohol	Acetic Acid	Amberlyst 15	1.86±0.10E-05	32
17	Amyl Alcohol	Acetic Acid	Amberlyst 36	1.71±0.04E-05	32
18	Benzyl Alcohol	Acetic Acid	Amberlyst 15	7.57±0.81E-05	38
19	Butanol	Butyric Acid	Amberlyst 15	5.59±0.43E-05	29
20	Butanol	Butyric Acid	Amberlyst 36	3.74±0.62E-05	29
21	Butanol	Butyric Acid	Amberlyst 70	1.80±0.16E-04	29
22	Butanol	Butyric Acid	Amberlyst 70	3.1±0.30E-04	25
23	Butanol	Propionic Acid	Dowex 50W-4	3.26±1.40E-04	34
24	Butanol	Butyric Acid	p-TSA	1.9±0.20E-03	25
25	Butanol	Acetic Acid	Smopex-101	1.08±0.28E-04	33
26	Butanol	Pentanoic Acid	Smopex-101	5.74±0.81E-05	33

Tabl	e 3.2 (cont'd)				
27	Butanol	Propionic Acid	Smopex-101	7.70±6.40E-05	33
28	Ethanol	Acetic Acid	Amberlyst 15	9.44±0.26E-05	21
29	Ethanol	Butyric Acid	Amberlyst 15	6.02±0.32E-05	29
30	Ethanol	Butyric Acid	Amberlyst 36	5.87±0.40E-05	29
31	Ethanol	Butyric Acid	Amberlyst 70	1.73±0.44E-04	29
32	Ethanol	Butyric Acid	Amberlyst 70	2.60±3.50E-04	25
33	Ethanol	Propionic Acid	Dowex 50W-4	2.96±1.40E-04	34
34	Ethanol	Butyric Acid	p-TSA	2.14±0.24E-04	25
35	Ethanol	Acetic Acid	Smopex-101	3.88±0.45E-04	33
36	Ethanol	Pentanoic Acid	Smopex-101	8.21±2.80E-05	33
37	Ethanol	Propionic Acid	Smopex-101	1.65±0.77E-04	33
38	Ethylene Glycol	Acetic Acid	Amberlyst 36	3.02±0.07E-05	39
39	Ethylene Glycol Mono Acetate	Acetic Acid	Amberlyst 36	6.58±0.41E-04	39
40	Heptanol	Butyric Acid	Amberlyst 70	9.76±14.8E-05	29
41	Heptanol	Butyric Acid	p-TSA	9.61±6.95E-04	29
42	Isobutanol	Butyric Acid	Amberlyst 15	5.81±0.22E-05	29
43	Isobutanol	Butyric Acid	Amberlyst 70	9.66±0.39E-05	29
44	Isobutanol	Propionic Acid	Dowex 50W-4	1.12±0.31E-04	22
45	Methanol	Butyric Acid	Amberlyst 15	2.27±0.68E-04	29
46	Methanol	Butyric Acid	Amberlyst 36	1.49±0.45E-04	29
47	Methanol	Butyric Acid	Amberlyst 70	4.29±0.75E-04	29
48	Methanol	Propionic Acid	Dowex 50W-4	4.90±0.38E-04	34
49	Methanol	Formic Acid	HCl	6.70±0.11E-02	30
50	Methanol	Acetic Acid	HCl	1.70±0.03E-02	30
51	Methanol	Propionic Acid	HCl	1.56±0.04E-02	30
52	Methanol	Butyric Acid	HCl	6.82±0.32E-03	30
53	Methanol	Pentanoic Acid	HCl	6.95±0.16E-03	30
54	Methanol	Octanoic Acid	HCl	7.12±0.19E-03	30
55	Methanol	Nonanoic Acid	HCl	7.19±0.19E-03	30
56	Methanol	Lauric Acid	HCl	7.53±0.19E-03	30
57	Methanol	Trimethyl Acetic Acid	HCl	6.74±1.12E-04	31
58	Methanol	Diethyl Acetic Acid	HCl	2.04±0.95E-04	31
59	Methanol	Dipropyl Acetic Acid	HCl	1.91±0.10E-04	31
60	Methanol	Dibutyl Acetic Acid	HCl	1.82±0.39E-04	31
61	Methanol	Diisobutyl Acetic Acid	HCl	9.01±2.38E-05	31

Tabl	e 3.2 (cont'd)				
62	Methanol	Betamethyl Valeric Acid	HCl	1.78±1.07E-03	31
63	Methanol	Acetic Acid	SAC-13	2.83±0.17E-04	35
64	Methanol	Propionic Acid	SAC-13	1.58±0.09E-04	35
65	Methanol	Butyric Acid	SAC-13	8.87±0.53E-05	35
66	Methanol	Hexanoic Acid	SAC-13	8.69±0.52E-05	35
67	Methanol	Caprylic Acid	SAC-13	6.51±0.41E-05	35
68	Methanol	Acetic Acid	Smopex-101	8.58±0.13E-04	33
69	Methanol	Pentanoic Acid	Smopex-101	1.49±0.17E-04	33
70	Methanol	Propionic Acid	Smopex-101	4.50±2.60E-04	33
71	Methanol	Acetic Acid	sulfuric acid	1.92±0.09E-02	35
72	Methanol	Propionic Acid	sulfuric acid	8.95±0.05E-03	35
73	Methanol	Butyric Acid	sulfuric acid	5.10±0.30E-03	35
74	Methanol	Caprylic Acid	sulfuric acid	8.33±0.41E-03	35
75	Methanol	Hexanoic Acid	sulfuric acid	6.95±0.49E-03	35
76	Octanol	Butyric Acid	Amberlyst 70	9.00±10.8E-05	29
77	Amyl Alcohol	Propionic Acid	Dowex 50Wx8-400	2.88±0.17E-04	34
78	Propanol	Butyric Acid	Amberlyst 15	5.69±0.22E-05	29
79	Propanol	Butyric Acid	Amberlyst 36	4.05±0.88E-05	29
80	Propanol	Butyric Acid	Amberlyst 70	1.39±0.08E-04	29
81	Propanol	Propionic Acid	Dowex 50W-4	3.32±1.60E-04	40
82	Propanol	Acetic Acid	Smopex-101	1.32±0.65E-04	33
83	Propanol	Pentanoic Acid	Smopex-101	7.53±0.52E-05	33
84	Propanol	Propionic Acid	Smopex-101	9.64±2.40E-05	33
85	Propylene Glycol	Acetic Acid	p-TSA	2.70±0.19E-3	41
86	Propylene Glycol monoacetate	Acetic Acid	p-TSA	2.40±0.21E-3	41

3.4.1 Rate constants for straight chain alcohols with common acid and catalyst

With the exception of methanol, varying the length of carbon chain for ethanol and higher alcohols does not change the rate constant significantly (Figure 3.1,Figure 3.2). As higher alcohols such as heptanol and octanol are used at low alcohol:acid ratios (~3:1), the rate constant slightly drops due to phase separation of the heavier esters formed from water.²⁹ The rate constant of methanol for both homogeneous and heterogeneous catalysis is considerably higher (2-2.5 times)

than the rate constants of C2-C8 linear primary alcohols, as might be expected because of the lack of steric hindrance from alkyl groups.

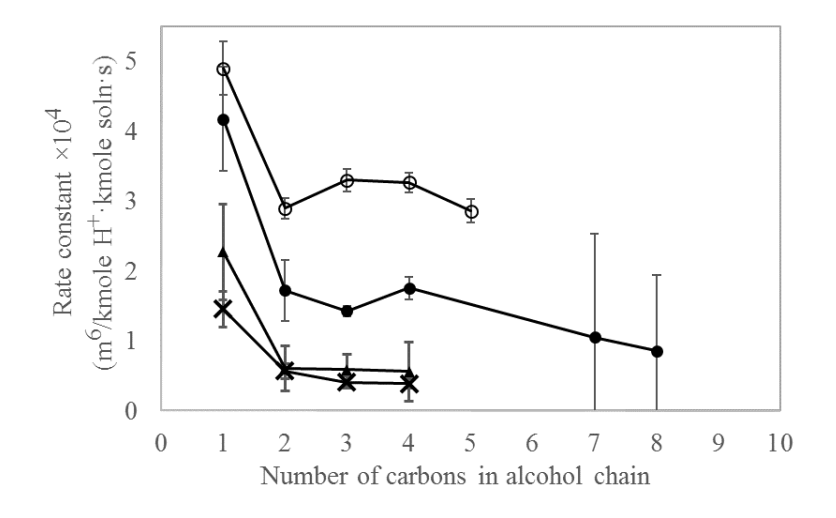


Figure 3.1: Non ideal rate constants at 60 °C for reaction families with differing number of carbons in primary alcohol chain with common carboxylic acid and catalyst. (●)-Butyric acid, Amberlyst 70 (▲)-Butyric acid, Amberlyst 15 (×)- Butyric acid, Amberlyst 36 (○)-Propionic acid, Dowex W50×4

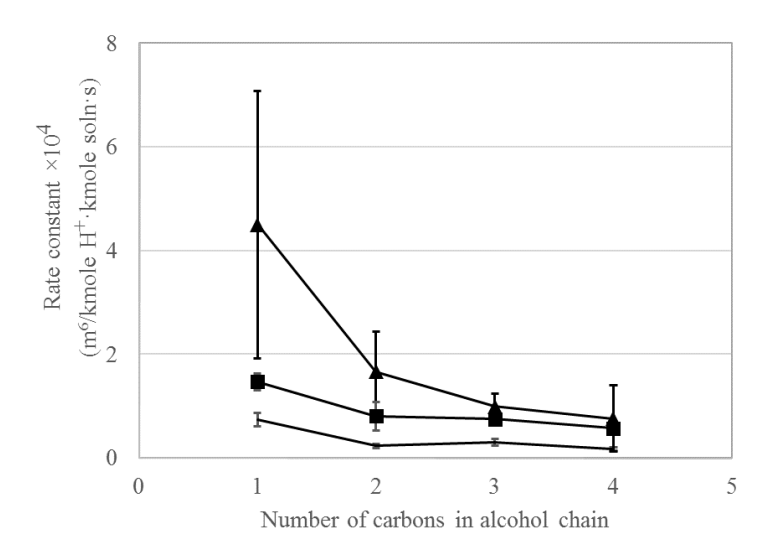


Figure 3.2: Non ideal rate constants at 60 °C for families of reactions with differing number of carbons in primary alcohol chain with common carboxylic acid and catalyst. (●)-Acetic acid, Smopex-101 (▲)-Propionic acid, Smopex-101 (■)-Pentanoic acid, Smopex-101

3.4.2 Rate constants for secondary alcohols with common acid and catalyst

Branched alcohols react slower than their primary isomers as expected due to increased steric hindrance (Figure 3.3). Within a level of branching the rates are similar, as seen with rates of acylation of 2-propanol and 2-butanol with propionic acid in presence of Dowex Wx4-500, and propionic acid with Smopex-101. Smopex-101 is a fibrous polymer supported sulfonic acid catalyst with a site concentration of ~3.2 equivalents per gram conventionally used as a metal scavenger. Isobutanol is not as sterically hindered as 2-butanol and has a higher rate constant, as is the case for 2-ethylhexanol and 4-heptanol.

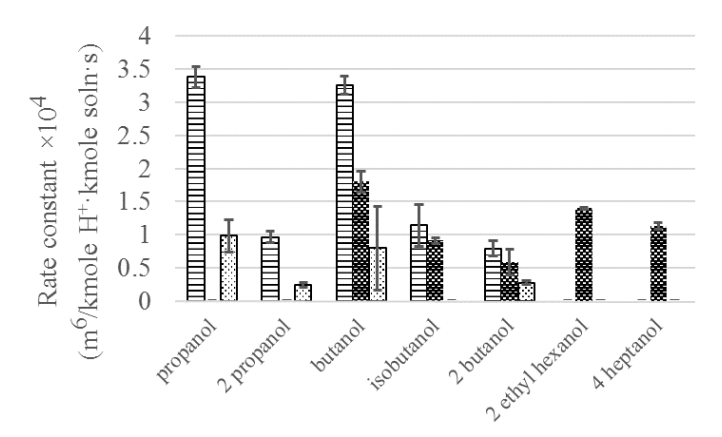


Figure 3.3: Non ideal rate constants at 60 °C for reaction families with branched alcohols with common carboxylic acid and catalyst. (

—)- Propionic acid, Dowex W4 (

—)-Butyric acid, Amberlyst 70 (
—)- Propionic acid, Smopex-101

3.4.3 Different primary carboxylic acids esterified by common alcohol and catalyst

Non ideal rate constants for different primary acids reach a plateau for acids higher than propionic acid for both homogeneous and heterogeneous acids (Figure 3.4, Figure 3.5). Formic acid reacts over 10 times faster than acetic or propionic acid with methanol (rate constant value of 0.19 (units), not shown in Figure 3.5)³⁰. In the presence of a strong mineral acid, the dissociation

of formic acid is greatly suppressed, so the increase in rate may be attributed to reactivity differences and not to significant autocatalysis.

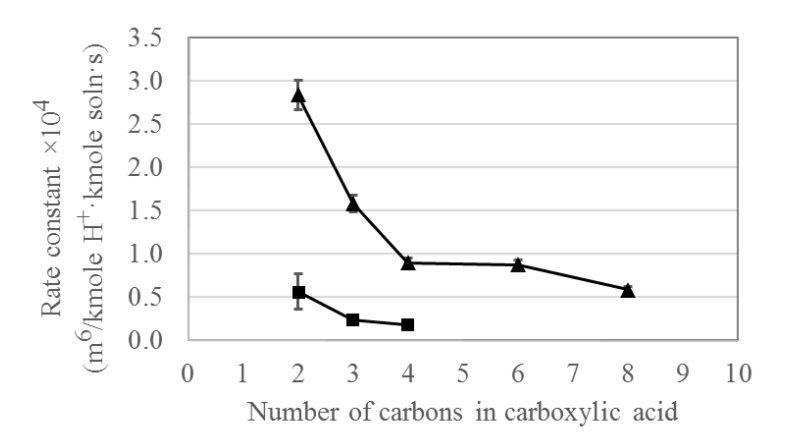


Figure 3.4: Non ideal rate constants at 60 °C for reaction families with differing number of carbons in primary carboxylic acid chain with common alcohol and catalyst. (▲)-Methanol, SAC-13, (■)-2-Propanol, Smopex-101

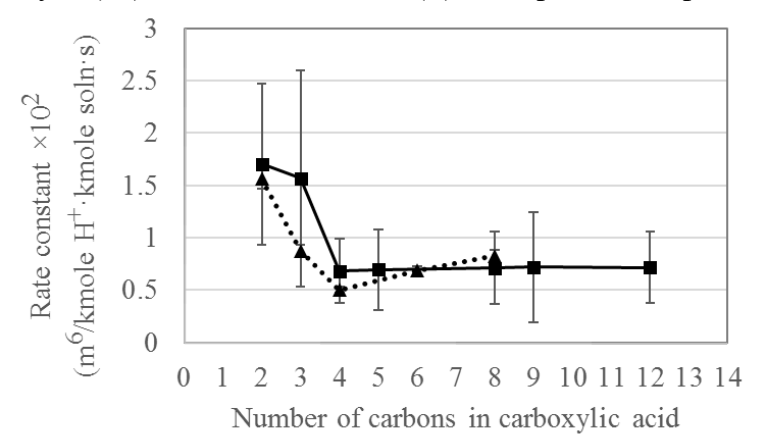


Figure 3.5: Non ideal rate constants at 60 °C for reaction families with differing number of carbons in primary carboxylic acid chain with common alcohol and catalyst. (▲)-Methanol, Sulfuric acid (■)- Methanol, Hydrochloric acid

3.4.4 Different branched carboxylic acids, same alcohol, same catalyst

Non ideal rate constants for carboxylic acids increase with the increase in branching. However, increasing the length of those branched chains does not have a significant steric effect as seen in the rate constants of diethyl acetic acid, dipropyl acetic acid and dibutyl acetic acid (Figure 3.6).³¹

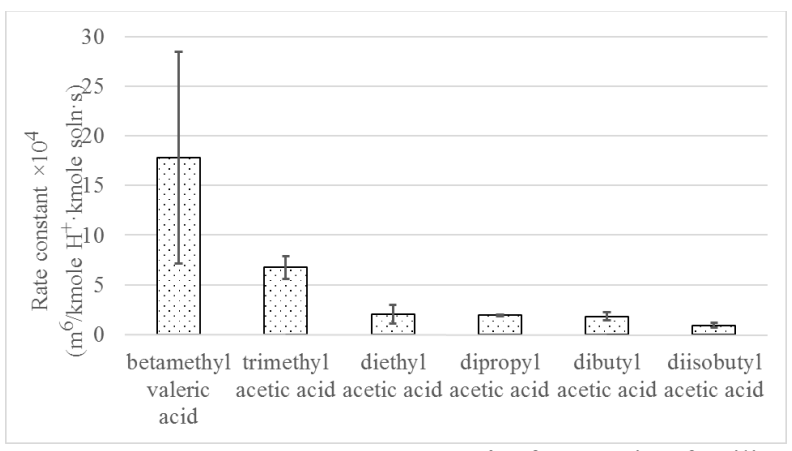


Figure 3.6: Non ideal rate constants at 60 °C for reaction families with differing number of carbons in branched carboxylic acid chain with methanol and hydrochloric acid catalyst

Table 3.3: Structures of branched carboxylic acids in Figure 3.6.

Table 3.3: Structures of branched carboxylic acids in Figure 3.6.			
beta-Methylvaleric acid	ОН		
Trimethylacetic acid	ОН		
Diethyl acetic acid	ОН		
Dipropyl acetic acid	ОН		
Dibutyl acetic acid	ОН		
Diisobutyl acetic acid	ОН		

3.4.5 Ratio of rate constants of the same reaction with different catalysts

Several examples of similar reactions carried out with different catalysts (homogeneous and heterogeneous) show that the ratio of turn over numbers (TON) for two catalysts is the same irrespective of the reaction. For example, methanol esterification of various acids shows the same turn-over ratio for sulfuric acid and SAC-13(Table 3.4).

Table 3.4: Ratio of rate constants at 60 °C based on non-ideal concentration model

	IIIO		1	
Alcohol	Carboxylic acid	Ratio of rate constants of two catalysts for different alcohols and carboxylic acids at 60 °C based on non-ideal concentration model	Ref.	
	Amberlyst 36/	/Amberlyst 15		
Methanol	Butyric acid	0.66	29,29	
Ethanol	Butyric acid	0.98	29,29	
Propanol	Butyric acid	0.70	29,29	
Butanol	Butyric acid	0.68	29,25	
Amyl Alcohol	Acetic acid	0.92	32,32	
	Smopex-101/	Dowex W×4		
2-Butanol	Propionic acid	2.87	33,34	
2-Propanol	Propionic acid	4.09	33,34	
Butanol	Propionic acid	4.24	33,34	
Ethanol	Propionic acid	1.79	33,34	
Propanol	Propionic acid	3.45	33,34	
Methanol	Propionic acid	1.31	33,34	
	SAC-13/su	ılfuric acid	•	
Methanol	Acetic acid	0.34	35,35	
Methanol	Propionic acid	0.28	35,35	
Methanol	Butyric acid	0.40	35,35	
Methanol	Hexanoic acid	0.22	35,35	
Methanol	Octanoic acid	0.17	35,35	
	Amberlyst	70/p-TSA		
4-Heptanol	Butyric acid	0.18	29,29	
Butanol	Butyric acid	0.20	29,29	
Butanol	Butyric acid	0.17	29,25	
Ethanol	Butyric acid	0.24	29,29	
Ethanol	Butyric acid	0.19	29,25	
Amberlyst 70/Amberlyst 15				
Ethanol	Butyric acid	3.01	29,29	
Ethanol	Butyric acid	2.40	29,25	
Propanol	Butyric acid	2.44	29,29	
Butanol	Butyric acid	2.96	29,29	
Butanol	Butyric acid	3.46	29,25	

The same is observed in the case of ethanol and butanol esterifying butyric acid in presence of Amberlyst 70 and *para*-Toluene sulfonic acid (*p*-TSA). Both cases indicate a similar reaction

mechanism for both homogeneous and the particular heterogeneous catalysts. The higher rate constant of p-TSA over Amberlyst 70 may be explained by the increased steric hindrance to the protonation of carboxylic acids by the bulky polymer backbone of Amberlyst 70 compared to acid sites in free solution.

This does not however explain the higher rate constants of Amberlyst 70 over Amberlyst 15. Amberlyst 15 has a higher cation exchange capacity, higher surface area and bigger pores. 42 However, the activity of Amberlyst 70 is higher per acid site (Table 3.3). This may be due to a combination of the effect of resin swelling and the fact that the acid sites are not saturated, i.e there are at any instant of time, enough available protonated carboxylic acid sites for alcohol molecules that diffuse into the catalyst. Resin catalysts are known to swell in the presence of certain polar solvents such as alcohols. Aliphatic and aromatic alcohols are able to diffuse through the bulk of the catalyst structure, thus making porosity not as important a factor as acid site strength. 43 The polymer backbone of Amberlyst 70 is halogenated. The presence of electron withdrawing groups is known to enhance the acid strength of Amberlyst 70 acid sites, making the turn over frequency of Amberlyst 70 higher. 44 In reactions with non-swelling solvents, one might expect the activity of Amberlyst 15 to be higher than Amberlyst 70.42

The activity of Smopex-101, a fibrous rather than resin catalyst with a lower acid site concentration with the same active group as Amberlyst 15 shows a higher activity. In this case, higher accessibility of acid sites in the fibrous catalyst rather than polymer resin may be said to cause the higher activity of Smopex-101.

3.5 Discussion

The non-ideal concentration model has been previously evaluated²⁵ for esterification reactions in Chapter 2 and is a useful method of reporting rate constants for maximum flexibility in reaction conditions of temperature, initial reactant composition and catalyst concentration. It has now been applied to several reactions with a view of comparing different reactants after normalizing for differences in solution density and accounting for non-ideal behavior. For a majority of reactions, with the exception of methanol and carboxylic acids smaller than butyric acid, increasing the number of alkyl groups in a carbon chain of either reactant does not have a significant polar or steric effect on reactivity. Reasonable estimates of rate constants for new reactions of interest involving several primary and secondary alcohols and carboxylic acids may be obtained from the data already available. The variation in rate constant values within the plateau region of reactivity for each reaction family ranges from 1 to 3% of the mean value, except for acetic acid esterification in the presence of Smopex-101, which had an error of 12% of the mean value. This is unsurprising as the confidence limits for reactions with Smopex-101 have relatively larger values (Table 3.1). The activation energies for a wide variety of carboxylic acids and alcohols is 50±10 kJ/mol, meaning the maximum error in the estimate of the rate constant is within 50% of its true value in the temperature range of 25 °C to 120 °C. This predictive capability enables the easy design of parallel reaction systems with multiple alcohols streams and multiple carboxylic acid streams commonly found in biomass conversion processes. Calculating the ratio of rate constants for two different catalysts for a number of reactions offers a simple way of evaluating similarity of mechanism between the two catalysts, and a number of such pairs of catalysts have been presented.

Esterification and hydrolysis reactions are considered to be predominantly sterically controlled. 13-15,36 The rate limiting step involves the attack of the alcohol on the carbonyl carbon of the protonated carboxylic acid. The reactivity of the carboxylic acid depends on the electrophilicity of the partially positive carbonyl carbon. Alkyl groups added to the carbon chain have an electron donating effect, effectively reducing the electrophilicity of the carbonyl carbon. The carbonyl carbon is sp² hybridized and the angle of attack of the nucleophile is affected by two factors. First, the repulsion of the high electron density region on the carbonyl oxygen atom, and second, the steric hindrance and repulsion of the OH and R group attached to the trigonal carbon atom. If portions of the carboxylic acid offer any steric hindrance to the angle of attack, the rate is reduced. Formic acid, having only a hydrogen atom, not only does not donate electron density to the carbonyl carbon, it has virtually no repulsive influence on the nucleophile, giving the alcohol a large geometric region of possible attack, thereby increasing the fraction of fruitful collisions between itself and formic acid. The methyl group on acetic acid donates electron density to the carbonyl carbon, and also reduces the region of successful attack of the nucleophile. The inductive effect drops in strength with increase in chain length, and steric effects dominate the reactivity of the bigger propionic acid. Butyric acid and higher acids show little difference in reactivity. The reactivity of the alcohol depends on its ability to attack the protonated carboxylic acid. Methanol, having only one alkyl carbon, offers the least steric hindrance and therefore has more success than ethanol and higher alcohols.

Little information was found on the structure-reactivity relationship of polyols such as ethylene glycol, propylene glycol, sorbitol, and glycerol which form an important portion of useful intermediates from biomass breakdown processes. However, the results of the study in Chapter 4 of propylene glycol esterification in the presence of *p*-TSA when normalized to the increased

concentration of hydroxyls in a diol, are close to the expected rate constant value for simple esterifications in *p*-TSA.

Dicarboxylic acid esterification reactions have also not been considered as they are strongly autocatalytic reactions even at room temperature and expressing catalyst concentration in the kinetic equation presents a challenge for most systems involving them. Additionally, obtaining accurate kinetic data for alcohol-dicarboxylic acid mixtures is made difficult by the almost instantaneous conversion of significant amounts of both to ester product.

Although the non-ideal concentration model works for a wide range of reaction conditions, in some cases where the reaction is conducted in a regime where the carboxylic acid is in excess of the alcohol and plays an important role in the catalysis, it fails to predict rates accurately irrespective of the activity coefficient model used when the reaction is started in excess ester or excess water.³⁷

3.5.1 Taft equation

Linear free energy relationships have been used extensively to quantify the link between the structure of a reactant in a reaction and the rate of the reaction. The Taft equation in particular has been used frequently to empirically relate rates of esterification reactions to steric effects in series of increasing alkyl chains in reactants, especially alcohols. ^{25,33,34} In this section, the non-ideal concentration based rate constants are related to the Taft steric equation, which relies on concentration based rates.

Taft's correlation for steric effect of substituents is as shown in Eq. 3.3.

$$\log\left(\frac{k_1}{k_{Ref}}\right) = \partial E_s \tag{3.3}$$

Where k_1 and k_{Ref} are concentration based rate constants of the reaction of interest and a reference reaction. E_S is the steric effect of substituents in reactants (relative to a reference reactant that has a short alkyl chain, usually the methyl group), is substituent specific, and the product of regression from different types of reactions. ∂ is the sensitivity of the reaction to steric effects of the substituent relative to the corresponding reaction that involves the reference reactant, and is a reaction specific parameter. The rate constants used in these studies are concentration based rate constants that do not explicitly account for non-idealities. An attempt to derive a relationship between non-ideal concentration rates and the steric effect of substituents follows:

Rate of a reaction is written as Eq. 3.4:

$$r = \mu_b C_{TS} \gamma_{TS} \tag{3.4}$$

In Eq. 3.4, μ_b is the frequency of the transition state crossing the activation barrier, C_{TS} and γ_{TS} are the concentration and activity coefficient of the transition state, respectively.

According to transition state theory, the transition state is considered to be in constant thermodynamic equilibrium with the reactants. The transition state formed in esterification is shown in Scheme 3.1.

Scheme 3.1: Rate limiting step of esterification reaction mechanism

$$R \xrightarrow{OH}^{+} + R^{-}OH \xrightarrow{HO} \xrightarrow{O-}R^{1} \xrightarrow{O-}R^{1} \xrightarrow{O-}R^{1} \xrightarrow{O-}R^{1}$$

Transition state

The equilibrium constant for transition state and reactants is expressed as in Eq. 3.5.²⁶

$$K^{TS} = \frac{C_{TS}\gamma_{TS}}{C_{R'OH}\gamma_{R'OH}C_{RCOOH}\gamma_{RCOOH}}$$
(3.5)

 C_{TS} , $C_{R'OH}$ and C_{RCOOH} are the concentrations of the transition state, alcohol and carboxylic acid respectively, while γ_{TS} , $\gamma_{R'OH}$, and γ_{RCOOH} are their activity coefficients.

Substituting for C_{TS} form Eq. 3.5 into the equation for rate (Eq. 3.4), we get Eq. 3.6.

$$r = \mu_b K^{TS} C_{R'OH} \gamma_{R'OH} C_{RCOOH} \gamma_{RCOOH}$$
 (3.6)

The frequency of the transition state crossing the barrier is expanded as Eq. 3.7.

$$\mu_b = \frac{k_B T}{\hbar} \tag{3.7}$$

In Eq. 3.7, k_B and h are Boltzmann and Planck's constant and T is temperature in Kelvin.

The thermodynamic definition of the reaction equilibrium constant is:

$$K^{TS} = \exp\left(\frac{-\Delta G^{TS}}{RT}\right) \tag{3.8}$$

Substituting for K^{TS} in the expression for rate (Eq. 3.6 and Eq. 3.7), we get Eq. 3.9,

$$r = \frac{k_B T}{\hbar} \exp\left(\frac{-\Delta G^{TS}}{RT}\right) C_{R'OH} \gamma_{R'OH} C_{RCOOH} \gamma_{RCOOH}$$
Rate
constant
k
(3.9)

In cases where the reaction solution is close to ideal, this expression becomes the law of mass action (Eq. 3.10).

$$r = kC_{ROOH}C_{RCOOH} (3.10)$$

In Eq. 3.10 above, the activity coefficients are all assumed to be unity and are lumped in with the rate constant k. Several kinetic studies of esterification reactions have concluded that activity based model better predicts experimental behavior, the rate constant is therefore expressed as Eq. 3.11.

$$r = kC_{R'OH}\gamma_{R'OH}C_{RCOOH}\gamma_{RCOOH}$$
 (3.11)

It should be noted that Eq. 3.11 above is for the forward reaction alone.

The rate constants used in the Taft equation are concentration based (mole/volume), which means in the application of the Taft equation to esterification, the activity coefficients are lumped in with the rate constants. Separating them from the rate constants, we get Eq. 3.12, which is rearranged to give Eq. 3.13.

$$\log\left(\frac{k_{1,C}}{k_{Ref,C}}\right) = \partial E_{s,C} = \log\left[\frac{\frac{k_B T}{\hbar} \exp\left(\frac{-\Delta G^{TS}}{RT}\right) \gamma_{R'OH} \gamma_{RCOOH}}{\frac{k_B T}{\hbar} \exp\left(\frac{-\Delta G^{Ref,TS}}{RT}\right) \gamma_{CH3OH} \gamma_{RCOOH}}\right]$$
(3.12)

$$\log\left(\frac{k_{1,C}}{k_{Ref,C}}\right) = \partial E_{s,C} = \left(\frac{-\Delta G^{TS}}{RT} - \frac{-\Delta G^{Ref,TS}}{RT}\right) + \log\left(\frac{\gamma_{R'OH}}{\gamma_{CH3OH}}\right)$$
(3.13)

The non-ideal concentration based rates and concentration based rates are then related as in Eq. 3.14.

$$\log\left(\frac{k_{1,C}}{k_{CH3,C}}\right) = \log\left(\frac{k_{1,NIC}}{k_{CH3,NIC}}\right) + \log\left(\frac{\gamma_{R'OH}}{\gamma_{CH3OH}}\right)$$
(3.14)

Or, in terms of the steric parameters, as in Eq. 3.15:

$$\partial E_{s,C} = \partial E_{s,NIC} + \log \left(\frac{\gamma_{R'OH}}{\gamma_{Ref,OH}} \right)$$
 (3.15)

Figure 3.7 shows the Taft equation plotted both as concentration and non-ideal concentration based rate constant ratios, to the reference reactant ethanol. E_S values used are reported in Table 3.5.

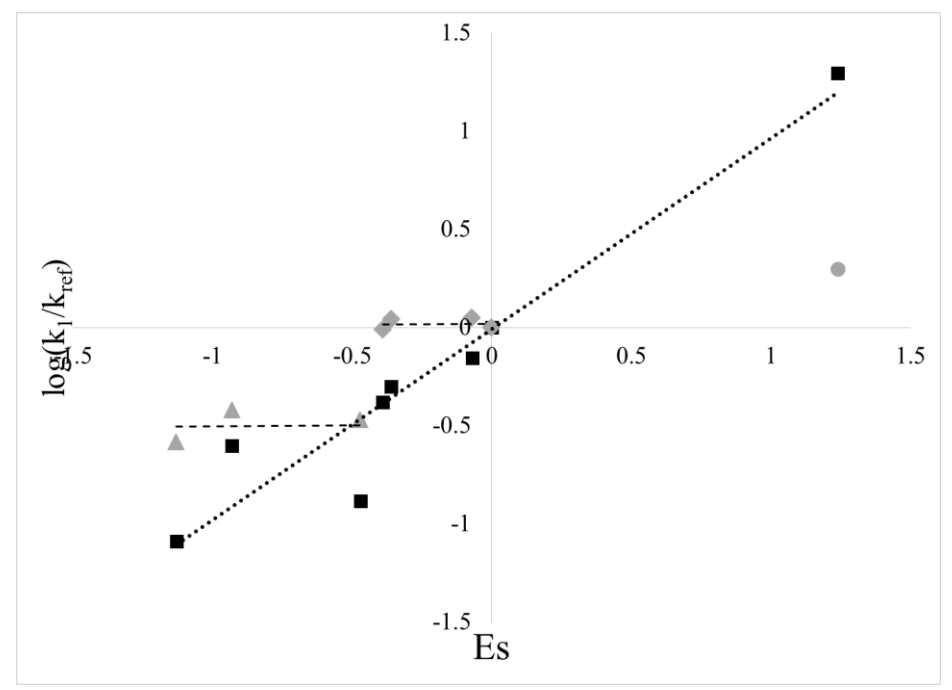


Figure 3.7: Taft equation applied to a candidate family of reactions (Reactions based on study by Erdem and Cebe)³⁴. Concentration based rate constant ratios (■), and non-ideal

concentration based rate constant ratios of methanol (●), primary alcohols (♦), and branched alcohols (▲) are plotted.

The dotted line shows the linear fit of the Taft equation for concentration based rate constant ratios to the ethanol rate constant from Erdem and Cebe³⁴. The data in grey are the non-ideal concentration based rate constant ratios to ethanol rate constant.

Table 3.5: Es values for each alcohol in Figure 3.7

Alcohol	Es
Methanol	1.24
Ethanol	0
n-Propyl	-0.07
alcohol	-0.07
<i>n</i> -Butyl	-0.36
alcohol	-0.50
<i>n</i> -Pentyl	-0.39
alcohol	-0.57
isobutyl	-0.93
acohol	-0.93
isopropyl	-0.47
alcohol	-0.47
2-Butyl	-1.13
alcohol	-1.13

The horizontal dashed lines show regions where there is little deviation in values of the two reaction families: esterification of propanoic acid with primary alcohols, and esterification of propanoic acid with branched alcohols. Both sets have almost no change in rate constant ratios. For a reference reactant within a family, $\log\left(\frac{k_{1,NIC}}{k_{CH3,NIC}}\right)$ is close to zero. This simple derivation indicates that the steric sensitivity parameter ∂ depends on the extent of non-ideality.

$$\partial E_{s,C} = 0 + \log \left(\frac{\gamma_{R'OH}}{\gamma_{CH3OH}} \right) \tag{3.16}$$

3.6 Conclusions

Using a non-ideal concentration model accounts for both, non-ideality and differences in initial molar compositions. Within a reactivity plateau, it is now possible now to have a quick theoretical estimate of reaction rate for a particular system from the data of a reference reaction. This makes process design easier for the flexible formation of esters in biorefineries. Reactants such as formic acid, acetic acid, and methanol, which lack attached alkyl groups, have much higher reaction rates in comparison to their longer hydrocarbon chain counterparts.

APPENDICES

Appendix D: Sample calculation of non-ideal concentration rate constant, knic

Non ideal rate constant calculated for acylation of propanol with butyric acid in presence of Amberlyst 36 from initial stages as: $k = \frac{\left(\frac{dx}{dt}\right)_{t=0}}{a_{acid}a_{alcohol}c_TW_{CAT}}$, where dx/dt is the absolute value of initial mole fraction change of any one reactant with respect to time, a_{acid} , $a_{alcohol}$ are mole fraction activities of carboxylic acid and alcohol, and w_{CAT} is the weight fraction of catalyst in the solution.

Experiment was conducted at 60° C, with an initial catalyst loading $w_{CAT} = 1$ wt.% (0.01 kg cat/kg soln), and an initial molar ratio of propanol: butyric acid = 3:1. Initial molar fractions of alcohol and carboxylic acid are 0.75 and 0.25 respectively.

Ion exchange capacity of Amberlyst 36 IE = 5.4×10^{-3} kmoles H⁺/kg cat.⁶¹

The initial rate was determined by a second order fit from data extrapolated to t=0.

$$\left(\frac{dx}{dt}\right)_{t=0} = 3.96 \pm 0.55 \times 10^{-6} s^{-1}$$

Solution molar density
$$C_T = \frac{N_T}{V_T} = \frac{3 \text{ kmoles propanol} + 1 \text{ kmol butyric acid}}{\left(\frac{3MW_{propanol}}{\rho_{propanol}} + \frac{MW_{butyric acid}}{\rho_{butyric acid}}\right)} = 12.11 \frac{\text{kmol}}{m^3},$$

where $MW_{propanol}$ and $MW_{butyric\ acid}$ are molar masses, and $\rho_{propanol}$ and $\rho_{butyric\ acid}$ are mass densities at 60 °C. Volume change on mixing, and due to reaction is considered to be negligible at 60 °C.

Mole fractions are calculated from the ratio of reactants to be 0.25 for butyric acid and 0.75 for propanol. Activity coefficients for butyric acid and propanol are 0.9784, 0.9966 using

UNIFAC. Activities are calculated to be at 0.244 for butyric acid and 0.747 for propanol using UNIFAC.

Hence $k=1.78\times 10^{-4}~kg~soln\cdot m^3~soln\cdot (kg~catalyst)^-1\cdot s^-1\cdot kmol^{-1}$. In terms of active site concentration of catalyst, $k_{NIC}=k\times IE\times \rho_{SOL}=4.1\times 10^{-5}~m^6~soln\cdot (kmoles~H^+)^{-1}\cdot (kmol~soln)^{-1}\cdot s^{-1}$.

Appendix E: Properties of alcohols, carboxylic acids and acid catalysts used in calculations

The following tables are properties used for calculations

Table 3.6: H⁺ concentrations of catalysts

Catalyat	kmol H+/kg
Catalyst	catalyst
Dowex	2.12E-03
50Wx8-400	2.12E-03
Amberlite IRA	4.40E-03
120	4.4015-03
Amberlyst 15	4.70E-03
Amberlyst 70	2.55E-03
Amberlyst 36	5.40E-03
sulfuric acid	1.02E-02
Amberlyst 39	5.00E-03
Amberlyst 35	5.20E-03
HC1	2.74E-02
Purolite	4.90E-03
HI	7.82E-03
SAC-13	1.31E-04
p-TSA	5.26E-03
Dowex 50W-4	4.55E-03
Smopex-101	3.20E-03

Table 3.7:Densities of alcohols at 60 °C

Tuble 5.7.D	Table 5.7. Delisities of alcohols at 00 C				
Alcohols	Density at 60 °C (kg/m³)	Molar Mass (kg/kmol)			
Methanol	754.7	32.0			
Ethanol	753.4	46.1			
Propanol	768.3	60.1			
2-Propanol	745.9	60.1			
Isopropanol	746.1	60.1			
Butanol	773.8	74.1			
2-Butanol	767.2	74.1			
Isobutanol	767.8	74.1			
Pentanol	748.8	88.1			
2-Ethyl	802.8	130.2			
Hexanol					
4-Heptanol	787.2	116.2			
Amyl Alcohol	784.0	88.2			
Octanol	798.9	130.2			
Ethylene Glycol	1100.0	62.1			
Diethylene Glycol	1200.0	106.1			
Triethylene Glycol	1150.0	150.2			
Isoamyl Alcohol	774.5	88.2			
Heptanol	787.2	116.2			
Ethylene Glycol	1110.0	62.1			
Benzyl Alcohol	1014.4	108.1			
Propylene Glycol	1005.3	76.1			

Table 3.8: Densities of carboxylic acids at 60 °C

Table 3.6. Delisitie	s of carboxyric acids	<u>at 00 C</u>
Carboxylic acids	Density at 60 °C (kg/m³)	Molar Mass (kg/kmol)
Acetic Acid	1005.588	60.05
Propionic Acid	952.62679	74.07548
Butyric Acid	921.03584	88.11
Pentanoic Acid	904.14871	102.13
Hexanoic Acid	892.30483	116.16
Caprylic Acid	910	144.21
Acrylic Acid	1005.69	72.06
Lactic Acid	1187.892	90.08
Octanoic Acid	910	144.21
Formic Acid	1220	46
Nonanoic Acid	900	158.23
Levulinic Acid	1107.891	116.11
Lauric Acid	800	200.3
Betamethyl Valeric Acid	896.15	132.158
Trimethyl Acetic		
Acid	884.6	102.132
Diethyl Acetic Acid	887.3	116.16
Dipropyl Acetic Acid	864	144.211
Methacrylic Acid	1020	86.06
Dibutyl Acetic Acid	840.7	172
Di-isobutyl Acetic		
Acid	840.7	172
Citric Acid	1104.142	192.124
Maleic Acid	1358.189	116.07
Decanoic Acid	893	172.26
Tartaric Acid	1745.109	150.087
Succinic Acid	1340.086	118.09

REFERENCES

REFERENCES

- (1) Larock, R. C. Comprehensive organic transformations; VCH New York, 1989; Vol. 315.
- (2) Acker, P. E. van; Mathieu, O.; Milner, R. J.; Pacynko, W. F. Ester co-production. US6093845 A, July 25, 2000.
- (3) Bam, N.; Drown, D. C.; Korus, R.; Hoffman, D. S.; Johnson, T. G.; Washam, J. M. Method for purifying alcohol esters. US5424467 A, June 13, 1995.
- (4) Masanori, O.; Seishiro, Y. Mixed sugar alcohol esters of higher and lower saturated fatty acids. US3649647 A, March 14, 1972.
- (5) M, G. C. Preparation of mixed esters of polyhydric alcohols. US2309949 A, February 2, 1943.
- (6) Drent, E. Process for the co-production of carboxylic acids and carboxylic acid esters. US4664851 A, May 12, 1987.
- (7) Warner, R. J.; Murphy, C. D.; Grajales, G. A. R.; Santiago, F. J. S.; Solorzano, F. A.; Torres, J. A. Process for the simultaneous coproduction and purification of ethyl acetate and isopropyl acetate. US6765110 B2, July 20, 2004.
- (8) Hinshelwood, C. N.; Legard, A. R. J. Chem. Soc. Resumed 1935, 1588–1591.
- (9) DeTar, D. F. J. Org. Chem. **1980**, 45, 5166–5174.
- (10) Eckey, E. W. J. Am. Oil Chem. Soc. **1956**, 33, 575–579.
- (11) Pfeffer, P. E.; Silbert, L. S. J. Org. Chem. 1976, 41, 1373–1379.
- (12) Srilatha, K.; Lingaiah, N.; Sai Prasad, P. S.; Prabhavathi Devi, B. L. A.; Prasad, R. B. N.; Venkateswar, S. *Ind. Eng. Chem. Res.* **2009**, *48*, 10816–10819.
- (13) Taft, R. W. J. Am. Chem. Soc. 1953, 75, 4538–4539.
- (14) Charton, M. J. Org. Chem. 1978, 43, 3995–4001.
- (15) Charton, M. J. Am. Chem. Soc. **1975**, 97, 1552–1556.
- (16) Loening, K. L.; Garrett, A. B.; Newman, M. S. J. Am. Chem. Soc. 1952, 74, 3929–3931.
- (17) Charton, M. J. Am. Chem. Soc. 1975, 97, 3694–3697.
- (18) Morgan, K. J.; Unwin, N. J. Chem. Soc. B Phys. Org. 1968, 880–884.
- (19) Ali, S. H.; Merchant, S. Q. Int. J. Chem. Kinet. **2006**, 38, 593–612.
- (20) Pöpken, T.; Götze, L.; Gmehling, J. Ind. Eng. Chem. Res. 2000, 39, 2601–2611.

- (21) Mazzotti, M.; Neri, B.; Gelosa, D.; Kruglov, A.; Morbidelli, M. *Ind. Eng. Chem. Res.* **1997**, *36*, 3–10.
- (22) Ju, I. B.; Lim, H.-W.; Jeon, W.; Suh, D. J.; Park, M.-J.; Suh, Y.-W. *Chem. Eng. J.* **2011**, *168*, 293–302.
- (23) Orjuela, A.; Yanez, A. J.; Santhanakrishnan, A.; Lira, C. T.; Miller, D. J. *Chem. Eng. J.* **2012**, *188*, 98–107.
- (24) Kolah, A. K.; Asthana, N. S.; Vu, D. T.; Lira, C. T.; Miller, D. J. *Ind. Eng. Chem. Res.* **2008**, *47*, 5313–5317.
- (25) Santhanakrishnan, A.; Shannon, A.; Peereboom, L.; Lira, C. T.; Miller, D. J. *Ind. Eng. Chem. Res.* **2012**, *52*, 1845–1853.
- (26) Eckert, C. A.; Hsieh, C. K.; McCabe, J. R. AIChE J. 1974, 20, 20–36.
- (27) Eckert, C. A. Ind. Eng. Chem. 1967, 59, 20–32.
- (28) Madon, R. J.; Iglesia, E. J. Mol. Catal. Chem. 2000, 163, 189–204.
- (29) Pappu, V. K. S.; Kanyi, V.; Santhanakrishnan, A.; Lira, C. T.; Miller, D. J. *Bioresour. Technol.* **2013**, *130*, 793–797.
- (30) Smith, H. A. J. Am. Chem. Soc. **1939**, 61, 254–260.
- (31) Smith, H. A. J. Am. Chem. Soc. **1940**, 62, 1136–1140.
- (32) Akbay, E. Ö.; Altıokka, M. R. Appl. Catal. Gen. **2011**, 396, 14–19.
- (33) Lilja, J.; Murzin, D. Y.; Salmi, T.; Aumo, J.; Mäki-Arvela, P.; Sundell, M. *J. Mol. Catal. Chem.* **2002**, *182–183*, 555–563.
- (34) Erdem B.; Cebe M, Zeitschrift für Physikalische, 2011, 225, 125-136.
- (35) Liu, Y.; Lotero, E.; Goodwin Jr., J. G. J. Catal. **2006**, 243, 221–228.
- (36) MacPhee, J. A.; Panaye, A.; Dubois, J.-E. *Tetrahedron* **1978**, *34*, 3553–3562.
- (37) Grob, S.; Hasse, H. *Ind. Eng. Chem. Res.* **2006**, *45*, 1869–1874.
- (38) Roy, R.; Bhatia, S. J. Chem. Technol. Biotechnol. 1987, 37, 1–10.
- (39) Schmid, B.; Döker, M.; Gmehling, J. Ind. Eng. Chem. Res. 2008, 47, 698–703.
- (40) Ali, S. H.; Tarakmah, A.; Merchant, S. Q.; Al-Sahhaf, T. *Chem. Eng. Sci.* **2007**, *62*, 3197–3217.
- (41) Santhanakrishnan, A.; Peereboom, L.; Miller, D. J.; Dumitrascu, A.; Smith, P. B. *Ind. Eng. Chem. Res.* **2013**, *52*, 9337–9342.

Included in this Section is a copy of the paper: Measurement of *p*-Toluenesulfonic Acid-Catalyzed Reaction Kinetics of 1,2-Propylene Glycol Acetylation Using *In Situ*¹H NMR Spectroscopy, by Arati Santhanakrishnan †, Lars Peereboom †, Dennis J. Miller †*, Adina Dumitrascu ‡, and Patrick B. Smith ‡

[†] Department of Chemical Engineering and Materials Science, Michigan State University, East Lansing, Michigan 48823, United States

[‡] Michigan Molecular Institute, 1910 West Saint Andrews Road, Midland, Michigan 48640, United States

Reprinted with permission from Ind. Eng. Chem. Res., 2013, 52 (27), pp 9337–9342

Copyright © 2013 American Chemical Society

4 Kinetics of *p*-Touenesulfonic Acid-Catalyzed 1,2-Propylene Glycol Acetylation

4.1 Abstract

The reaction kinetics of the acetylation of 1,2-propylene glycol (PG) catalyzed by *p*-toluenesulfonic acid (*p*-TSA) determined using an *in-situ* ¹H NMR method by collaborating researchers were modeled. Both primary and secondary mono-acetate esters of PG were observed as well as the di-ester. The reaction kinetics were characterized as a function of PG to acetic acid (AA) stoichiometry, *p*-TSA concentration, and temperature. The acetylation reactions and the transacetylation of diester with PG were modeled as reversible second order reactions. Equilibrium constants were determined experimentally for each reaction. Activation energies for the consecutive acetylation of PG and PGMA are 56 and 47 kJ/mol, respectively. The activation energy for intermolecular transacetylation of PG with its diacetate ester to form PG monoacetate is 63 kJ/mol. The rate constants obtained from the model, when normalized to the two hydroxyls present per molecule of diol, are close to the expected value of the universal rate constant for *p*-TSA esterification calculated in Chapter 2.

4.2 Introduction

Esters of glycols and other polyols have many industrial applications including as coalescing agents, lubricants, intermediates to polyurethane foams, plasticizers, and emulsifiers in the food processing industry. The conventional route for their synthesis is the acylation of polyols with a carboxylic acid in the presence of acid catalysts. Typically, the reaction system consists of the esterification reactions of alcohols and subsequent hydroxyl esters with carboxylic acids to form esters and water, and disproportionation reactions involving the transesterification of the

monoesters to form diesters and glycol (Scheme 4.1). The usage of glycol esters in a wide variety of applications requires the optimization of esterification processes for high yields of either monoesters or diesters with high purity, warranting a thorough understanding of the kinetics of glycol esterification systems.

In this study, a candidate reaction system consisting of propylene glycol reacting with acetic acid in the presence of *para*-toluene sulfonic acid has been studied to model the effect of initial reactant molar ratios, temperature, catalyst loading and non-ideality of solutions on the rate of reaction and equilibrium composition with a kinetic model that uses non-ideal concentrations. Using propylene glycol instead of ethylene glycol enables differentiation between primary and secondary monoesters and to understand their interactions and individual rates of further esterification. Propylene glycol (PG) is a large commodity chemical with annual global sales of about \$150 million⁶. Acetate esters of PG are excellent model compounds for further chemistry, and their formation has not yet been studied in detail. The acetylation of PG with acetic acid (AA) to form either primary (PGMA1) or secondary (PGMA2) mono-acetate esters and the subsequent acetylation with another acetic acid molecule to form propylene glycol diacetate (PGDA) (Scheme 4.2) is a commercially valuable process.

Commercial processes now exist to make propylene glycol from glycerol, which in turn is a side product of biodiesel synthesis. Bio-based acetic acid may be produced readily from ethanol. Kinetic models of the esterification of acetic acid with propylene glycol that account for both non

ideality of the solutions and a wide range of reaction conditions enable simulations for the design of future biorefinery processes.

Scheme 4.2: Acetylation of 1,2 - propylene glycol with acetic acid.

4.3 Materials and Methods

Acetic acid (AA), 1,2-propylene glycol (PG), propylene glycol diacetate (PGDA), and *p*-toluene sulfonic acid monohydrate (*p*-TSA) were obtained from Sigma Aldrich and used without further purification.

As part of a collaborative research project, kinetic experiments for acetylation of PG were conducted at Michigan Molecular Institute by Dr. Patrick B. Smith and Dr. Adina Dumitrascu using an in situ H¹ NMR method that enabled real time sample measurements and the accurate quantification of the primary and secondary monoesters.

Transacetylation reactions were carried out at Michigan State University in 75-ml stainless steel batch autoclaves in a Parr 5000 Multireactor system. PG and PGDA were loaded into the autoclave and the mixture was heated to reaction temperature, at which time *p*-TSA catalyst was injected into the reaction fluid. Samples (~1.0 ml) were taken periodically, diluted ten-fold in acetonitrile prior to injection, and then analyzed in a Varian 450 gas chromatograph fitted with a thermal conductivity detector (Varian Medical Systems Inc., Palo Alto, CA). Separation was done on a 0.53 mm ID Aquawax-DA 30 m capillary column with 1.0µm film thickness, a helium carrier gas flow rate of 10 ml/min, an injector temperature 250 °C, and detector temperature 240 °C. The initial column temperature was held at 40 °C for 1 min, ramped to 130 °C at 30 °C/min, ramped to 150 °C at 5 °C/min, and finally ramped to 200 °C at 30 °C/min and held for 2 min. Standards of known composition in the range of interest were prepared and run in the chromatograph before and after reaction samples to calibrate the response factor of each component of the reaction. PGMA was determined stoichiometrically from the amount of PGDA consumed in the reaction mixture.

4.4 Results

The full list of experiments conducted either at the Michigan Molecular Institute or at Michigan State University are recorded in Table 4.1.

4.4.1 Equilibrium constants

The activity-based equilibrium constants for Reactions 1 and 2 in Scheme 4.3 (Eq. 4.1) were obtained from experimental data at long reaction times where equilibrium was reached (Figure 4.1).

Scheme 4.3: Simplified reaction scheme for kinetic model

Table 4.1: Summary of reactions and experimental conditions

Experiment	Temperature (°C)	catalyst loading (kg cat/ kg soln)	initial molar ratio	Figure No.
Esterification			PG:AA	
1	63	0.012	1: 1	4.6
2	63	0.016	2: 1	4.7
3	63	0.008	1: 2	4.2
4	75	0.008	1: 2	4.8
5	75	0.012	1: 1	4.9
6	75	0.006	1: 1	4.10
7	75	0.025	1: 1	4.11
8	75	0.063	1: 1	4.12
9	86	0.012	1: 1	4.13
10	86	0.016	2: 1	4.14
11	86	0.008	1:2	4.15
Hydrolysis			PGDA: Water	
12	64	0.01	3: 1	4.16
13	75	0.01	3: 1	4.3
14	86	0.01	3: 1	4.17
Transacetylation			PGDA:PG	
15	85	0.007	1: 1	4.4
16	75	0.004	3: 1	4.18
17	65	0.007	1: 3	4.19

$$K_{a,m} = K_{x,m} K_{\gamma,m} = \prod_{i=1}^{Nc} (x_i \gamma_i)_{EQ}^{\nu_i}$$
 (4.1)

Here x_i , y_i , and v_i represent the mole fraction, activity coefficient, and stoichiometric coefficient of component i in the reaction mixture at equilibrium. The equilibrium constant for the

transacetylation reaction, $K_{a,3}$, is equal to the ratio of the other two equilibrium constants (i.e $K_{a,3}$ = $K_{a,1}/K_{a,2}$). UNIFAC (UNIversal Functional Activity Coefficient) was used to estimate activity coefficients of components⁷.

A van't Hoff plot of both acetylation reactions shows a slight temperature dependence (exothermic) for $K_{a,1}$, but a constant value for $K_{a,2}$ (Figure 4.1). Although only two temperatures were used for this analysis, a number of values at each temperature show a consistent difference for $K_{a,1}$, for a relatively small difference in temperature (~10°C). This warranted the inclusion of a temperature dependence for $K_{a,1}$, and consequently $K_{a,3}$, in the regression analysis discussed in the next section. The heat of reaction of PG acetylation (Reaction 1 of Scheme 4.3) and thus PG-PGDA transacetylation (Reaction 3 of Scheme 4.3) is -10 kJ/mol.

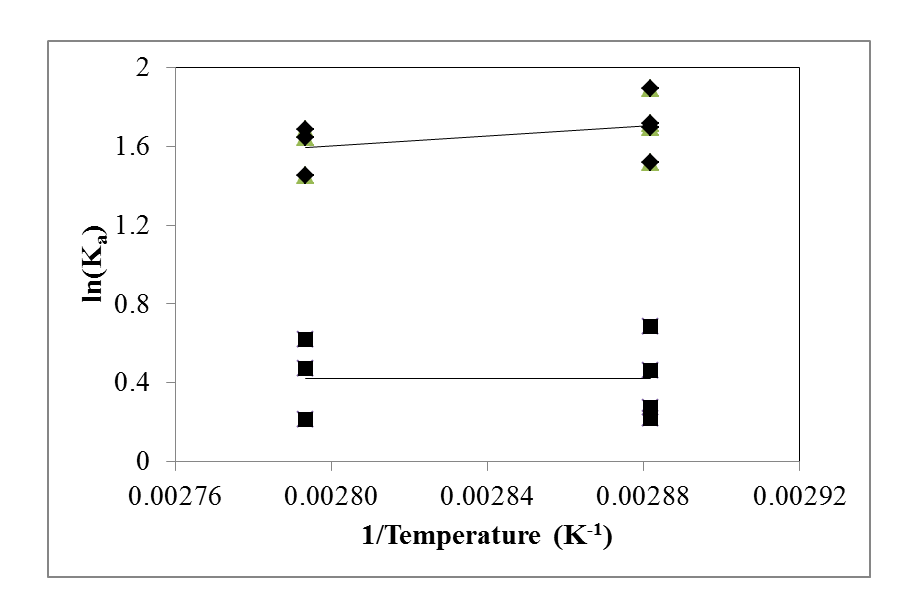


Figure 4.1: Van't Hoff plot of experimental activity-based equilibrium constants for the acetylation of PG and PGMA $(•) - K_{al}$; $(•) - K_{a2}$.

4.4.2 Kinetic modeling

The NMR kinetic data for PG acetylation were modeled as a set of elementary, reversible, consecutive reactions (Scheme 4.3). The reaction of PG with PGDA to give PGMA (propylene

glycol monoacetate) (k_3) in an intermolecular transacetylation is also included in the model to account for interconversion of the esters. Reverse reaction rates (hydrolysis of PGMA and PGDA, and conversion of PGMAs to PGDA and PG) are accounted for by the equilibrium constants and forward rate constants ($k_{-m} = k_m/K_m$ for reaction m in Scheme 4.3). Initially, a more complex reaction network that treated the primary and secondary PGMA esters as separate species was considered (Scheme 4.2); however, experimental concentration profiles showed a constant molar ratio of primary to secondary monoesters of approximately 1.7 at all stages of reaction, evidence that interconversion of the two PGMA esters is significantly faster than PG acetylation. This observation, along with the challenge of preparing pure primary or secondary PGMA standards, led to the decision to treat the primary and secondary monoacetates as one entity.

The sealed NMR tube used in reaction studies is modeled as a stirred batch reactor. The change in number of moles of component $i(N_i)$ participating in m reactions can be expressed as

$$\frac{dN_i}{dt} = N_T \frac{dx_i}{dt} = \left(\sum_{m=1}^m \theta_{i,m} r_m\right) V \tag{4.2}$$

where N_T is the total number of moles in the reactor, V is the volume of the reacting phase, r_m is the rate of reaction m per unit volume, and x_i is the mole fraction of component i in the liquid mixture. The parameter $\theta_{i,m}$ is the ratio of stoichiometric coefficients of component i with respect to the reference component in reaction m.

Eq. 4.2 can be simplified by assuming total molar concentration of the liquid phase C_T to be constant $(V/N_T = 1/C_T)$, as total number of moles is conserved in the reaction system and reaction volume is assumed constant during the run under isothermal conditions.

$$\frac{dx_i}{dt} = \frac{1}{C_T} \left(\sum_{m=1}^m \theta_{i,m} r_m \right) \tag{4.3}$$

Reaction rate r_m is expressed in terms of an elementary rate law with the product of solution density C_T and species activity a_i representing each species in the rate expression. This product, termed "non-ideal concentration" ($C_Tx_i\gamma_i$ or $C_i\gamma_i$), has been found in earlier work to be the basis for a universal approach to esterification kinetics. ^{8–10} Rates of formation of propylene glycol mono acetate (PGMA) and propylene glycol diacetate (PGDA), and the transacetylation of PG and PGDA to PGMA, can thus be expressed in terms of the activities of propylene glycol (PG), acetic acid (PGMA), and water (PGMA), and water (PGMA), and PGMA, and water (PGMA), the concentration of catalyst in the reaction mixture; the solution density PGMA, and PGMA, the forward rate constants. The number of moles and thus activity of water in the reaction mixture is calculated from the reaction stoichiometry. (PGMA) activity coefficient model is used to calculate the activity coefficients of each species in the system.

Table 4.2: UNIFAC groups and their counts in reaction components

Component name	Group	Count
PG	CH3	1
	CH2	1
	СН	1
	ОН	2
Acetic acid	CH3	1
	СООН	1
PGMA	CH3	1
	CH2	1
	СН	1
	CH3COO	1
	ОН	1
PGDA	CH3	1
	CH2	1
	СН	1
	CH3COO	2
Water	H2O	1

Table 4.3: Group volume and surface area contributions

Group	$\mathbf{R}_{\mathbf{k}}$	Qk
CH3	0.9011	0.848
CH2	0.6754	0.54
COOH	1.3013	1.224
CH3COO	1.9031	1.7280
H2O	0.9200	1.4000
OH	1.0000	1.2000
СН	0.4469	0.2280

Table 4.4: UNIFAC group binary interaction parameters

Name	CH2	ОН	H2O	СНЗСОО	СООН
CH2	0	986.5	1318	232.1	663.5
ОН	156.4	0	353.5	101.1	199
H2O	300	-229.1	0	72.87	-14.09
СН3СОО	114.8	245.4	200.8	0	660.2
СООН	315.3	-151	-66.17	-256.3	0

$$r_1 = w_{CAT} C_T^2 k_1 \left[a_{PG} a_{AA} - \frac{a_{PGMA} a_W}{K_{a,1}} \right]$$
 (4.4)

$$r_2 = w_{CAT} C_T^2 k_2 \left[a_{PGMA} x_{AA} - \frac{a_{PGDA} a_W}{K_{a,2}} \right]$$
 (4.5)

$$r_3 = w_{CAT} C_T^2 k_3 \left[a_{PGDA} a_{PG} - \frac{a_{PGMA}^2}{K_{a,3}} \right]$$
 (4.6)

Five ordinary differential equations (one for each chemical species in the system) were assembled from Eq. 4.3 through Eq. 4.6; these equations were simultaneously integrated and regressed to experimental data to estimate kinetic parameters using the functions nlinfit and ode23 from the optimization toolbox of Matlab 7.12.0. To simplify parameter fitting, the rate constant k_3 for the transacetylation reaction of PG with PGDA to give PGMA was first determined using only experimental data for that reaction (Experiments 15-17 of Table 4.1). Then, using the value for k_3 , the hydrolysis and acetylation reactions were fit together to give the values of k_1 and k_2 (Experiments 1-14). Optimization was done by minimizing the sum of squared differences between calculated (x_{i-calc}) and experimental (x_{i-exp}) species mole fractions (Eq. 4.7),

$$F_{min}^2 = \frac{1}{n} \sum_{samples} \sum_{i=1}^{N_C} (x_{i-exp} - x_{i-calc})^2$$
 (4.7)

where n is the number of experimental samples withdrawn in each experiment and N_c is the number of reacting components in each experiment. Optimized kinetic parameters are reported in **Error!** Reference source not found.

Table 4.5 Optimized kinetic parameters with 95% confidence limits for PG acetylation with *p*-TSA catalyst

	Reaction 1: Acetylation of PG to PGMA						
$k_{0,1}$	$3.13 \pm 0.05 \times 10^{6}$	m ³ soln·kg soln/kg cat/kmol/s					
$E_{a,1}$	55700 ± 50	kJ / kmol					
$K_{a,1}$	exp(1255/T -1.91)						
	Reaction 2: Acetylati	on of PGMA to PGDA					
$k_{0,2}$	$5.22 \pm 0.25 \times 10^4$	m ³ soln·kg soln/kg cat/kmol/s					
$E_{a,2}$	47000 ± 140	kJ / kmol					
$K_{a,2}$	1.52						
	Reaction 3: Transacetylation	on of PG + PGDA to PGMA					
$k_{0,3}$	$9.05 \pm 0.34 \times 10^6$	m ³ soln·kg soln/kg cat/kmol/s					
$E_{a,3}$	63900 ± 630	kJ / mol					
$K_{a,3}$	$K_{a,1}/K_{a,2}$						

The rate constant values at 60 °C of PGMA formation and PGDA formation calculated from the parameters in **Error! Reference source not found.** are found to be 2.4×10^{-3} and 2.2×10^{-3} m³ soln·kg soln/kg cat/kmol/s. These values are very close to the rate constant value at 60 °C of the acylation of ethanol and *n*-butanol with butyric acid in the presence of *p*-TSA (2.1×10^{-3}). The values of $E_{a,1}$ and $E_{a,2}$ are in the range of 50 ± 10 kJ/mole, which is typical of esterification reaction activation energies. Figure 4.2 through Figure 4.4 compare the predicted and experimental species mole fractions vs. time for acetylation, hydrolysis, and transacetylation reactions.

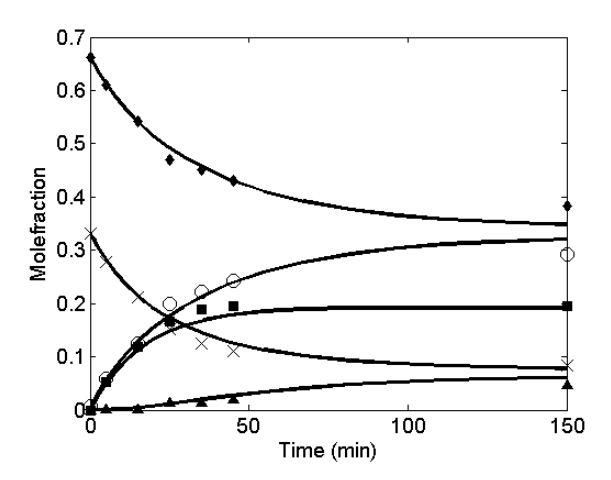


Figure 4.2: Experimental and predicted concentration profiles of PG acetylation (Experiment 3: 63 °C, 0.008 kg cat/kg soln, initial molar ratio PG:AA = 1:2) (——) – UNIFAC activity based model prediction; (♠) – acetic acid; (■) – propylene glycol monoacetate; (▲) – propylene glycol diacetate; (×) –propylene glycol; (○) – water.

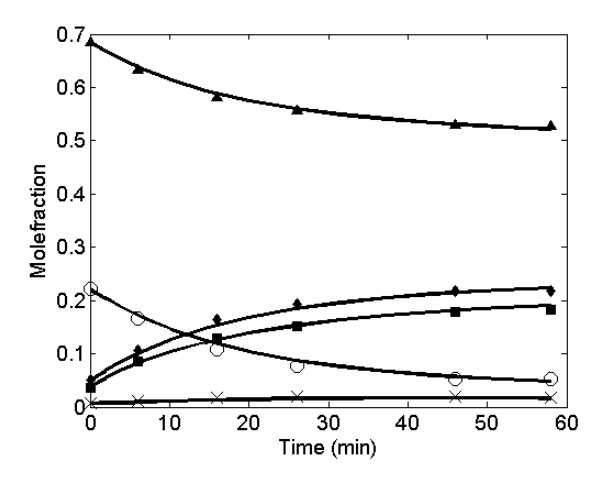


Figure 4.3: Experimental and predicted concentration profiles of PGDA hydrolysis (Experiment 13: 75 °C, 0.010 kg cat/kg soln, initial molar ratio PGDA:water = 3:1) (——) – UNIFAC activity based model prediction; (♠) – acetic acid; (■) – propylene glycol monoacetate; (▲) – propylene glycol; (○) – water.

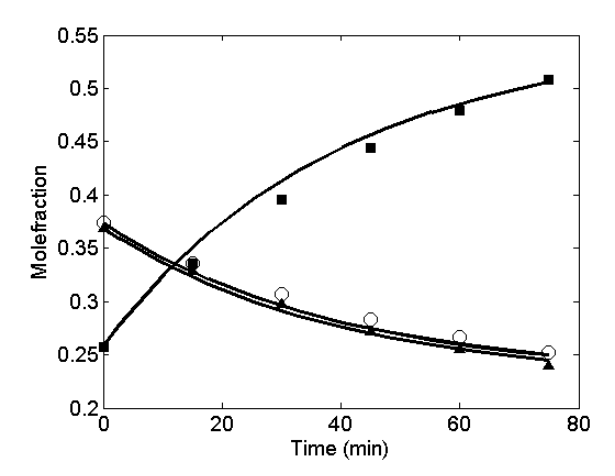


Figure 4.4:Experimental and predicted concentration profiles of PG-PGDA transacetylation (Experiment 15: 85 °C, 0.007 kg cat/kg soln, initial molar ratio PGDA:PG = 1:1) (——) − UNIFAC activity based model prediction; (♦) – acetic acid; (■) – propylene glycol monoacetate; (▲) – propylene glycol diacetate; (×) –propylene glycol; (○) – water.

The model was found to predict experimental behavior accurately with the value of absolute residuals (predicted minus experimental mole fraction) averaged over all species at all data points for all experiments equal to 0.0098. A parity plot of PGMA experimental and predicted mole fractions for every data point in every experiment, which demonstrates the overall quality of model fit to data, is shown in Figure 4.5.

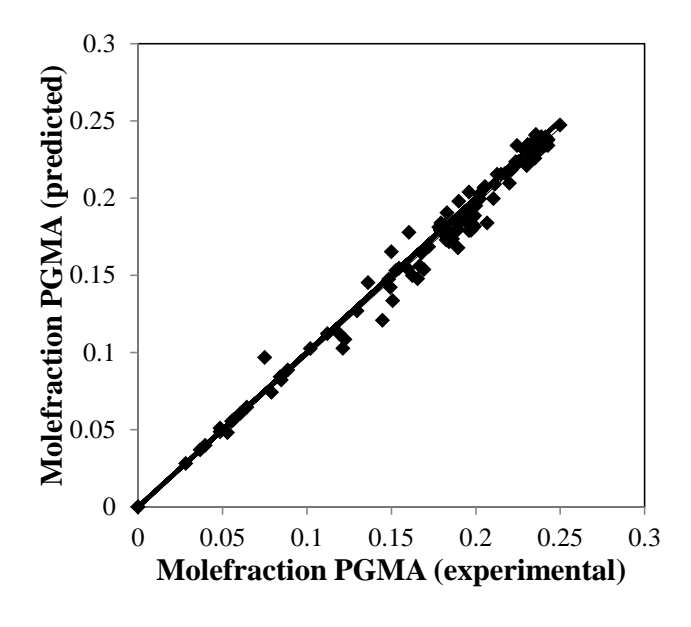


Figure 4.5: Parity plot of kinetic model fit for PGMA mole fractions in experiments

The absolute residual for each experiment are shown in Table 4.6. Predicted and experimental mole fraction profiles for all experiments are given in Figure 4.6 through Figure 4.19 of Appendix F. Raw NMR data from experiments conducted at Michigan Molecular Institute and Michigan State University are given in Table 4.7 through Table 4.23 of Appendix G.

Table 4.6: Absolute residuals for each experiment

Tubic	1.0.71050141016	esiduals for each each each each each each each each	porimont	
Experiment	Temperature	loading	Initial molar	$\mathbf{F_{abs}}^{\mathbf{a}}$
Experiment	(°C)	(kg cat/ kg	ratio	rabs
	(0)	soln)	Tatio	
Acetylation		50111)	PG:AA	
1	63	0.012	1: 1	0.016
2	63	0.016	2: 1	0.011
3	63	0.008	1: 2	0.009
4	75	0.008	1: 2	0.009
5	75	0.012	1: 1	0.009
6	75	0.006	1: 1	0.008
7	75	0.025	1: 1	0.009
8	75	0.063	1: 1	0.008
9	86	0.012	1: 1	0.009
10	86	0.016	2: 1	0.010
11	86	0.008	1:02	0.009
Hydrolysis			PGDA:	
Trydrorysis			Water	
12	64	0.01	3: 1	0.008
13	75	0.01	3: 1	0.013
14	86	0.01	3: 1	0.016
Transacetylation			PGDA:PG	
15	85	0.007	1: 1	0.006
16	75	0.004	3: 1	0.009
17	65	0.007	1: 3	0.008

 $^{a}F_{abs}$ is the absolute value of predicted minus experimental mole fraction averaged over all species and all data points for the experiment.

4.5 Conclusions

Reaction kinetics and equilibrium constants for the reversible liquid phase acetylation of PG with AA using *p*-toluenesulfonic acid as catalyst have been determined in the range of 63 °C – 85 °C. The experiments were conducted and analyzed using an *in-situ* ¹H NMR technique that quantified all reactants and products except water in the reaction mixture over time. The experimental data were fit to a homogeneous activity-based model that describes the experimental behavior. Heats of reaction were calculated from experimentally determined equilibrium constants. The reaction of PG with PGDA to form PGMA was found to proceed at rates comparable to the acetylation reactions; interconversion of PGMA primary and secondary isomers was rapid, giving an equilibrium molar ratio of primary:secondary of 1.7:1 under all reaction conditions. The non-ideal concentration model rate constants were calculated at 60 °C for PGDA formation from PGMA and acetic acid gives rate constant values similar to those obtained for butyric acid esterification with ethanol and *n*-butanol in the presence of *p*-TSA. This similarity provides further impetus to use the non-ideal concentration model for esterification kinetics.

APPENDICES

Appendix F: Predicted and experimental mole fraction profiles of all experiments in PG esterification with acetic acid (Chapter 2)

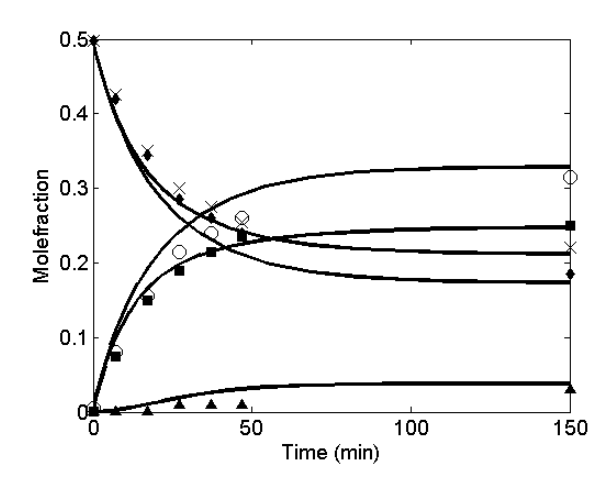


Figure 4.6: Experimental and predicted concentration profiles of PG acetylation (Experiment 1: 63 °C, 0.012 kg cat/kg soln, initial molar ratio PG:AA=1:1) (———) – UNIFAC activity based model prediction; (♠) – acetic acid; (■) – propylene glycol monoacetate; (▲) – propylene glycol diacetate; (×) –propylene glycol; (○) – water

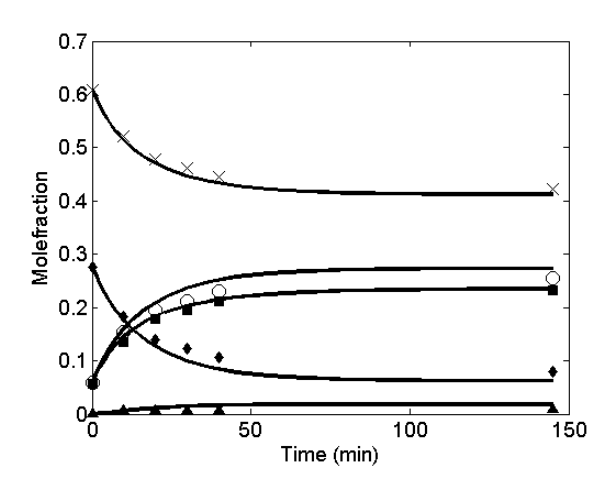


Figure 4.7: Experimental and predicted concentration profiles of PG acetylation (Experiment 2: 63 °C, 0.016 kg cat/kg soln, initial molar ratio PG:AA=2:1) (———) – UNIFAC activity based model prediction; (♠) – acetic acid; (■) – propylene glycol monoacetate; (▲) – propylene glycol diacetate; (×) –propylene glycol; (○) – water

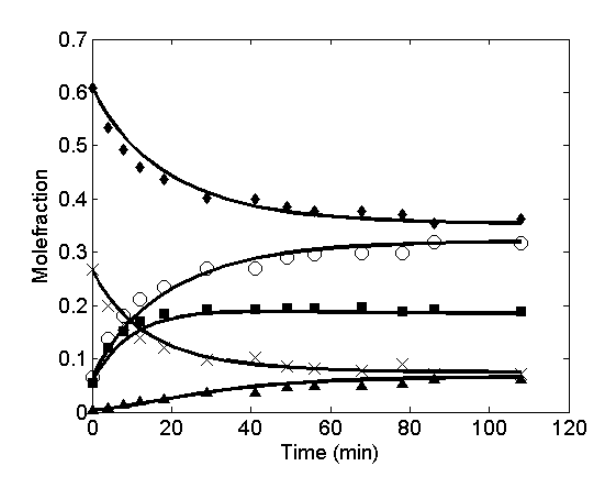


Figure 4.8: Experimental and predicted concentration profiles of PG acetylation (Experiment 4: 75 °C, 0.008 kg cat/kg soln, initial molar ratio PG:AA=1:2) (———) – UNIFAC activity based model prediction; (♠) – acetic acid; (■) – propylene glycol monoacetate; (▲) – propylene glycol diacetate; (×) –propylene glycol; (○) – water

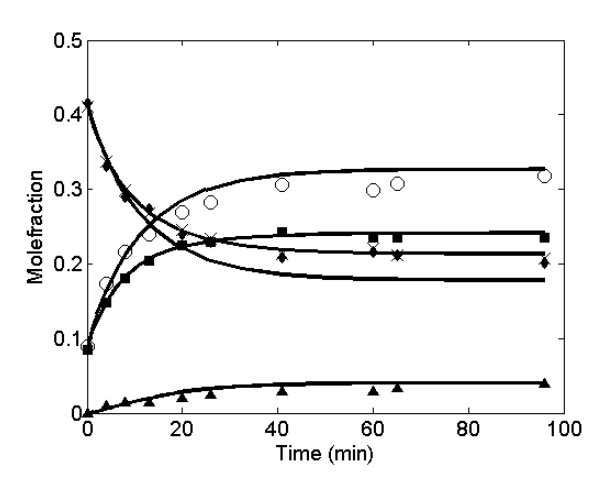


Figure 4.9: Experimental and predicted concentration profiles of PG acetylation (Experiment 5: 75 °C, 0.012 kg cat/kg soln, initial molar ratio PG:AA=1:1) (——) – UNIFAC activity based model prediction; (♠) – acetic acid; (■) – propylene glycol monoacetate; (▲) – propylene glycol diacetate; (×) –propylene glycol; (○) – water

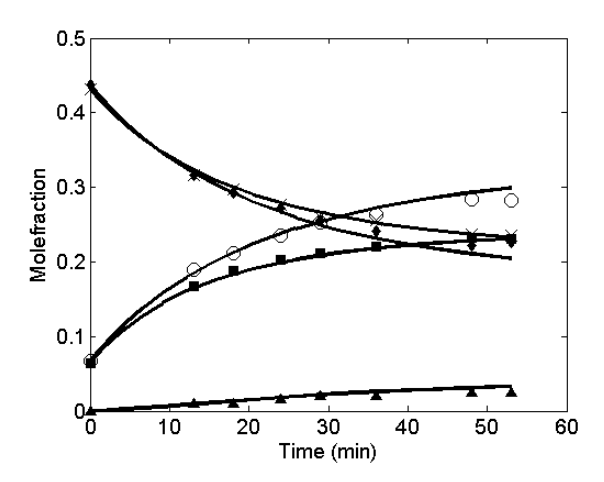


Figure 4.10: Experimental and predicted concentration profiles of PG acetylation (Experiment 6: 75 °C, 0.006 kg cat/kg soln, initial molar ratio PG:AA=1:1) (——) – UNIFAC activity based model prediction; (♦) – acetic acid; (■) – propylene glycol monoacetate; (▲) – propylene glycol diacetate; (×) – propylene glycol; (○) – water

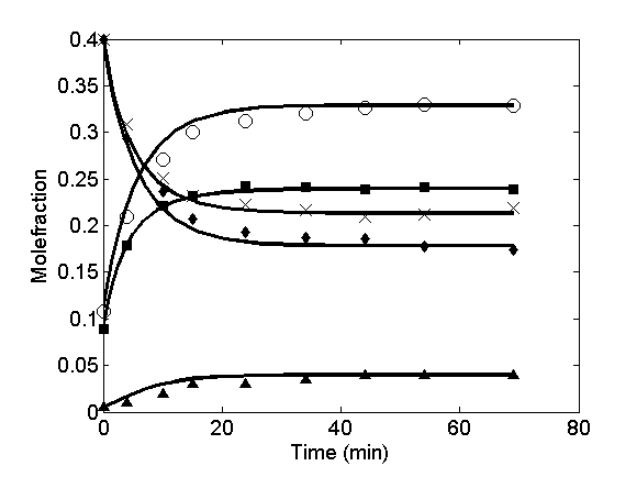


Figure 4.11: Experimental and predicted concentration profiles of PG acetylation (Experiment 7: 75 °C, 0.025 kg cat/kg soln, initial molar ratio PG:AA=1:1) (——) – UNIFAC activity based model prediction; (♠) – acetic acid; (■) – propylene glycol monoacetate; (▲) – propylene glycol diacetate; (×) – propylene glycol; (○) – water

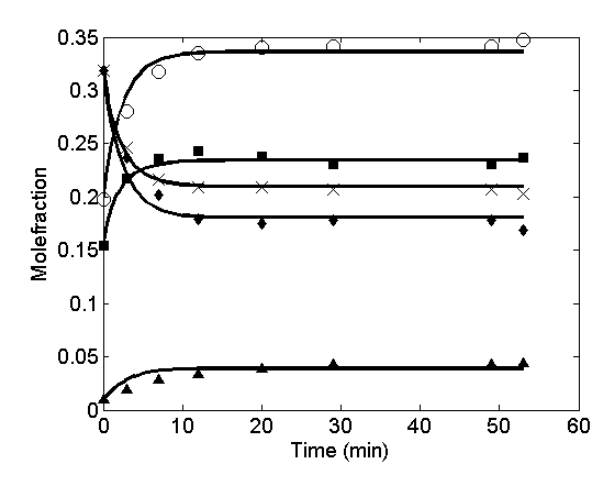


Figure 4.12: Experimental and predicted concentration profiles of PG acetylation (Experiment 8: 75 °C, 0.063 kg cat/kg soln, initial molar ratio PG:AA= 1:1) (———) – UNIFAC activity based model prediction; (♠) – acetic acid; (■) – propylene glycol monoacetate; (▲) – propylene glycol diacetate; (×) – propylene glycol; (○) – water

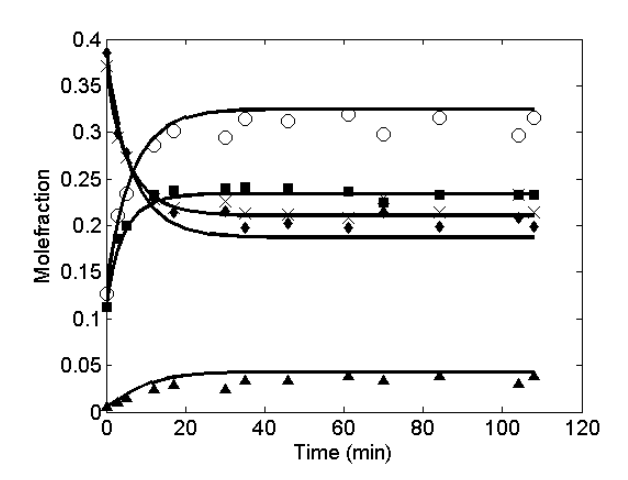


Figure 4.13: Experimental and predicted concentration profiles of PG acetylation (Experiment 9: 86 °C, 0.012 kg cat/kg soln, initial molar ratio PG:AA=1:1) (——) – UNIFAC activity based model prediction; (♠) – acetic acid; (■) – propylene glycol monoacetate; (▲) – propylene glycol diacetate; (×) – propylene glycol; (○) – water

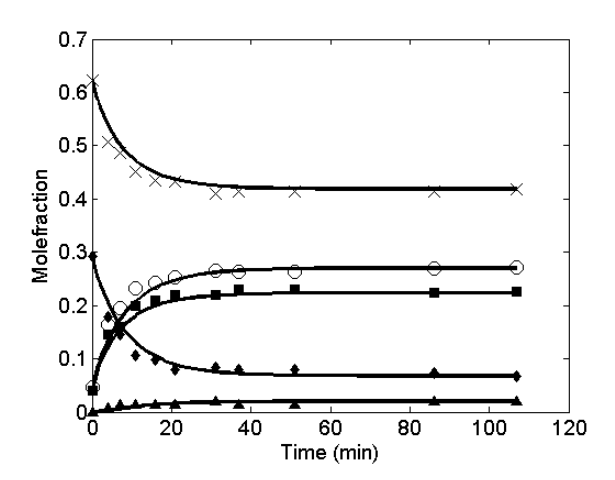


Figure 4.14: Experimental and predicted concentration profiles of PG acetylation (Experiment 10: 86 °C, 0.016 kg cat/kg soln, initial molar ratio PG:AA=2:1) (——) – UNIFAC activity based model prediction; (♠) – acetic acid; (■) – propylene glycol monoacetate; (▲) – propylene glycol diacetate; (×) – propylene glycol; (○) – water

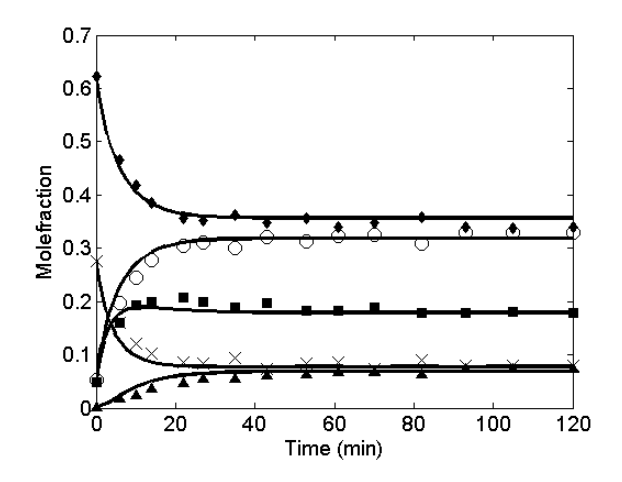


Figure 4.15: Experimental and predicted concentration profiles of PG acetylation (Experiment 11: 86 °C, 0.008 kg cat/kg soln, initial molar ratio PG:AA= 1:2) (——) – UNIFAC activity based model prediction; (♦) – acetic acid; (■) – propylene glycol monoacetate; (▲) – propylene glycol diacetate; (×) – propylene glycol; (○) – water

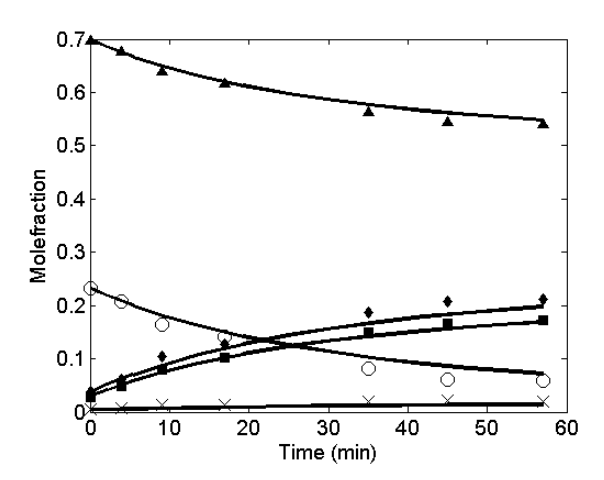


Figure 4.16: Experimental and predicted concentration profiles of PGDA hydrolysis (Experiment 12: 63 °C, 0.013 kg cat/kg soln, initial molar ratio PGDA:water = 3:1) (——) – UNIFAC activity based model prediction; (♦) – acetic acid; (■) – propylene glycol monoacetate; (▲) – propylene glycol diacetate; (×) – propylene glycol; (○) – water

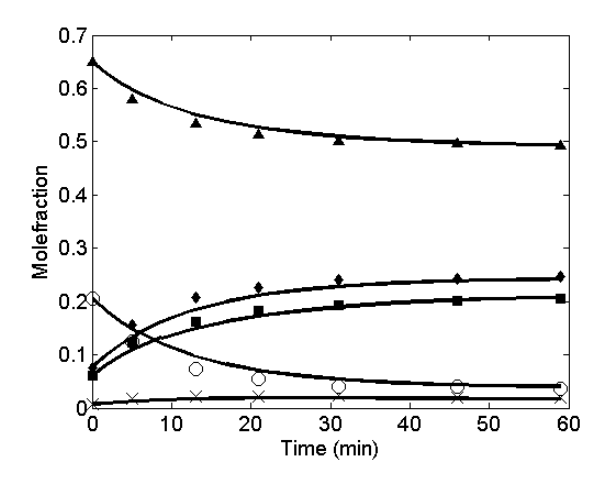


Figure 4.17: Experimental and predicted concentration profiles of PGDA hydrolysis (Experiment 14: 86 °C, 0.010 kg cat/kg soln, initial molar ratio PGDA:water = 3:1) (——) – UNIFAC activity based model prediction; (♦) – acetic acid; (■) – propylene glycol monoacetate; (▲) – propylene glycol diacetate; (×) – propylene glycol; (○) – water

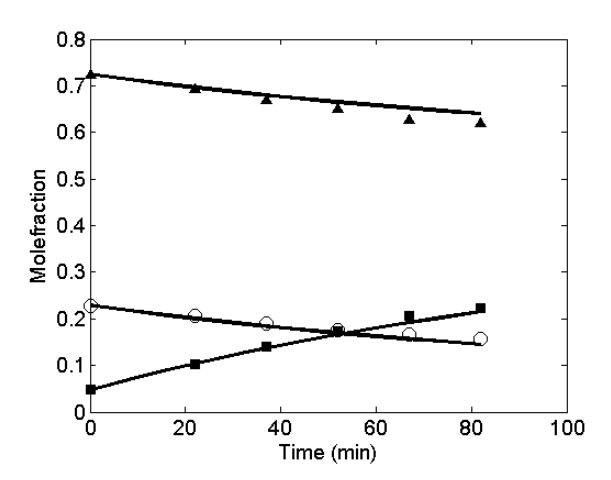


Figure 4.18: Experimental and predicted concentration profiles of PG transacetylation (Experiment 16: 75 °C, 0.004 kg cat/kg soln, initial molar ratio PGDA:PG=3:1) (——) − UNIFAC activity based model prediction; (♦) – acetic acid; (■) – propylene glycol monoacetate; (▲) – propylene glycol diacetate; (×) –propylene glycol; (○) – water

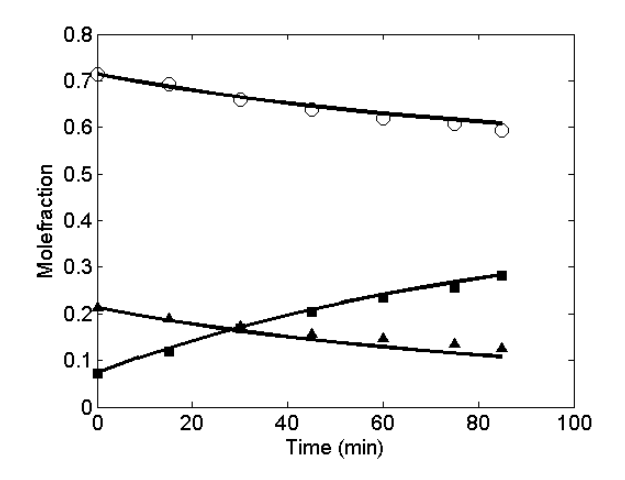


Figure 4.19: Experimental and predicted concentration profiles of PG transacetylation (Experiment 17: 65 °C, 0.007 kg cat/kg soln, initial molar ratio PGDA:PG=1:3) (——) − UNIFAC activity based model prediction; (♦) – acetic acid; (■) – propylene glycol monoacetate; (▲) – propylene glycol diacetate; (×) –propylene glycol; (○) – water

Appendix G. Raw data from propylene glycol esterification with acetic acid (conducted at Michigan Molecular Institute)

Data in Table 4.7 through Table 4.23 present relative molar quantities of each species as determined from *in-situ* NMR spectra of the reaction mixture.

Table 4.7: Experiment 1

Time (min)	AA	PGMA1	PGMA2	PGDA	PG
0	100	0.001	0.001	0.001	100
7	84	10	5	0.001	85
17	69	20	10	0.001	70
27	57.002	26	12	2	60
37	52.002	27	16	2	55
47	48.002	30	17	2	51
150	37.002	31	19	6	44

Table 4.8: Experiment 2

Time (min)	AA	PGMA1	PGMA2	PGDA	PG
5	83	12	5	0.001	183
15	55.002	27	14	2	157
25	42.002	34	20	2	144
35	37.002	38	21	2	139
45	32.002	40	24	2	134
150	24.002	46	24	3	127

Table 4.9: Experiment 3

Time (min)	AA	PGMA1	PGMA2	PGDA	PG
0	100	0	0	0	50
5	91.998	6	2	0.001	42
15	82	12	6	0.001	32
25	71.002	17	8	2	23
35	69	19	10	2	19
45	66	20	10	3	17
150	59	19	11	7	13

Table 4.10: Experiment 4

Time (min)	AA	PGMA1	PGMA2	PGDA	PG
4	187	11	6	1	82
8	163	26	11	2	61
12	150	33	13	4	50
16	141	35	17	6	43
22	133	37	19	7	37
33	122	39	20	11	30
45	120	39	19	11	31
53	118	41	19	14	26
60	116	41	19	15	25
72	116	42	19	15	24
82	112	38	19	16	27
90	109	40	19	19	22
112	111	39	19	19	22

Table 4.11: Experiment 5

Time (min)	AA	PGMA1	PGMA2	PGDA	PG
4	84	11	6	0	83
8	67	21	9	2	68
12	59	25	12	3	61
17	56	28	14	3	55
24	49	30	16	4	50
30	47	31	16	5	48
45	43	33	17	6	44
64	45	33	16	6	46
69	44	33	16	7	44
100	42	33	16	8	43

Table 4.12: Experiment 6

Time (min)	AA	PGMA1	PGMA2	PGDA	PG
6	88	9	4	0	87
19	64	23	11	2	64
24	59	26	12	2	60
30	55	27	14	3	56
35	52	29	14	4	53
42	49	30	15	4	52
54	45	31	16	5	48
59	46	30	17	5	48

Table 4.13: Experiment 7

Time (min)	AA	PGMA1	PGMA2	PGDA	PG
4	81	12	6	1	81
8	59	25	11	2	62
14	48	31	14	4	51
19	42	32	15	6	47
28	39	32	17	6	45
38	38	32	17	7	44
48	38	32	17	8	43
58	36	33	16	8	43
73	35	32	16	8	44

Table 4.14: Experiment 8

Time (min)	AA	PGMA1	PGMA2	PGDA	PG
4	66	22	10	2	66
7	49	30	15	4	51
11	42	32	17	6	45
16	37	33	17	7	43
24	36	32	17	8	43
33	37	33	15	9	43
53	37	31	17	9	43
57	35	32	17	9	42

Table 4.15: Experiment 9

Time (min)	AA	PGMA1	PGMA2	PGDA	PG
6	79	15	8	1	76
9	61	23	15	2	60
11	57	27	14	3	56
18	47	31	17	5	47
23	44	31	18	6	45
36	44	33	16	5	46
41	41	32	18	7	44
52	42	30	20	7	44
67	41	31	18	8	43
76	44	30	16	7	47
90	41	29	19	8	44
110	42	31	16	6	47
114	41	29	19	8	44

Table 4.16: Experiment 10

Time (min)	AA	PGMA1	PGMA2	PGDA	PG
4	44	4	2	0	94
8	27	14	8	1	77
11	21	14	9	2	70
15	16	19	11	2	68
20	15	21	11	2	66
25	12	22	11	2	65
35	13	23	11	3	63
41	12	21	14	2	63
55	12	23	12	2	63
90	11	22	12	3	63
111	10	22	12	3	63

Table 4.17: Experiment 11

Time (min)	AA	PGMA	PGMA2	PGDA	PG
5	192	10	5	0.1	85
11	139	31	17	5	48
15	125	33	25	7	36
19	114	36	23	11	30
27	105	36	25	14	25
32	104	36	23	16	25
40	107	37	19	16	28
48	104	36	23	18	22
58	107	34	21	19	25
66	100	36	18	20	25
75	105	35	22	20	22
87	108	37	17	19	27
98	102	34	20	22	24
110	102	33	22	22	24
125	102	36	18	22	24

Table 4.18: Experiment 12

Time	AA	PGMA1	PGMA2	PGDA	PG
(min)					
5.0	5.2	1.5	2.4	95.5	0.7
9.0	8.4	3.7	3.0	92.5	0.9
14.0	14.3	6.1	4.8	87.4	1.7
22.0	17.4	8.4	5.5	84.3	1.7
40.0	25.7	12.7	7.7	76.9	2.6
50.0	28.5	14.2	8.6	74.3	2.8
62.0	28.9	15.0	8.5	73.8	2.7

Table 4.19: Experiment 13

Time(min)	AA	PGMA1	PGMA2	PGDA	PG
4.0	6.9	2.4	2.6	94.0	0.9
10.0	14.5	6.7	4.9	86.9	1.4
20.0	22.5	11.1	6.7	79.8	2.4
30.0	26.5	13.4	7.6	76.3	2.8
50.0	30.0	15.4	9.0	72.8	2.8
62.0	30.0	15.8	9.4	72.4	2.4

Table 4.20: Experiment 14

Time (min)	AA	PGMA1	PGMA2	PGDA	PG
5	10.6	4.9	3.6	90.5	1.0
10	21.8	10.7	6.3	80.6	2.3
18	29.0	14.5	8.2	74.2	3.2
26	31.6	16.1	9.3	71.6	3.0
36	33.6	17.3	9.6	69.8	3.3
51	33.7	18.0	10.2	69.1	2.7
64	34.3	18.3	10.3	68.6	2.8

Table 4.21: Experiment 15

Time	mole fractions					
(min)	PG	PGMA1	PGDA	PGMA2		
0	0.71	0.049	0.213	0.024		
15	0.69	0.079	0.189	0.039		
30	0.66	0.112	0.173	0.055		
45	0.64	0.137	0.158	0.067		
60	0.62	0.156	0.147	0.077		
75	0.61	0.172	0.136	0.085		
85	0.59	0.186	0.126	0.095		

Table 4.22: Experiment 16

Time	mole fractions					
(min)	PG	PGMA1	PGDA	PGMA2		
0	0.228	0.032	0.72	0.015		
22	0.206	0.068	0.69	0.033		
37	0.190	0.094	0.67	0.046		
52	0.177	0.116	0.65	0.058		
67	0.166	0.138	0.63	0.068		
82	0.157	0.148	0.62	0.075		

Table 4.23: Experiment 17

Time	mole fractions					
(min)	PG	PGMA1	PGDA	PGMA2		
0	0.373	0.171	0.369	0.087		
15	0.336	0.223	0.328	0.113		
30	0.306	0.263	0.298	0.132		
45	0.283	0.296	0.272	0.148		
60	0.266	0.319	0.255	0.160		
75	0.252	0.339	0.240	0.169		

REFERENCES

REFERENCES

- (1) Vahteristo, K.; Laari, A.; Haario, H.; Solonen, A. Chem. Eng. Sci. 2008, 63, 587–598.
- (2) Gryglewicz, S.; Piechocki, W.; Gryglewicz, G. *Bioresour. Technol.* **2003**, 87, 35–39.
- (3) Ehrlich, A.; Smith, M. K.; Patton, T. C. J. Am. Oil Chem. Soc. 1959, 36, 149–154.
- (4) Morgan, P. W. Ind. Eng. Chem. Anal. Ed. 1946, 18, 500–504.
- (5) Seiden, P. Purifying propylene glycol monoesters using vacuum distillation. US3669848 A, June 13, 1972.
- (6) Shelley, S. Chem. Eng. Prog. **2007**, 103, 6–9.
- (7) Fredenslund, A.; Jones, R. L.; Prausnitz, J. M. *AIChE J.* **1975**, *21*, 1086–1099.
- (8) Eckert, C. A. Ind. Eng. Chem. 1967, 59, 20–32.
- (9) Eckert, C. A.; Hsieh, C. K.; McCabe, J. R. AIChE J. **1974**, 20, 20–36.
- (10) Santhanakrishnan, A.; Peereboom, L.; Miller, D. J.; Dumitrascu, A.; Smith, P. B. *Ind. Eng. Chem. Res.* **2013**, *52*, 9337–9342.

5 Catalytic epoxidation of propylene glycol and its acetates

5.1 Abstract

The base-catalyzed, gas-phase epoxidation of propylene glycol and its acetates to propylene oxide (PO) is investigated in a laboratory-scale fixed-bed reactor. Potassium salts (0.5-2.5 mmol/g) on silica gel support are identified as selective catalysts for the reaction. A temperature of 400 °C with short contact times has been found to be optimal, giving a maximum PO selectivity of 88% and 50% conversion of propylene glycol acetates. Higher temperatures and higher potassium loadings on silica gel lead to collapse of the support, resulting in reactor plugging. Pre- and post-reaction catalysts have been characterized by N₂ adsorption, XPS, EDS and FTIR. Bulk potassium carbonate has been found to be the stable active species on the support surface during reaction for loadings greater than 1.5 mmol/g K⁺ on silica. At lower loadings, potassium silicate is the active component. The use of a stable, low surface area silica support prevents the collapse of the support structure, leading to higher conversions without sacrificing selectivity.

5.2 Introduction

Propylene oxide (PO) is a valuable intermediate chemical with a global market of more than 9.2 million tonnes in 2014 that is expected to steadily increase in the future. PO is used to make many everyday products such as defoamers, anti-freeze, and lubricants in the form of polyglycols, polyurethanes and polyglycol ethers. Conventionally, PO is manufactured by the chlorohydrin process (Scheme 5.1) or by organic peroxidation (Scheme 5.2); both processes rely heavily on the availability of petroleum derived propylene. The chlorohydrin process involves

addition of stoichiometric amounts of chlorine and requires the disposal of aqueous solutions of sodium or calcium chloride of forty times the volume of PO produced, making the process a waste water burden.² The organic peroxidation route produces either *tert*-butanol or 1-phenyl ethanol as co-products, depending on whether the organic peroxide used is synthesized from *tert*-butane or ethyl benzene, respectively. These processes also produce side products such as methyl formate, which has a boiling point close to PO, making it difficult to separate. In the interest of reducing our reliance on fossil sources and shifting to more environmentally friendly processes, alternate routes to make propylene oxide are being investigated.

Scheme 5.2: *tert*-Butyl peroxide process

Although routes to make biomass based propylene are being investigated,³⁻⁶ clean and economical alternatives to the above mentioned processes for PO production are still under development, the most promising being the HPPO process (Dow Chemical). Biodiesel production by transesterification of triglycerides produces glycerol as a side product, providing the

opportunity to build reaction networks with glycerol as a building block. One such reaction of glycerol is hydrogenolysis to propylene glycol, which is being extensively studied^{7–10} and is commercially practiced by Archer Daniels Midland.¹ Thus, instead of the traditional pathway to propylene glycol from propylene derived propylene oxide, the pathway to propylene oxide from bio-glycerol derived propylene glycol becomes an attractive option.

Studies focusing on producing propylene oxide from propylene glycol in literature are broadly of two categories (Scheme 5.3). One route is the direct dehydration of propylene glycol to propylene oxide. The other is indirect; propylene glycol is converted to its esters with an abundantly available carboxylic acid, and the ester-glycol mixture formed is then converted to propylene oxide. The majority of catalysts tested for both routes were alkali or alkaline earth metal salts on neutral or weakly acidic supports such as silica and alumina. Other supports such as magnesium oxide, carbon and germanium dioxide loaded with similar base salts gave much lower yields (<7% by mole). Supports such as silica and supports such as salts gave much lower yields (<7% by mole).

Scheme 5.3: Routes from propylene glycol to propylene oxide

The optimized yield reported in multiple studies from both these routes using a variety of catalysts and processes is ~30%. The highest reported PG/PGMA conversions were for cesium on silica at 52%. Sodium and lithium gave maximum yields of 20 % and 3%, respectively.

The reaction of PG and its acetates to PO occurs at high temperature (>300 °C) in the gas phase and proceeds with the formation of various side products (Scheme 5.4). Most of these studies screen a number of catalysts, but good process design requires a thorough understanding of the effect of process parameters as well as fundamental catalyst properties.

In this study, several candidate catalysts were chosen and a detailed investigation of the effect of reaction temperature from 340°C to 420°C, feed material (PG vs. PG acetates), contact time, and the loading of catalytic salt on the support was conducted. Characterization of catalysts via N₂ BET surface area measurement and FTIR, XPS, and EDS surface analysis has also been done.

5.3 Materials and Methods

5.3.1 Materials

Reagent grade propylene oxide (99%, Sigma Aldrich Corp., St. Louis, Missouri), n-propanal (97%, Sigma Aldrich Corp., St. Louis, Missouri), PGDA (99.7%, Sigma Aldrich Corp., St. Louis, Missouri), acetic acid (glacial, Emanuel Merck Damstadt Chemicals, Philadelphia, Pennsylvania), PG (A.C.S Reagent, Jade Scientific Inc., Westland, Michigan), allyl alcohol(99%, ACROS Organics, New Jersey), 2-ethyl-4-methyl-1,3-dioxolane (Alfa Aesar, Ward Hill, Massachusetts), allyl acetate (99%, Sigma Aldrich Corp., St. Louis, Missouri), water (HPLC solvent, JT Baker Reagent Chemicals, Phillipsburg, New Jersey), acetone (JT Baker Reagent Chemicals, Phillipsburg, New Jersey), acetone (JT Baker Reagent Chemicals, Phillipsburg, New Jersey), cesium nitrate, potassium hydroxide (pellets, A.C.S Reagent, >85%, Sigma Aldrich Corp., St. Louis, Missouri), potassium acetate (>98%, Sigma Aldrich Corp., St. Louis, Missouri), potassium silicate (99%, anhydrous, Alfa Aesar, Ward Hill, Massachusetts), silica gel

(high purity grade, 60 Å, 35-70 mesh, 0.212-0.5 mm diameter, Sigma Aldrich Corp., St. Louis, Missouri), and controlled pore glass (507 Å, 200-400 mesh, 40-75 μ m, Controlled Pore Glass Inc., Lincoln Park, New Jersey) were used without further purification. The properties of Amberlyst 15 used to prepare feed are reported in the literature.²⁰

5.3.2 Feed preparation

Water content of propylene glycol and propylene glycol diacetate was measured by Karl Fischer titration and gas chromatography. Traces of water (<0.1 weight %) were found in both chemicals. Small amounts (<1% on basis of weight) of acetic acid were found in propylene glycol diacetate. Weighed amounts of propylene glycol and propylene glycol diacetate were dried with activated Drierite in their respective containers. After allowing the containers to sit overnight, the resulting solutions were again analyzed for water content and impurities using Karl Fischer and gas chromatography. PGDA and PG were then mixed in a 1:1 molar ratio with 2% by weight Amberlyst 15 catalyst (dried in a vacuum oven at 100°C for well over 2 days), and freshly activated drierite granules in a batch reactor set up at 70 °C. The final mixture was composed of 55 mol% primary and secondary propylene glycol monoacetates (in a ratio of primary:secondary = 1.7:1) and 22.5 mol% each of propylene glycol and propylene glycol diacetate.

5.3.3 Catalyst preparation

Catalysts were prepared by incipient wetness.¹² Pore volume of fresh silica support was measured to be 0.69 cc/g. Basic salt catalyst was impregnated by filling the pore volume with a solution containing the desired loading of the catalyst material. The catalyst was dried at 120°C overnight, and then calcined for 6 hrs. at 550°C under a steady flow of nitrogen gas prior to use.

5.3.4 Fixed bed reactor and condensation system

The reactor used was either a stainless steel or quartz tube of 0.5 in outer diameter and 43 cc volume. A thermoprobe (stainless steel or quartz) well was fitted axially along the length of the reactor to facilitate temperature readings at different positions during the course of the reaction. The furnace was a brass tube 12 inches in length with high performance (313 W, 120V) electrical heating tape wrapped snugly around it, and the rate of heating was regulated by a PID controller. Temperature readings inside the reactor were recorded in a data logger, initially at different positions along the length of the reactor and the pre-heat zone to get the temperature profile, and then during the remainder of the experiment, at the middle of the reactor bed zone. Borosilicate beads (2mm) or silicon carbide were used as packing material below and above the catalyst bed. Liquid feed was introduced at the top of the reactor through a 1/16" Stainless Steel tube just above the pre-heating zone. Liquid flow rate was maintained by an HPLC pump (Varian), or in the case of experiments with PO as feed, a syringe pump was used. Inert gas nitrogen (unless otherwise mentioned) flowed concentrically around the feed tube. Inert gas flow rate was maintained by a mass flow controller.

The reactor outlet connects to a two-chamber condenser system fitted with a three-way valve to direct product mixture to either chamber to enable continuous operation. The collection vessels (50 cc) were fitted with dip tubes and valves to collect samples during reaction. Depending on the cooling requirements of the product mixture, one or two stage condensation systems were used with either ice-water baths or at ~-79°C in dry ice-acetone baths. Non-condensable gases flowed out of a vent at the top of the collection vessels. Flow rate out of the reactor was measured by a gas bubble meter and recorded at regular intervals to ensure continuity of flow. The reactor

was also fitted with a pressure gauge (0-100psig) to monitor fluctuations in pressure in the reactor. The reaction was run at 1 atm, but a sudden rise indicated reactor plugging.

Before and after a reaction, weights of the reactor system and collected samples were recorded to calculate total mass recovery. The reactor was heated to the required temperature with a steady nitrogen flow rate. After the reactor stabilized at the required temperature, liquid feed flow was started (~0.1 mL/min). The first sample was collected after 3 hours, and 3-4 subsequent samples were collected at 1.5-2 hour intervals. Sample collection was alternated between the two collection vessels.

5.3.5 Analysis

Samples collected were diluted 10-fold in a solution of acetonitrile containing 5wt% decanol as the internal standard. All products were quantified by a Varian 450 GC (Varian Medical Systems Inc., Palo Alto, CA) fitted with two detectors, a thermal conductivity detector and a flame ionization detector. Separation was done on a 0.53mm ID Aquawax-DA 30 m capillary column with 1.0µm film thickness. Helium carrier gas flow rate was set to 10 mL min⁻¹. Injector temperature was 250 °C. The following temperature program was used: initial column temperature of 37 °C was held for 4 min, ramped to 90 °C at 10 °C/min and held for 3 min, then ramped to 150 °C at 10 °C/min, and finally ramped to 230 °C at 30 °C/min and held for 2 min. The temperatures of the TCD and FID were 240 °C and 300 °C, respectively.

Mass balances, propylene glycol backbone balance (Eq. 5.1), acetate species balances (Eq. 5.2) and overall carbon balances were done to ensure that the sample composition is representative of the reaction; these balances were consistently above 93% closure. Carbon balance values are reported in the Appendix H for each reaction in **Error! Reference source not found.**.

$$Acetate\ balance = \frac{n_{PGMA} + 2n_{PGDA} + n_{AA} + n_{allyl\ acetate}}{n_{0.PGMA} + 2n_{0.PGDA} + n_{0.AA}}$$
(5.1)

Propylene glycol balance =
$$\frac{n_{remaining \, reactants} + n_{products}}{n_{0,PGMA} + n_{0,PGDA} + n_{0,PG}}$$
(5.2)

 $n_{remaining \ reactants} + n_{products} = n_{PGMA} + n_{PGDA} + n_{PG} + n_{PO} + n_{propanal} + n_{acetone} + n_{allyl \ alcohol} + n_{allyl \ acetate} + 2n_{dioxolane}$

Conversion, PO selectivity, and PO yield were calculated from Eq. 5.3, 5.4, and 5.5 respectively.

$$conversion = \frac{initial\ moles\ feed-final\ moles\ feed}{initial\ moles\ feed} \tag{5.3}$$

$$PO\ selectivity = \frac{moles\ PO\ formed}{moles\ feed\ reacted} \tag{5.4}$$

$$PO \ yield = conversion \times PO \ selectivity$$
 (5.5)

5.3.6 Catalyst characterization

Qualitative FTIR studies of prepared and post-reaction catalysts were done. The catalyst samples were ground together with KBr in a 2% by weight mixture and pressed into a transparent tablet at 10000 psi in a dye press for approximately 5 minutes. The tablet was inserted into the FTIR spectrometer that was continually purged with nitrogen. Multiple spectra from 4000 cm⁻¹ to 500 cm⁻¹ were taken with each sample.

Thermogravimetric analyses were done in a TGA Q500 using a Hi-Res TGA furnace control method to determine decomposition temperatures.

Surface areas and pore size distributions were obtained from nitrogen adsorption and desorption isotherms obtained from an ASAP 2010 (Micromeritics Instrument Corporation, Norcross, Georgia). Base and acid site concentrations were determined from carbon dioxide and ammonia temperature programmed desorptions in an Autochem II Chemisorption Analyzer (Micromeritics Instrument Corporation, Norcross, Georgia).

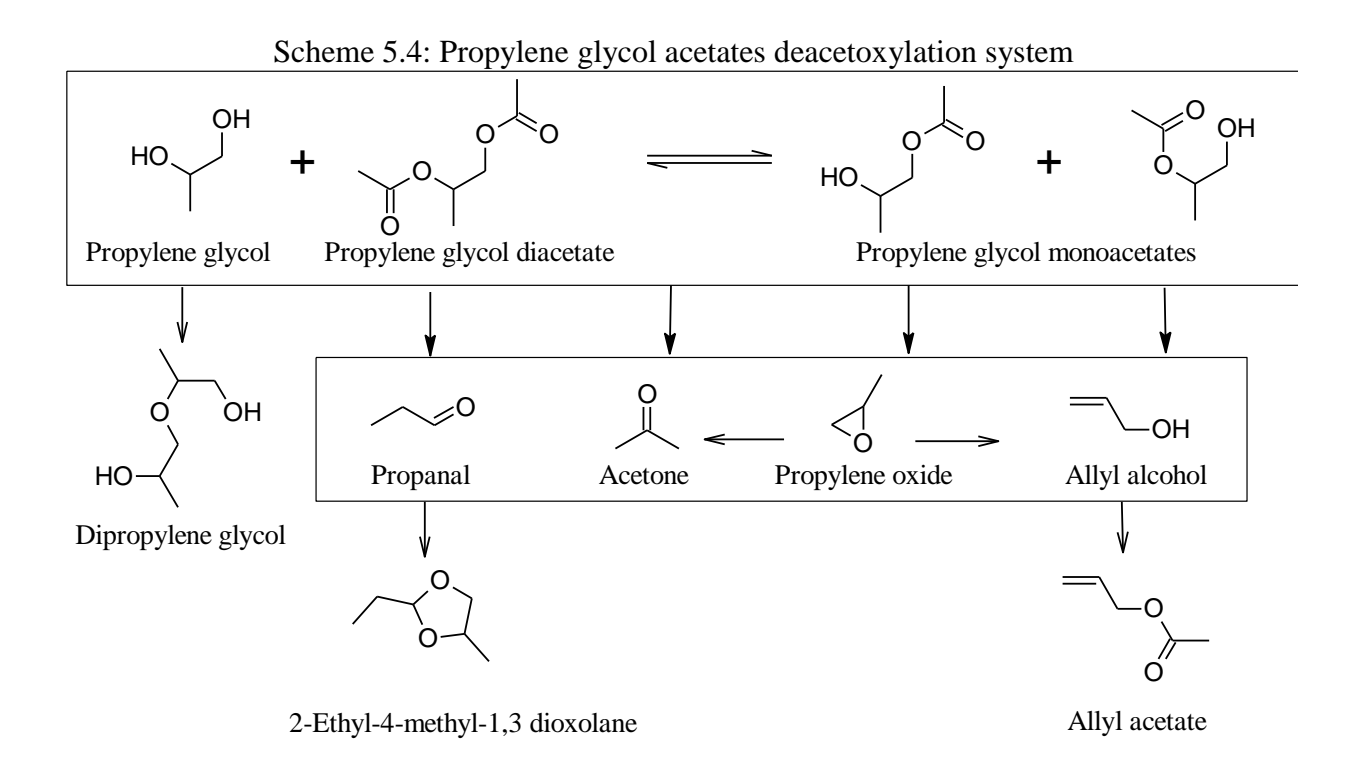
SEM images were obtained in an EVO-LS-25 (Carl Zeiss Microscopy, Thornwood, New York) variable pressure scanning electron microscope with a beam energy of 15-20 kV and an EDAX Pegasus camera. EDS analysis was done using TEAM software. XPS analysis was done using a Magnesium non chromatic source with a pass energy of 189 eV for survey scans and 29.5 eV for spectra. Spectra were collected at a base pressure of 5×10⁻⁸ Torr. Spectra were fitted and analyzed using PHI Multipak (Physical Electronics Inc.) software. A take-off energy of 45° was used.

5.4 Results

5.4.1 Thermodynamic Analysis of Reaction Network

An estimate of the feasibility of the reaction was obtained from Gibbs energies of reactions. The details of the parameters used are reported in Appendix K. Speculative mechanisms of the major reactions in the system are reported in Appendix J in Scheme 5.6. PO is formed from PG and its acetates by intramolecular substitution. Propanal, acetone and allyl alcohol are formed from PG by elimination mechanisms. Di-propylene glycol and other ethers are formed by intermolecular substitution. Propanal further reacts with PG to form a secondary side product, a 1,3-dioxolane. Allyl alcohol esterifies acetic acid to form allyl acetate. The isomerization of PO, a strained molecule, to its side products propanal and acetone by 1,2 H shifts, and to allyl alcohol by 1,4 H

shifts, is also highly favorable according to Gibbs energy estimates from this study and from literature. 18,19



5.4.2 Control Reactions

Preliminary reactions were carried out to understand the effect of thermal conditions and catalytic activity of the support. No reaction of PGMA was observed in reactions at 420 °C when the reaction was run with silica beads but no catalyst or support, indicating that the reaction is catalytic, and that the nature of the heating material used is inert.

Experiments with PO as feed in the absence of any catalyst were conducted to gauge if there is a thermal limit to selectivity. They showed little to no conversion of PO at reaction

conditions, a result in agreement with literature. ¹⁸ However, the mass balances for these reactions were poor, owing to the high volatility of both the reactants and the products. Experiments were also conducted with PO feed with catalyst, which showed up to 35% conversion to side products at 450 °C and 16% conversion at 400 °C. These findings are sufficient to state that PO is converted, but quantification of conversion rate is difficult without better product collection techniques. The boiling points of PO, propanal, acetone and allyl alcohol are 34 °C, 42 °C, 56 °C and 97 °C respectively, whereas the boiling points of PG, PGMA and PGDA are all within the range of 189 °C-191 °C. Thus, for low conversions of PO only feed, the boiling point of the reaction mixture was much lower than the boiling point of reaction mixtures with PG-PGMA feed. (Mass balances for experiments starting from PGMA feed were >93 %). Liquid nitrogen and dry-ice acetone baths proved unsuccessful in achieving total carbon recovery for PO isomerization experiments. Future attempts at doing PO isomerization kinetic experiments might include trapping PO chemically. Mass left behind in reactor was calculated from weight measurements before and after reaction, and did not account for a significant fraction of the feed.

The presence of acid sites is known to strongly favor the formation of propanal from PG, as well as the isomerization of PO. Less than 1% by mole of products, consisting only of propanal, were formed with reaction or PO over untreated silica gel support. This is expected because of the presence of a few acidic silanol groups on silica gel, leading to acid-catalyzed elimination. This was confirmed from ammonia TPD of the silica gel support, showing 1.8 mmol/g of acid sites for untreated silica gel, while calcined silica gel had an acid site density of 0.02 mmol/g rendering the support inert for all practical purposes. Further evidence of the near absence of hydroxyl groups in calcined silica gel support is provided from XPS spectra in Section 5.4.4.8.

5.4.3 Cesium nitrate on silica gel

The highest conversions reported in the literature were from cesium nitrate on silica, with a reported conversion of 52%. ¹² Early runs were conducted to attempt to replicate the results from literature. Cesium nitrate on silica catalyst was prepared by a method as close as possible to the literature description. ¹² Reaction conditions were maintained at reported conditions of a weight hour space velocity of 1.7 hr⁻¹ and a reaction temperature of 400 °C. However, the reactor was repeatedly found to plug at temperatures higher than 380 °C. This is probably due to fusion of cesium nitrate at around 400 °C, and the possible collapse of silica from reacting with alkali salts. ²¹ Experiments conducted at or below 375 °C are reported in Table 5.1.

Table 5.1: List of reactions run with 1.5 mmol/g CsNO3 on silica gel catalyst with space velocity =1.7 g feed/g catalyst/h

	Tomn	Conv.		Select	tivity (%)		Yield
No.	Temp (°C)	(%)	PO	Propanal	Acetone	Allyl alcohol	PO
1	351	36	10	13	18	5	4
2	351	18	29	29	16	11	5
3	352	20	26	31	17	11	5
4 ^a	374	46	9	34	18	9	4
5	384	29	13	43	28	12	4
6 ^b	375	44	13	6	4	3	5

a: partial pressure of feed reduced by half

b: PG only feed used

The reactions show results similar to other alkali metal catalysts at those conditions. Experiments at identical conditions to check the reproducibility (R2, R3) demonstrate good reproducibility. As temperature rises, the selectivity of feed to propylene oxide rises and then drops off, while selectivity to propanal increases. An increase in feed concentration in the gas phase leads to a decrease in selectivity of propylene oxide (R4), as expected. The overall yield of propylene oxide did not rise above ~ 6% on a molar basis.

A comparison experiment done at 375°C with pure propylene glycol as feed (R6) showed that the selectivity to propylene oxide was much higher than propanal selectivity. However, up to 72% of the reacted propylene glycol was consumed in the formation of ethers such as di propylene glycol and others, whereas with a mixture with propylene glycol acetates, selectivity to ethers was minimal. Therefore, a feed of a mixture of propylene glycol and its acetate mono and di-esters was used as feed in all successive reactions. Since the optimum results obtained for cesium catalysts were no higher than 5% yield, weaker base metal potassium was considered. Sodium and lithium showed poor results in literature.¹³

5.4.4 Potassium salt catalysts

Potassium catalysts on silica gave the next best conversion of ~45% in literature, in addition to being less expensive than cesium and rubidium. Detailed reaction studies were therefore conducted with potassium hydroxide catalyst to understand the effect of space velocity, temperature and concentration of base on silica gel (Table 5.2). A later experiment conducted with potassium catalyst on a stabilized, low surface area silica support, Controlled Pore Glass (Controlled Pore Glass Inc.) was also compared with the silica gel based catalysts to determine the effect of surface area, discussed in Section 5.4.4.8.

Table 5.2: List of experiments with KOH on silica gel

NI.	Loading (mmol	Temp	WHSV	Conv.			Yield		
No.	K ⁺ / g catalyst)	(°C)	(h ⁻¹)	(%)	РО	Propanal	Acetone	Allyl alcohol	PO
7	2.5	400	1.7	37	81	11	6	2	30
8	2.5	400	1.7	34	83	7	8	2	28
9	0.5	400	1.7	50	52	28	10	10	26
10	0.5	400	3.4	44	64	22	9	5	28
11 ^c	0.5	400	3.4	45	65	22	9	4	29
12	1.5	400	1.7	50	38	37	14	11	19
13	0.5	400	6.7	33	71	22	5	3	23
14	2.5	400	3.4	20	70	13	10	7	14
15	2.5	400	3.4	22	80	9	5	6	18
16	2.5	420	3.4	36	67	18	10	5	24
17	2.5	370	3.4	12	50	26	13	11	6
18	2.5	440	3.4	30	64	14	17	5	19

c: Methyl ethyl ketone promoter added, no improvement observed

5.4.4.1 Mass transport limitations

The effect of intraparticle mass transport limitation was determined by calculating the observable modulus and invoking the Weisz Prater criterion²² using data from a reaction at the lowest space velocity (highest contact time). The observable modulus $\phi_w = 1.11 \times 10^{-4}$, effectiveness factor η is >=0.99, and the rates observed can be assumed to be close to intrinsic rates. Details of calculations are reported in Appendix L.

5.4.4.2 Effect of weight hour space velocity

Weight hour space velocity (WHSV, g feed/g catalyst/hr), which is inversely related to contact time, was varied by increasing the amount of catalyst loaded into the reactor (R9-11, R13). There is an increase of conversion with decrease in WHSV as expected, but selectivity increases with increasing WHSV (Figure 5.1), indicating that isomerization of propylene oxide to side products propanal, acetone and allyl alcohol plays an important role in selectivity. PO

isomerization experiments were not successful due to due to difficulty in product collection. Additional experiments done at much higher space velocities are discussed later in Section 5.4.4.7.

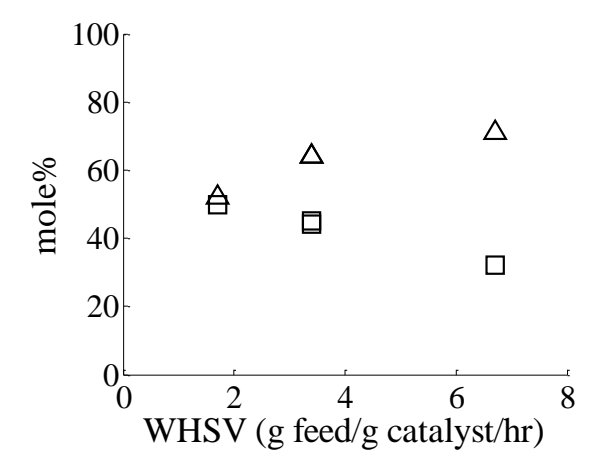


Figure 5.1: Conversion (\square), PO selectivity (Δ) vs weight hour space velocity. (T= 400 °C, 0.5 mmol/g of KOH in catalyst

The order of reaction was estimated using reaction runs at different contact times using integrated rate equations. A first order reaction rate fits the data reasonably well; corresponding zero-order and second-order fits gave poorer results. (Figure 5.2).

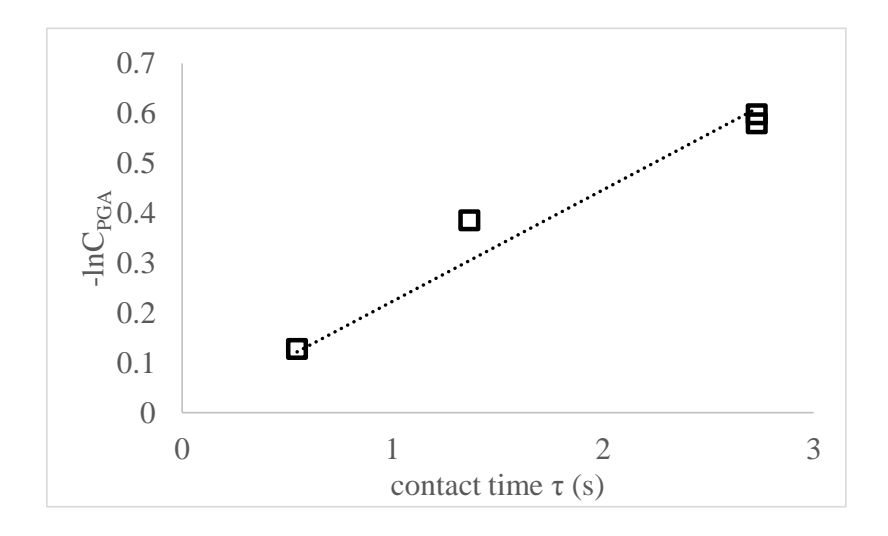


Figure 5.2: Rate constant vs contact time for a first order reaction A straight line through the origin fits the data with an R^2 value of 0.94

5.4.4.3 Effect of temperature

Figure 5.3 shows the dependence of conversion and selectivity on temperature of reaction. Conversion increases with temperature as expected until 420 °C, after which conversion is found to drop due to agglomeration of catalyst particles that results in poor accessibility to active sites in the catalyst.

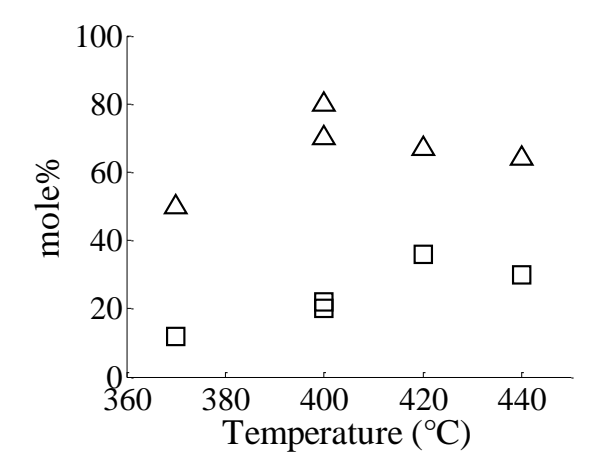
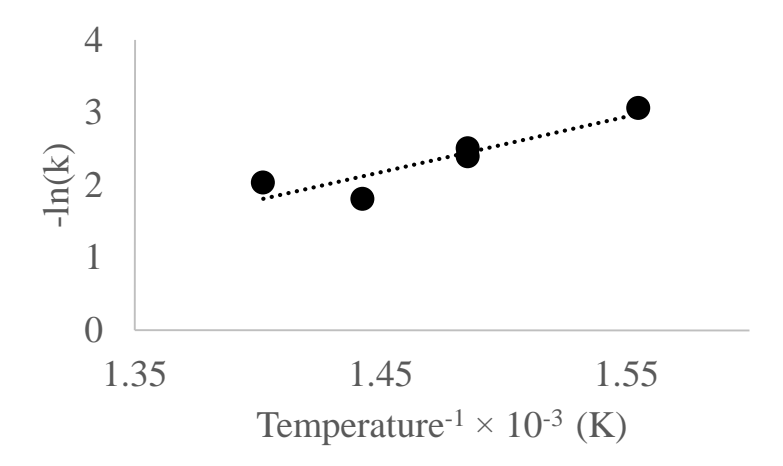


Figure 5.3: Conversion (\square), PO selectivity(Δ), temperature. (WHSV= 1.7 g feed/g cat/ h), loading = 2.5 mmol/g of KOH in catalyst) (R14 – R18)

Selectivity to propylene oxide is similarly shown to increase up to ~80% at lower temperatures and then decrease at higher temperatures. This is expected to result from higher rates of isomerization of propylene oxide and a preference for elimination reactions to propanal, acetone, and allyl alcohol over substitution reactions to propylene oxide at higher temperatures. Optimum temperature for selectivity is 400 °C, whereas overall yield is highest at 420 °C. A composite activation energy is obtained from an Arrhenius plot (Figure 5.4) of reactions over the temperature range of 370 °C to 440 °C.



 $E_a = 89.9 \text{ kJ/mole}, k_0 = 3.08 \times 10^7 \text{s}^{-1}$

Figure 5.4: Arrhenius plot of composite reaction of PGA to products (R14-R18)

The rate constant in Figure 5.4 is derived from first order kinetics in a plug flow reactor. Ln k = $-\ln(1-X)/\tau$ where X is conversion on basis of PG and PGA, while τ is the contact time of the feed in the reaction bed. Activation energy is obtained from the slope to be 89.9 kJ/mole, while a composite pre-exponential factor is obtained from the exponent of the intercept as 3.08×10^7 s⁻¹.

5.4.4.4 Effect of catalyst loading

The effect of the loading of KOH on silica gel was studied (R7 – R9, R12 of Table 5.2). At higher loadings, conversion was found to significantly drop, although there was a sharp increase in PO selectivity (Figure 5.5). This is a result of the silica pore structure collapsing at higher base loading, as described below.

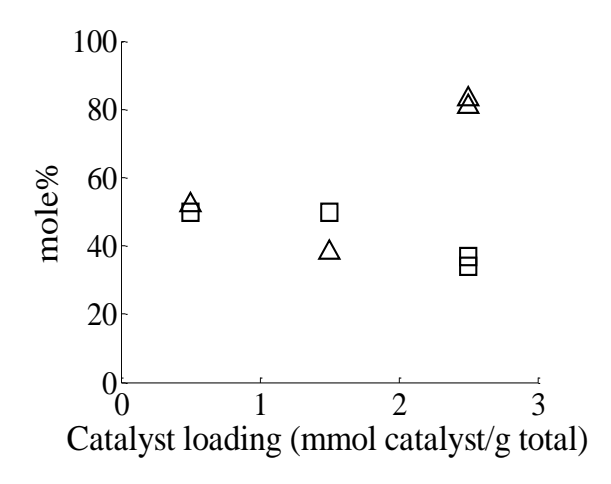


Figure 5.5: Conversion (\square), PO selectivity (Δ) vs catalyst loading. (T= 400 °C, WHSV = 1.7 g feed/g cat/h)

5.4.4.5 Surface area studies

Surface areas measured by BET/nitrogen method at various stages of catalyst preparation and post reaction are reported (Table 5.3). As catalyst loading is increased, the silica support is collapsed to greater degrees, leading to a corresponding decrease in surface area of catalyst.

Table 5.3: Surface areas of KOH on silica gel catalysts and supports determined by N₂ adsorption (BET method)

Catalyst	Surface area (m²/g)
Silica gel uncalcined	514
Silica gel calcined	474
2.5 mmol KOH/g on SiOx (impregnated, dried at 100 °C)	27
2.5 mmol/g KOH on SiOx calcined (fresh)	3.0
2.5 mmol/g KOH on SiOx calcined (used)	0.2
1.5 mmol KOH/g catalyst used	12
0.5 mmol KOH/g catalyst used	94
0.5 mmol/g KOH on silica gel (fresh, calcined)	115

The compounded effect of surface area and catalyst loading is considered in greater detail in Section 5.4.4.8.

5.4.4.6 Chemical nature of catalyst during reaction

Alkali metal salts on silica can react or remain unchanged, depending on a number of factors including temperature, basicity and loading of alkali metal, and type of support used, which in turn affects the activity and selectivity of the catalyst. Acetic acid is liberated during the conversion of propylene glycol acetates. It may therefore be hypothesized that potassium hydroxide on the support is neutralized to potassium acetate, which in turn ketonizes to potassium carbonate with the liberation of acetone at ~400 °C, as described in Scheme 5.5. Potassium carbonate may be the stable form of the catalyst under reaction conditions.

Scheme 5.5: Formation of potassium carbonate on surface of catalyst during reaction

1) Reaction in catalyst bed: liberation of acetic acid

propylene glycol mono acetate propylene oxide acetic acid

2) Potassium hydroxide reacts to form potassium acetate

$$HO-K$$
 + \longrightarrow O

potassium acetate

3) Ketonization of potassium acetate

$$O = \left(\begin{array}{c} \Delta \\ O - K \\ \text{potassium carbonate} \end{array} \right) + \left(\begin{array}{c} O \\ - K \\ \end{array} \right)$$

Thermogravimetric analysis of neat potassium acetate shows a sharp weight loss at approximately 400 °C (Figure 5.6).

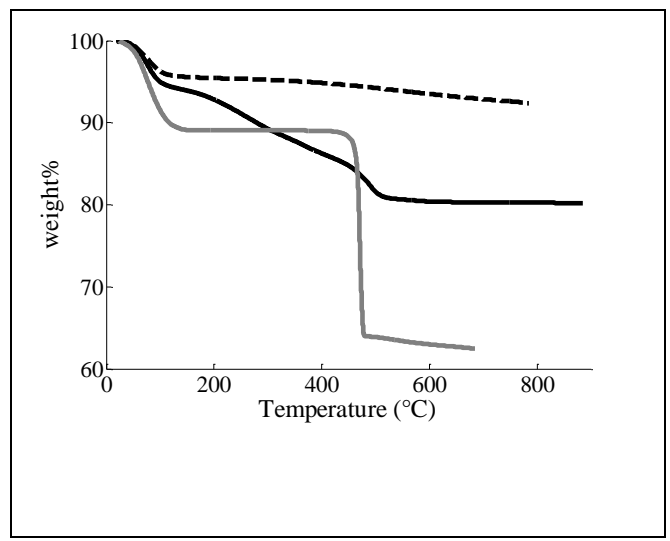


Figure 5.6:Thermogravimetric analyses 1.

(——) KOAc on silica, 2. (——) silica gel, 3.

(——) neat KOAc

The weight loss recorded is equal to the expected stoichiometric loss of acetone in the conversion of potassium acetate to potassium carbonate via ketonization (Reaction 3 of Scheme 5.5). Silica gel loaded with potassium acetate undergoes sharp weight losses at 120 °C, 250 °C and 380 °C. The first is the loss of water molecules on the silica gel support, identical to the weight loss peak in silica gel alone at the same temperature. The second drop is the loss of water remaining from the preparation stage, and the third is the ketonization of potassium acetate to potassium carbonate. Calculations show that the third peak is equal to the expected stoichiometric loss in weight from acetone (29.3%) (calculations in Appendix M). Unfortunately, the amount of acetone liberated from the catalyst during experiments (expected to be ~0.5-2.5 mmol) was miniscule comparison to the acetone produced as a side product of formation of propylene oxide to be accurately quantified. The TGA of silica gel shows the loss of hydroxyl groups with increase in temperature. K₂CO₃ has a decomposition temperature higher than 800 °C.²¹ Acetic acid liberated

during reaction apparently reacts with potassium hydroxide to form potassium acetate, which subsequently becomes potassium carbonate after ketonization (Scheme 5.5).

5.4.4.7 Experiments with KOAc, K₂CO₃ and K₂SiO₃ based catalysts

At loadings of catalyst higher than 2.5 mmol KOH/g, the catalyst was found to plug the reactor similar to cesium nitrate from dissolution of silica, forming glassy non porous clumps at room temperature at loadings higher than 5 mmol KOH/g. In order to make catalysts with higher concentrations of base salt on support, catalysts made with weaker basic salt KOAc were tested and are reported in Table 5.4. A loading of 5 mmol/g KOAc on silica was found to have no significant improvement over 2.5 mmol/g KOAc on silica (R19 and R20). It is also observed that the activity of the KOAc catalyst is very similar to a KOH catalyst of the same loading (R14 and R15 of Table 5.2).

Table 5.4: Experiments conducted with KOAc at temperature of 400C and WHSV = 3.4 g feed/ g cat/h

No	Loading (mmol	Temp	WHSV	Conv.			Yield		
	K ⁺ / g catalyst)	(°C)	(h ⁻¹)	(%)	РО	Propanal	Acetone	Allyl alcohol	PO
19	2.5	400	3.4	21	72	12	16	0	15
20	5.0	400	3.4	22	60	14	16	10	13

Reactions using K_2CO_3 as base salts on support were then carried out to compare their activity and selectivity with the KOH and KOAc catalysts. These along with other reactions using K_2CO_3 are reported in Table 5.5.

Table 5.5: Experiments conducted with 1.25 mmol K₂CO₃/g catalyst at 400 °C

No.	Catalyst	WHSV	Conv. (%)	•						
NO.	base on silica gel	(h ⁻¹)		РО	Propanal	Acetone	Allyl alcohol			
21	K ₂ CO ₃	3.4	25	67	25	7	3	17		
22 ^d	K ₂ CO ₃	3.4	30	63	26	9	3	19		
23	K ₂ CO ₃	17.1	12	84	12	3	2	29		
24 ^d	K ₂ CO ₃	17.1	8	88	9	2	0.2	20		

d: carbon dioxide used as feed carrier gas instead of nitrogen

R14, R19 and R21 with KOH, KOAc and K2CO3 loaded on silica show similar conversion and selectivity at identical reaction conditions. An additional experiment carried out (R 22) to determine the effect of carbon dioxide as feed carrier gas was done, however, no significant improvement was observed in the reaction yield or conversion.

Additional experiments done with very high weight hour space velocities of 17.1 h⁻¹, or short contact times of 0.56 s (R23, R24 in Table 5.5) yielded selectivity as high as 88%, but with correspondingly lower PGMA conversion of 8% by mole.

5.4.4.8 FTIR and XPS analysis of catalysts

To ascertain the presence of carbonate species, FTIR spectra of fresh and used KOH and KOAc catalysts were obtained (Figure 5.7).

e: partial pressure of feed reduced by half

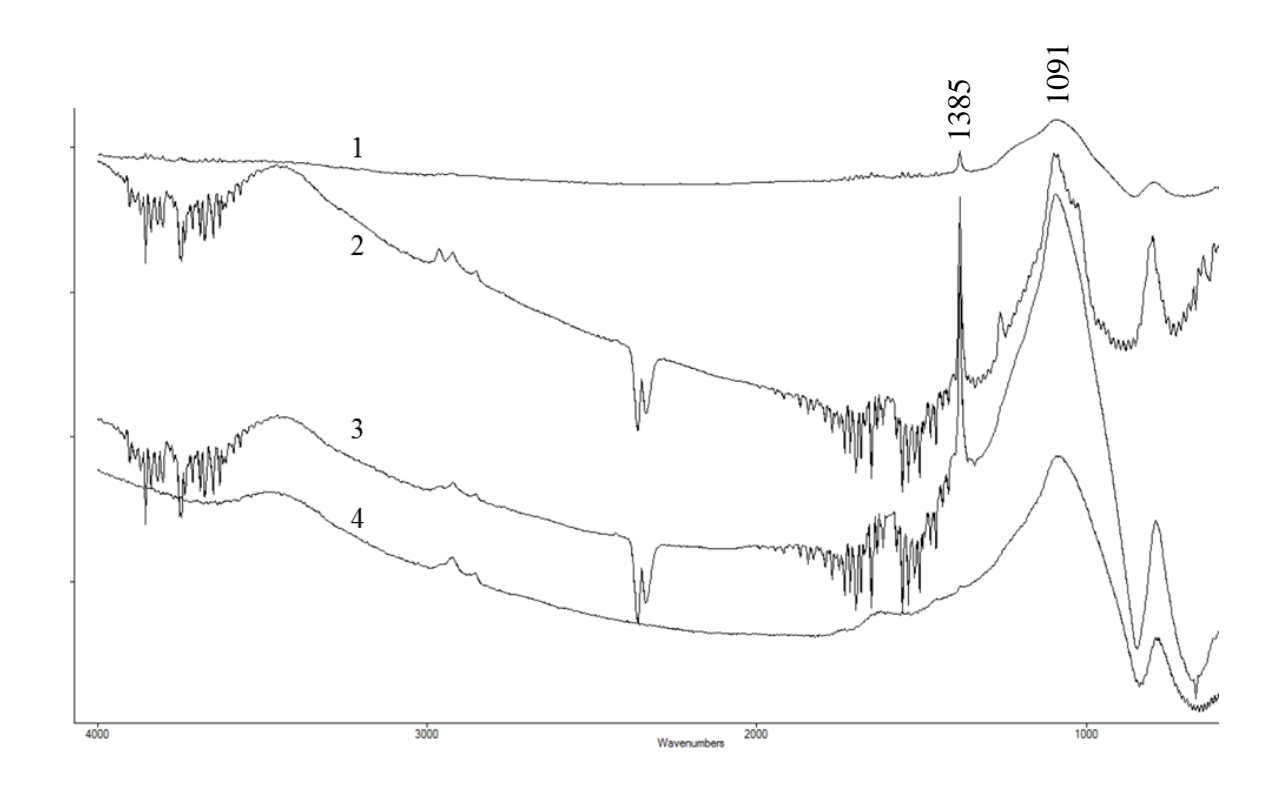


Figure 5.7: Absorbance FTIR analyses of fresh and used catalyst samples. (1: 1.25 mmol/g K₂CO₃ on silica, 2: post reaction 2.5 mmol KOAc/g on silica, 3: post reaction 2.5 mmol/g KOH on silica, 4: unused 2.5 mmol/g KOH on silica)

The sharp peak at 138 cm⁻¹ has been previously characterized as the presence of bulk carbonate,²³ while 1541 cm⁻¹ is associated with supported carbonate. No peak is observed at 1541 cm⁻¹, associated with bicarbonate or supported carbonate species on silica.²³ Si-O-Si bending in silica is observed at 810 cm⁻¹ in the silica gel spectrum. The large peak at 1091 cm⁻¹ is attributed to Si-O-Si bond stretching,^{23–26} with the shoulder being attributed to skeletal stretching.²⁶ The presence of Si-O-K bonds in potassium silicate would shift the stretching peak to lower wave numbers due to the lengthening of the bond,^{26,27} but the Si-O-Si stretching peak remains at 1091 cm⁻¹ indicating that no significant potassium silicate is present. IR spectra of neat potassium silicate and potassium silicate on silica gel show a characteristic peak at 958 cm⁻¹, not seen in fresh

or used spectra of any loading of KOH, KOAc or K₂CO₃ catalysts. There is, however, a shift to lower wave numbers of the Si-O-Si bending peak to 788 cm⁻¹, indicating an increase in proportion of non-bonding oxygens.²⁶

FTIR spectra of used samples of lower loadings of KOH (0.5 mmol and 1.5 mmol /g catalyst), and K2CO3 on CPG are shown in Figure 5.8.

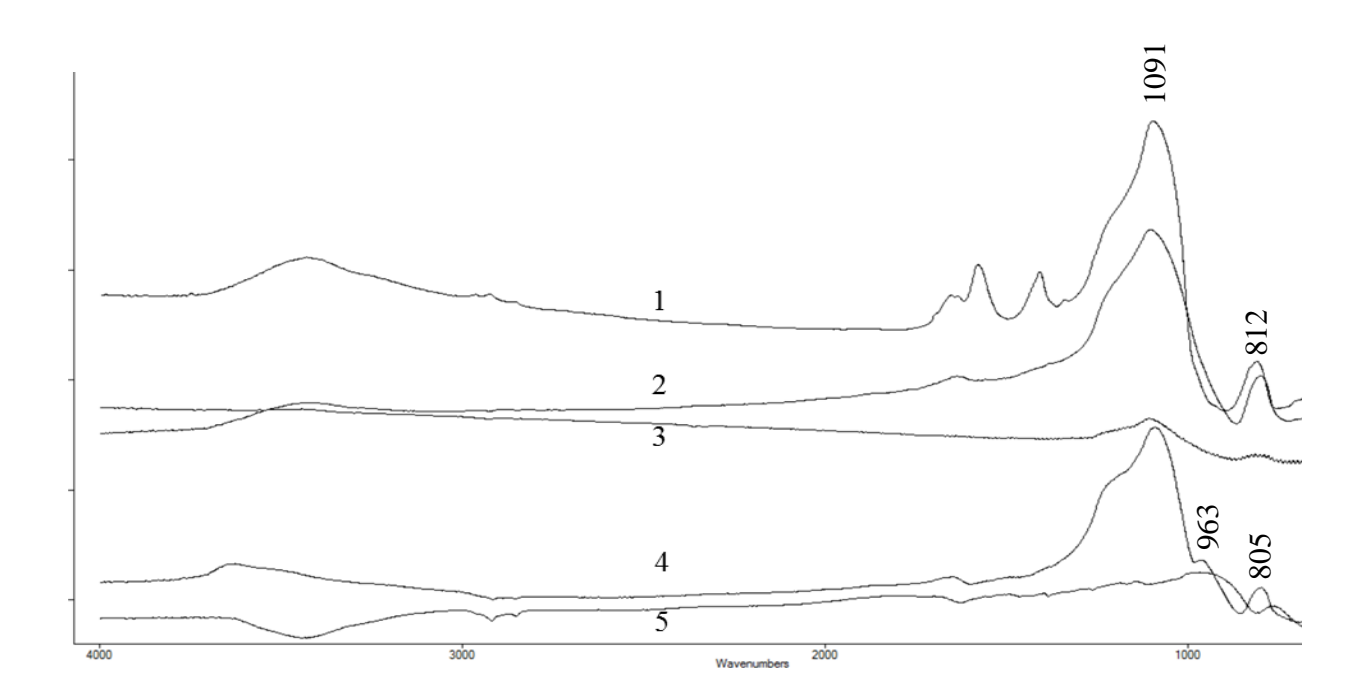


Figure 5.8: Absorbance FTIR analyses of fresh and used catalyst samples. (1: silica gel support, 2: calcined fresh 1.5 mmol KOH/g on silica, 3: post reaction 1.5 mmol/g KOH on silica, 4: unused 1.25 mmol/g K₂SiO₃ on silica, 5: neat K₂SiO₃)

There is no bulk carbonate peak observed in lower loading KOH catalysts and in potassium carbonate on CPG. Calculations done to estimate monolayer coverage of catalyst show that there is less than monolayer coverage of potassium salts on the surface for the catalysts with lower loadings and Controlled Pore Glass due to their much higher surface areas.

No peak is observed at 1541 cm⁻¹, associated with bicarbonate or supported carbonate species on silica.²³ It therefore becomes probable that there are some Si-O-K bonds formed in the micropores of the silica gel, but not enough to be visible on the IR spectra. There is no prominent silicate peak observed on these catalysts either, although there is a slight bump on the lower wavenumber side of the Si-O-Si peak at 1091 cm⁻¹. There is no significant shift in Si-O-Si stretching or bending peaks.

In order to ascertain the presence of Si-O-K bonds on lower loading KOH catalysts or on K_2CO_3 on controlled pore glass, XPS spectra of post reaction samples of those catalysts were obtained.

Table 5.6: Binding energy peaks from XPS spectra for calcined support silica gel, neat K₂O:SiO₂ and neat K₂CO₃.

Sample	K ₂ C0	O_3	K ₂ O:S	SiO ₂	Silica gel	calcined
	Binding Energy	Area %	Binding Energy	Area %	Binding Energy	Area %
C 1s	284.4	14.7	283.4	7.1	Energy	70
	285.3	32.7	284.8	83.6		
	287.1	51.4	286.3	0.6		
	288.8	1.1	287.8	8.8		
O 1s	531.7	16.8	530.6	43.7	533.1	
	533.1	64.3	532	56.4		
	534.8	18.9				
Si 2p	NA	NA			103.9	
K 2p	292.5	63.6	292.6			
	295.3	28.7	295.4			

Silica gel calcined at 550 for 6 hours (Table 5.6) shows only one peak in its Si 2p spectra at 103.9 eV, and one peak in its O 1s spectra at 533.1 eV. Both these are attributed to vitreous silica with no non-bridging oxygens.²⁸ The binding energy of Si atoms depends on the nature of the O atoms bonded to it. Since K atoms are much less electronegative than Si atoms, the valence

electron density around a non-bridging O atom is higher. The mutual screening leads to destabilization, leading to lower binding energies. The Si 2p spectra for K₂O:SiO₂ shows lower values of binding energy for Si atoms in the presence of K₂O. The O 1s values of neat potassium silicate show a peak for bridging O (533.1 eV) and another peak for non-bridging O attached to K atoms at lower binding energies of 528-530 eV.²⁹ Carbonate and bicarbonate peaks for C 1s spectra are at 287 eV and 289 eV respectively.³⁰ This is confirmed from the samples of neat K₂O:SiO₂ and neat K₂CO₃. The C1s spectra of K₂O:SiO₂ shows some adventitious carbon probably deposited during analysis at 284-285 eV.

Table 5.7: Binding energy peaks from XPS spectra for 2.5 mmol K⁺/g catalyst made from KOH, KOAC and K₂CO₃.

Troff, from and freedy.									
	2.5 mmol/g KOH on silica gel		2.5 mm KOAc or		1.25 m K ₂ CO ₃ o		1.25 m K ₂ CO ₃ o		
Sample				gel		gel		l	
	Post re	eaction	Post rea	ction	Calcined,	unused	Post rea	Post reaction	
	Binding	Area %	Binding	Area	Binding	Area	Binding	Area	
	Energy	Alea %	Energy	%	Energy	%	Energy	%	
C 1s	285.3	54.6	284.9	29.4	285.2	15.6	283.9	15.8	
	286.4	34.6	286.8	70.6	286.9	84.4	284.9	47.4	
	289.2	10.8					286.9	27.9	
							288.4	5.4	
							289.8	3.4	
O 1s	530.7	4.2	530	1	530.8	7.7	531.1	8.6	
	532.2	56	532.3	18	532.1	31	532.5	27.2	
	533.7	34.5	533.7	40.9	533.4	44.6	533.7	19.7	
	534.5	5.4	534.5	40.2	534.5	16.8	534.5	44.6	

Table 5.7 shows the binding energies from XPS spectra for 2.5 mmol K^+/g catalyst made from KOH, KOAC and K_2CO_3 . The peaks from C 1s spectra at 286.4-286.9 eV may be attributed to the bulk carbonate found on these catalysts from post reaction FTIR runs, along with lower peaks 284-285 eV attributed to lower oxidation states of C 1s, are probably due to carbonaceous

deposits during reaction or contamination during XPS analysis. Strong peaks at 532.2-534.5 eV are attributed to bridging O atoms in the silica support bulk and the bulk carbonate species. There are probably minor amounts of Si-O-K bonds present, as visible from lower peaks at ~530 eV²⁶.

Table 5.8 shows binding energy peaks for lower loadings of KOH on silica gel (0.5 and 1.5 mmol/g). The C 1s spectra for 0.5 mmol/g KOH do not show any significant amounts of peaks at 287 eV or higher both before and after reaction, whereas 1.5 mmol/g KOH on silica gel shows small amounts of carbonate at 286.5 eV. Definite peaks at 528-530 eV confirms the presence of Si-O-K bonds that prevail during reaction for both lower loadings on silica gel and controlled pore glass (CPG) catalysts.

Table 5.8: Binding energy peaks from XPS spectra for lower loadings of KOH on silica gel (0.5 and 1.5 mmol/g)

	01 K	OH OH SHI	ica gei (0.5 a	na 1.5 n	iiioi/g)	
	0.5 mm	nol/g	0.5 mm	nol/g	1.5 mm	ol/g
Sample	KOH or	silica	KOH on	silica	KOH on	silica
	ge	1	gel		gel	
	Calcined, unused		Post rea	ction	Post rea	ction
	Binding	Area	Binding Area		Binding	Area
	Energy	%	Energy	%	Energy	%
C 1s	281.7 86.8		282.5	29.4	283.3	41.8
	285.1	13.2	284.9	27.5	285	40.1
			286.4	2.8	286.5	13.5
			287.9	1.9	288	4.7
O 1s	528.5	4.7	528.7	3.5	528.9	2
	531.2	6.2	530.1	11.2	530.7	8.3
	532.8	89.1	531.4	23.1	532.1	32.5
			532.5	53	533.1	47.6
			533.6	9.2	534.3	9.6

A potassium silicate catalyst of loading 1.5 mmol/g shows similar activities as the lower loadings of KOH on silica gel (R25 of Table 5.9). This is further proof of the chemical nature of those catalysts.

Table 5.9: Potassium silicate on silica gel at 400 °C

No	Catalyst base on	Loading (mmol	WHSV	Conv.		Selectivity (%)				
No.	silica gel	K ⁺ / g catalyst)	(h ⁻¹)	(%)		Propanal	Acetone	Allyl alcohol	РО	
25	K ₂ SiO ₃	1.5	3.4	53	42	33	10	15	22	

The above findings indicate that in the case of lower loadings of KOH on silica gel, the primary active component is potassium silicate. At higher loadings (>1.5 mmol K/g catalyst), there is a substantial change to potassium carbonate, which is present as bulk on the surface of the catalyst, and is the primary active component.

5.4.4.9 Monolayer coverage calculations and controlled pore glass catalysts

The effect of the loading of KOH on silica gel was studied earlier on in our experiments (R7-9, and R12 of Table 5.2). At higher loadings, conversion was found to significantly drop, although there was a sharp increase in PO selectivity (Figure 5.5). The effect of catalyst loading is compounded with the effect of catalyst surface area. As catalyst loading is increased, the silica support is collapsed to greater degrees, leading to a corresponding decrease in surface area of catalyst (Table 5.3 in section 5.4.4.5 and Table 5.10 below). This prompted a more detailed look into the nature of the catalysts when impacted by one of the two or both factors.

Table 5.10: Surface areas of catalysts and supports determined by N₂ adsorption (BET method)

Catalyst	Surface area (m²/g)
1.25 mmol/g K ₂ CO ₃ on SiOx calcined (fresh)	2.5
Unsupported K ₂ CO ₃	3.0
Controlled pore glass (CPG)	37
1.25 mmol/g K ₂ CO ₃ on CPG calcined (fresh)	34
1.25 mmol/g K ₂ CO ₃ on CPG calcined (used)	32

Among the silica gel catalysts, simple calculations show that at the loading equal to full monolayer coverage of the two dimensional silica surface, the conversion is the highest. Assuming a hexagonal or cuboid arrangement of silica molecules, the number of moles of Si-O- bonds available on the surface approximated to a plain two dimensional areas was calculated. This gives us the maximum loading for a monolayer coverage. This optimal monolayer value is a loading of 1.5 mmol/g KOH, in which the surface area of the support is decreased to 12 m²/g, which is seen in Figure 5.10.

Surface area measurements of catalyst and support show an almost complete collapse of silica surface area (from $514 \text{ m}^2/\text{g}$ to $0.2 \text{ m}^2/\text{g}$) at high (2.5 mmol/g) loadings of KOH. There is some collapse to $27 \text{ m}^2/\text{g}$ on impregnation of KOH, but after calcination, the surface area is further reduced to $3.0 \text{ m}^2/\text{g}$. This is attributed to temperature dependent structural modification of silica in presence of alkali salts. The surface area of the neat potassium carbonate salt used in experiments was measured to be $2.5 \text{ m}^2/\text{g}$, nearly identical to loaded potassium carbonate. Reactions R21in Table 5.5 and R25 in Table 5.11 compare the activity and selectivity of the same

molar loading of neat K₂CO₃ and 1.25 mmol/g K₂CO₃ on silica with identical contact time and temperature.

Table 5.11: Experiments done to determine the effect of surface area with 1.25 mmol/g K₂CO₃

No.	Support	Temp (°C)	WHSV	Conv.		Selectivity (%)				
110.	Support	(°C)	(h ⁻¹)	(%)	PO	Propanal	Acetone	Allyl alcohol	PO	
26 ^f	Neat	400	1.7	29	53	30	15	2	12	
27 ^g	CPG	400	3.4	44	75	14	7	4	33	

f: neat potassium carbonate used without silica support

time, and are used to compare the activity of different catalysts. Neat K_2CO_3 has a turn over number of $\sim 3.40 \, h^{-1}$ and loaded K_2CO_3 has a turn over number of $\sim 7.1 \, h^{-1}$. Although neat K_2CO_3 has more moles of K^+ by weight, they are less dispersed. The surface density of neat K_2CO_3 is 0.19-0.2 mmol/g of catalyst, whereas the saturated monolayer surface density of supported K_2CO_3 is 0.25-0.29 mmol/g. Reactions R24 and R26 compare the effect of support surface area: both activity and selectivity of the controlled pore glass is higher, indicating that higher surface areas and higher loadings are optimal for selectivity.

Separate experiments with controlled pore glass were done (R 26) to separate the effect of surface area and catalyst loading. In order to disperse higher loadings, higher surface area supports that are chemically stable were required. Controlled pore glass was much more stable towards the attack of potassium base salts, with a surface area of 32 m²/g such that at loadings as high as 2.5 mmoles/g K+, the surface of the catalyst was not fully covered, and no drop in conversion was observed (R 26), in fact, the advantage of higher loadings, the higher selectivity is also achieved.

g: potassium carbonate on controlled pore glass with higher surface area support
Turn over numbers are a measure of moles reacted per mole of base site on catalyst in unit

The turn over number for K_2CO_3 on CPG is $10.4 \, h^{-1}$. This is much higher than the aforementioned turn over numbers for neat K_2CO_3 and loaded K_2CO_3 on silica gel.

FTIR spectra of CPG catalysts are shown in Figure 5.9. There is a distinct peak at the same wavenumber as the peak attributed to bulk potassium silicate at 964 cm $^{-1}$. There is no shift in the Si-O-Si stretching peak at 1091 cm $^{-1}$. This indicates that the K_2SiO_3 observed on the post reaction sample of K_2CO_3 supported on CPG is bulk silicate. There is no visible peak for bulk carbonate at 1385 cm $^{-1}$ for spectra of fresh or post reaction catalyst.

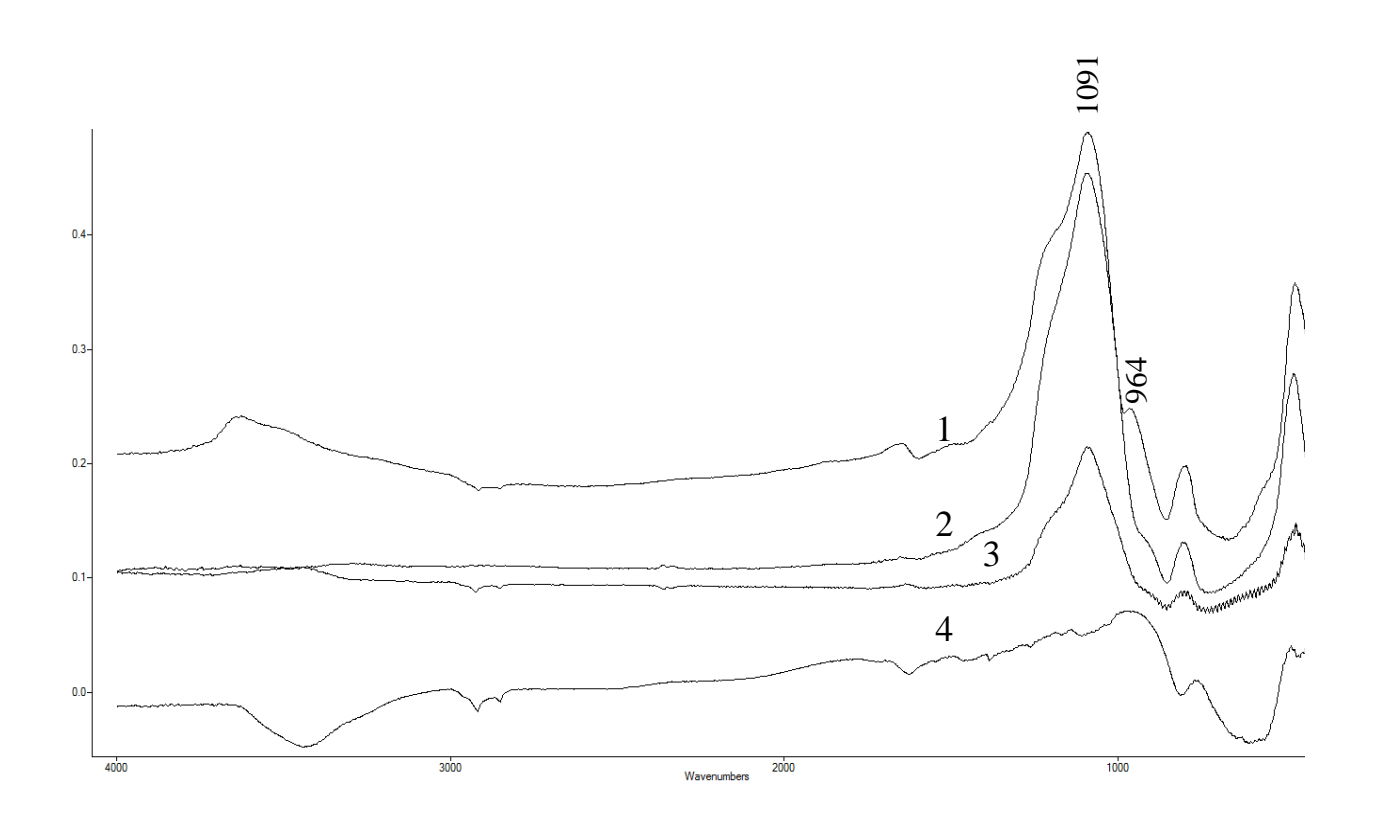


Figure 5.9: Absorbance FTIR analyses of fresh and used catalyst samples. (1: K₂SiO₃ on silica gel, 2:1.25 mmol/g K₂CO₃ on CPG post reaction, 3: 1.25 mmol/g K₂CO₃ on CPG calcined, unused, 4: K₂SiO₃, neat)

Table 5.12: Binding energy peaks from XPS spectra for K_2CO_3 on CPG before and after use

IX ₂ C	K ₂ CO ₃ on Cl O before and after use										
	1.25 m	mol/g	1.25 m	mol/g							
Sample	K_2CO_3	on CPG	K_2CO_3	on CPG							
	Calcined	, unused	Post re	action							
	Binding	Area %	Binding	Area %							
	Energy	Alea %	Energy	Alea %							
C 1s	281.4	31.2	281.4	14.9							
	284.9	61.9	284.8	33.9							
	286.4	3.2	286.3	3.1							
	287.9	3.8	287.8	2.7							
O 1s	530	5.4	528.5	1.7							
	531.8	37.8	530.2	7							
	532.6	56.8	531.6	28.5							
			532.5	54.7							
			533.7	8.2							
Si 2p			101.6	7.4							
-			103.2	92.7							

Table 5.12 shows binding energy peaks for K₂CO₃ on CPG before and after use. As expected, K₂CO₃ on CPG shows small amounts of carbonate on its surface. Peaks at 528-530 eV post reaction confirms the presence of Si-O-K bonds that prevail during reaction for controlled pore glass (CPG) catalyst.

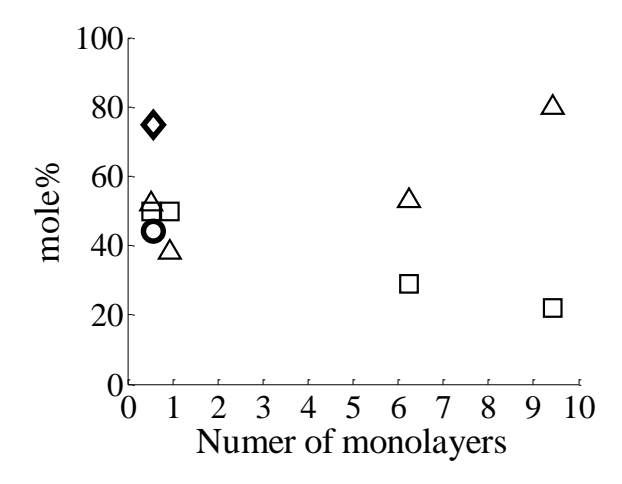


Figure 5.10: Conversion on silica gel catalysts (\square), PO selectivity on silica gel catalysts (Δ), conversion on CPG catalyst (\circ), PO selectivity on CPG catalyst (\diamond) vs percentage coverage of potassium base salt on silica surface. (T= 400 °C, WHSV = 3.4 g feed/g cat/h). Percentage coverage >100% if surface is fully saturated, and more than one layer of potassium salt is present

Figure 5.10 shows the dependence of conversion and PO selectivity on the coverage of potassium salt on the support. At coverage of more than a monolayer, conversion steadily decreases while PO selectivity increases. This effect has been recorded previously for alkali metal salts on silica. 32,33 As was seen in Section 5.4.4.8, the catalysts loaded with more than a monolayer show the formation of bulk carbonate species, while those that have less than the full coverage do not show the presence of a bulk carbonate peak. This indicates that the active component of catalyst in the cases of more than monolayer coverage is potassium carbonate, which is a selective catalyst for PO, but has poor activity. PO selectivity is not merely a function of conversion. Potassium carbonate loaded on controlled pore glass shows similar high selectivity at high conversions. Conversion appears to be a strong function of percentage surface area of support covered. Irrespective of the loading, conversion is high ~50%, as long as surface coverage < 100%. In the case of silica gel supported KOH catalysts, it is possible that only the base on the outside of the

catalyst is converted to K₂CO₃, while the basic species in the first layer is K-O-Si bonds, visible as 528-530 eV peak in O 1s XPS spectra. Table 5.13 shows the calculations for Figure 5.10.

Table 5.13: Monolayer coverage calculations

Catalyst	Surface area (m²/g)	Monolayer surface loading (mmol/g)	No. of layers of base deposited	monolayer surface density (mmol/m²)	Conversion	PO selectivity
2.5 mmol/g KOH on silica gel	2	0.265	9.4	0.13	22	80
Neat potassium carbonate	3	0.4	6.3	0.13	29	53
1.5 mmol/g KOH on silica gel	12	1.615	0.93	0.13	50	38
0.5 mmol/g KOH on silica gel	85	9.4	0.05	0.0059	50	52
1.25 mmoles K2CO3 on CPG	32	4.3	0.58	0.078	44	75

EDS and XPS atomic concentrations provide atomic concentration data for the post reaction catalysts and are reported in Table 5.18 through Table 5.20 in Appendix M.

5.5 Conclusions and recommendations for future work

The reaction system of propylene glycol and its acetates to propylene oxide and its side products in the presences of alkali metal salts on silica gel has been characterized. Early reactions with cesium nitrate on silica gel were unsuccessful, due to the dissolution of silica gel at high temperatures. A maximum yield of 6% was achieved at lower temperatures. Potassium base salts were found to be less corrosive to the support up to loadings of 3 mmol/g. The effect of weight

hour space velocity was studied, and the reaction was determined to be first order with respect to CPGA. Conversion decreases with decreasing contact time, however, selectivity increases, indicating that PO isomerization is an important reaction in the system. The effect of temperature was studied; conversion increases with temperature up to 420 and then drops due to accelerated agglomeration of catalyst particles. A composite activation energy of Ea = 89.9 kJ/mole was obtained based on first order kinetics. Selectivity decreases as temperature is increased, this could be due to the domination of elimination reactions to propanal, acetone and allyl alcohol over substitution reaction to propylene oxide, and increased PO isomerization. The trade-off between selectivity and conversion reaches an optimum value of 32% at 420 °C.

The activity of KOH, KOAc and K₂CO₃ based catalysts on silica gel are similar. FTIR and XPS studies confirm that for loadings of higher than monolayer coverage the active component at reaction conditions is bulk carbonate, irrespective of the starting material. For lower loadings that are sub monolayer, the active component consists of Si-O-K bonds. Surface area studies of the catalyst at different stages of preparation and post reaction have been studied. Monolayer coverage calculations of different catalysts show that sub monolayer coverage loadings are optimal for high conversions. Controlled pore glass is a stable high surface area support that allows high conversions without sacrificing selectivity. FTIR and XPS spectra show that the active component of K₂CO₃ loaded CPG catalyst is potassium silicate at reaction conditions.

The high conversion and selectivity of catalysts with CPG as support is promising for further optimization of PO yields. High surface areas allow for monolayer coverage even at high alkali loadings, making high conversions possible along with high selectivity. Future studies at higher loadings of potassium for full coverage, and higher surface areas might be conducted.

Characterizing PO isomerization kinetics would be helpful to understand the limit of PO yield achievable.

APPENDICES

Appendix H: List of all experiments with reaction conditions, conversion, selectivity and carbon recovery

Table 5.14: List of all experiments with reaction conditions, conversion, selectivity and carbon recovery

	Metal Loading	Feed rate	Wt.	Carrier gas	Temp	WHSV (g	Conv.	onv. Selectivity					C
No	(mmol M/ g catalyst)	(g/min)	(g)	(g/min)	(°C)	feed/g cat/h)	(%)		(%)				rec
				N ₂ unless otherwise stated				РО	Propanal	Acetone	Allyl alcohol		(%)
Cesium nitrate catalyst runs													
1	1.5	0.1	3.5	0.1	351	1.7	36	10	13	18	5	4	86
2	1.5	0.1	3.5	0.1	351	1.7	18	29	29	16	11	5	95
3	1.5	0.1	3.5	0.1	352	1.7	20	26	31	17	11	5	90
4 ^a	1.5	0.1	3.5	0.2	374	1.7	46	9	34	18	9	4	97
5	1.5	0.1	3.5	0.1	384	1.7	29	13	43	28	12	4	96
6 ^b	1.5	0.1	3.5	0.1	375	1.7	44	13	6	4	3	5	78
	Potassium hydroxide catalyst runs												
7	2.5	0.1	3.5	0.1	400	1.7	37	81	11	6	2	30	101
8	2.5	0.1	3.5	0.1	400	1.7	34	83	7	8	2	28	99
9	0.5	0.1	3.5	0.1	400	1.7	50	52	28	10	10	26	93
10	0.5	0.1	1.8	0.1	400	3.4	44	64	22	9	5	28	98
11 ^c	0.5	0.1	1.8	0.1	400	3.4	45	65	22	9	4	29	97
12	1.5	0.1	1.8	0.1	400	3.4	50	38	37	14	11	19	100
13	0.5	0.1	0.9	0.1	400	6.7	33	71	22	5	3	23	99
14	2.5	0.1	1.8	0.1	400	3.4	20	70	13	10	7	14	99
15	2.5	0.1	1.8	0.1	400	3.4	22	80	9	5	6	18	99
16	2.5	0.1	1.8	0.1	420	3.4	36	67	18	10	5	24	100
17	2.5	0.1	1.8	0.1	370	3.4	12	50	26	13	11	6	100
18	2.5	0.1	1.8	0.1	440	3.4	30	64	14	17	5	19	101

Table	e 5.14 (cont'd)												
Potassium acetate catalyst runs													
19	2.5	0.1	1.8	0.1	400	3.4	21	72	12	16	0	15	95
20	5	0.1	1.8	0.1	400	3.4	22	60	14	16	10	13	101
Potassium carbonate runs													
21	2.5	0.1	1.8	0.1	400	3.4	25	67	25	7	3	17	98
22 ^d	2.5	0.1	1.8	0.1	400	3.4	30	63	26	9	3	19	114
23	2.5	0.1	0.4	0.1	400	17.1	12	84	12	3	2	29	109
24 ^e	2.5	0.1	0.4	0.1	400	17.1	8	88	9	2	0.2	20	94
25	2.5	0.1	1.8	0.1	400	3.4	53	42	33	10	15	22	98
26 ^f	2.5	0.1	3.5	0.1	400	1.7	29	53	30	15	2	12	96
27 ^g	2.5	0.1	1.8	0.1	400	3.4	44	75	14	7	4	33	100

a: partial pressure of feed reduced by half

b: PG only feed used

c: feed mixed with 40% by mole methyl ethyl ketone found to promote reaction in previous study. ¹³ No significant improvement found in present study.

d: carbon dioxide used as feed carrier gas instead of nitrogen

e: partial pressure of feed reduced by half

f: neat potassium carbonate used without silica support

g: potassium carbonate on controlled pore glass with higher surface area support

Appendix I: Calibration plots for all components in reaction system

The following plots (Figure 5.11 through Figure 5.20) show calibrations of standards prepared to determine response factors of each component in the reaction system, determined by the slope of area ratio over weight ratio of component over internal standard decanol.

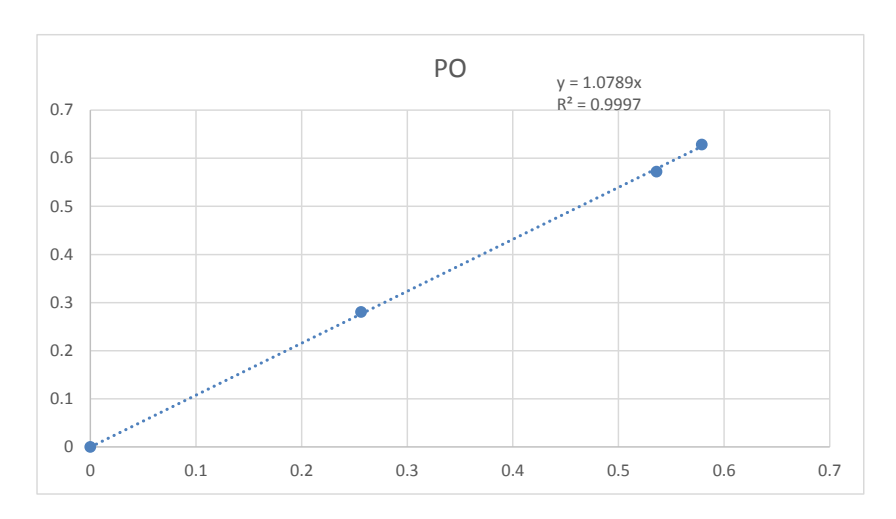


Figure 5.11: Plot of area ratio vs weight ratio of PO over internal standard decanol

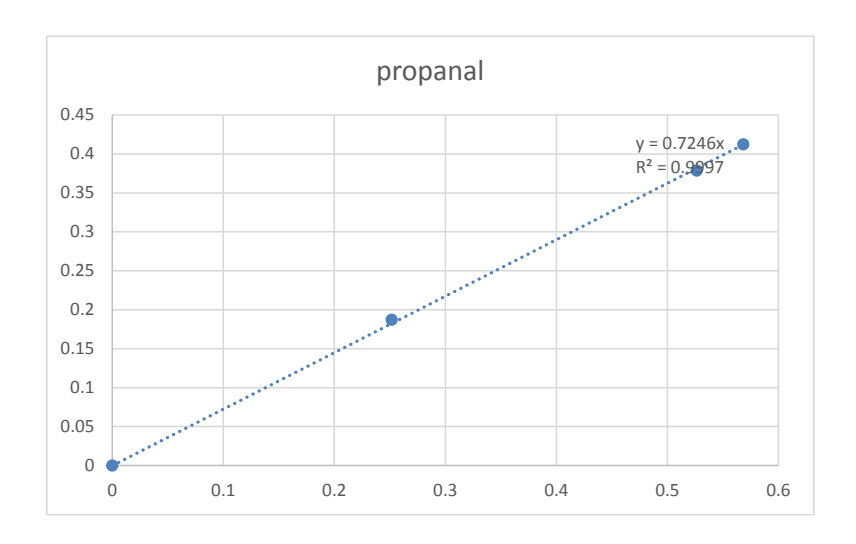


Figure 5.12: Plot of area ratio vs weight ratio of propanal over internal standard decanol

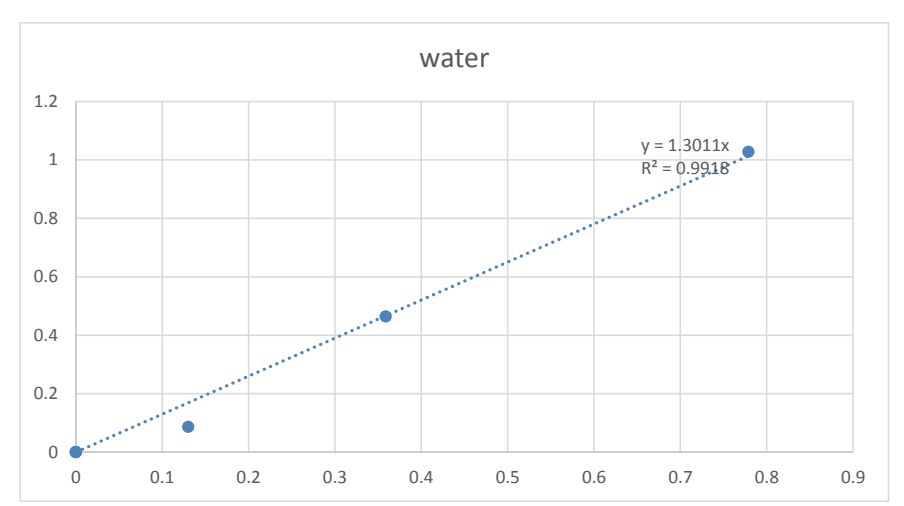


Figure 5.13: Plot of area ratio vs weight ratio of water over internal standard decanol

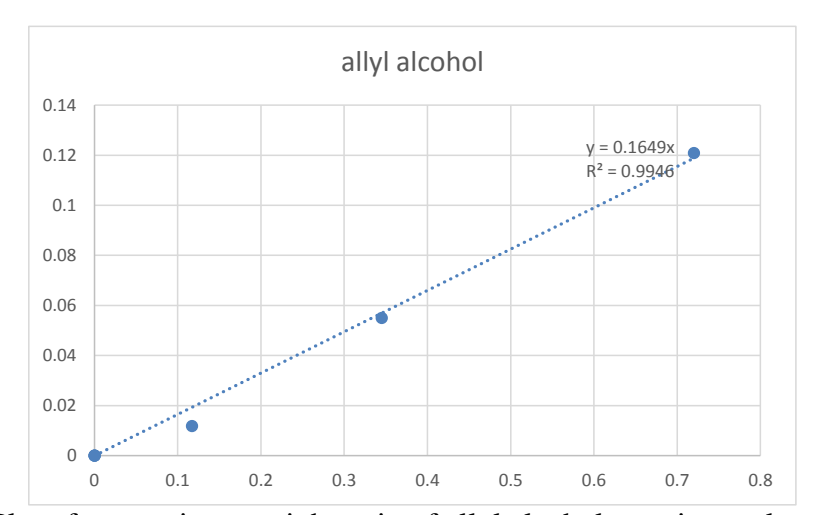


Figure 5.14: Plot of area ratio vs weight ratio of allyl alcohol over internal standard decanol

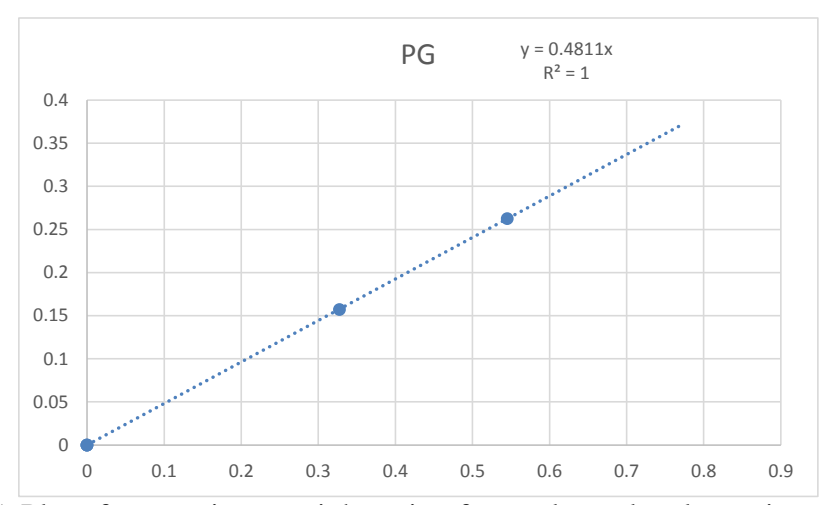


Figure 5.15: Plot of area ratio vs weight ratio of propylene glycol over internal standard decanol

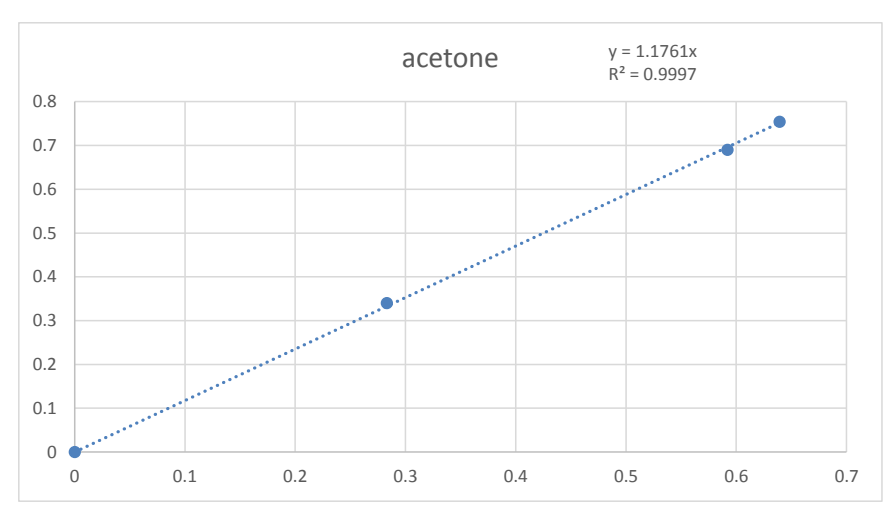


Figure 5.16: Plot of area ratio vs weight ratio of acetone over internal standard decanol

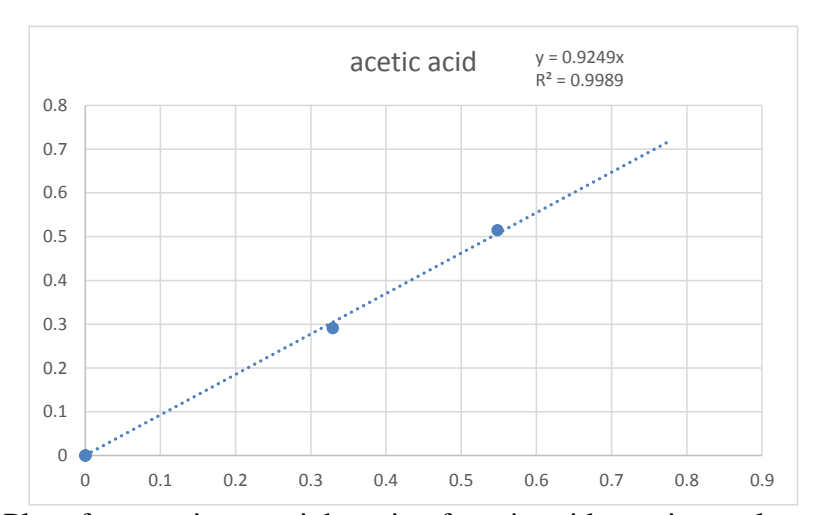


Figure 5.17: Plot of area ratio vs weight ratio of acetic acid over internal standard decanol

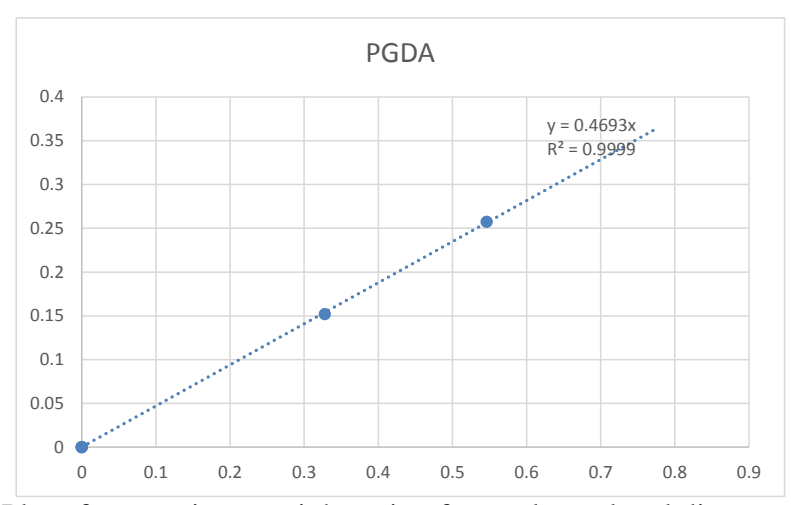


Figure 5.18: Plot of area ratio vs weight ratio of propylene glycol diacetate over internal standard decanol

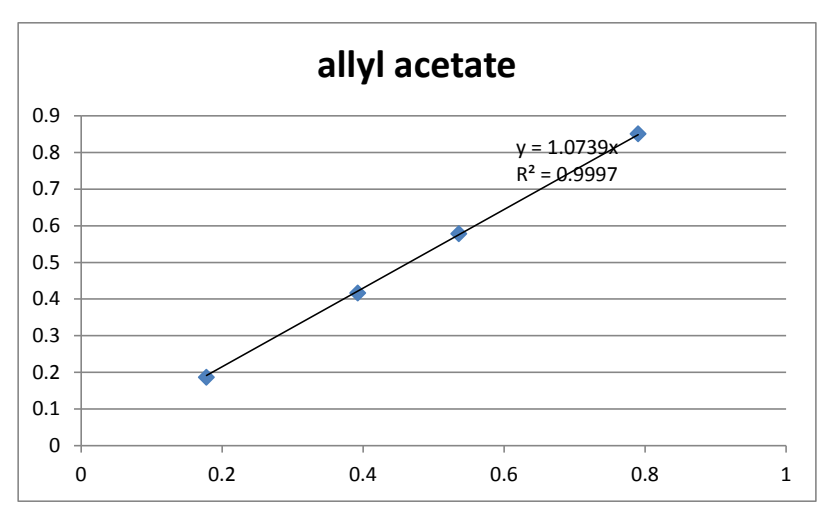


Figure 5.19: Plot of area ratio vs weight ratio of allyl acetate over internal standard decanol

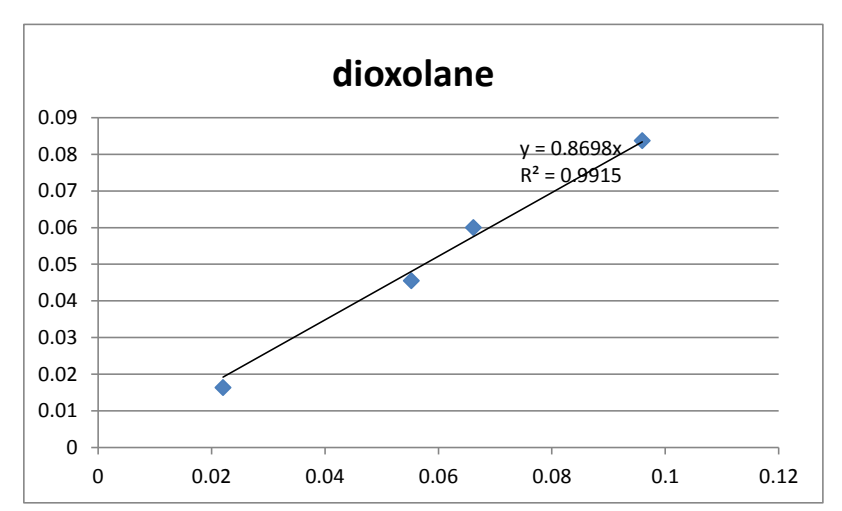
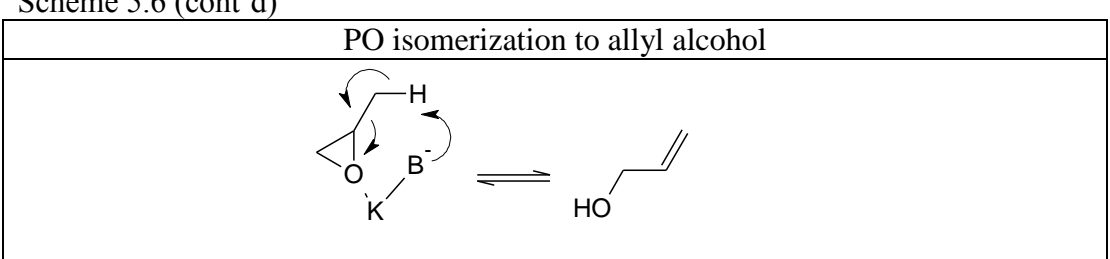


Figure 5.20: Plot of area ratio vs weight ratio of 2-ethyl,4-methyl,1,3-dioxolane over internal standard decanol

Appendix J: Mechanisms for major reactions in reaction system

Scheme 5.6: Mechanisms for formation of PO and its isomers
Formation of PO from PGA
$\begin{array}{cccccccccccccccccccccccccccccccccccc$
Formation of acetone from PGA
B H O O + OH
Formation of propanal from PGA
B H O O + OH OH
Formation of allyl alcohol from PGA
HO K O HO HO HO HO HO HO HO
PO isomerization to propanal
K_{B-} HO O
PO isomerization to acetone
$ \begin{array}{c} $

Scheme 5.6 (cont'd)



Appendix K: Gibbs energy of reaction and equilibrium constants at reaction temperature

Gibbs energies of formation in the gas phase were calculated for each component in the reaction system by a polynomial function (Eq. 5.6) found in literature (Table 5.15).³⁴ The Gibbs energies of the major reactions and equilibrium constants for major reactions in the system were then calculated at reaction temperature of 673 K (Table 5.16).

$$G_f = A + BT + CT^2 + DT^3 + ET^4 (5.6)$$

Table 5.15: Gibbs energy polynomial function values and Gibbs energy of formation at standard conditions (298 K) and at reaction temperature (673 K)

$\Delta G_{ m f}$						ΔG_{f}	
component	A	В	C	D	E	(298 K) (kJ/mol)	(673 K) (kJ/mol)
						` /	` /
PO	-8.2E+01	1.4E-01	1.8E-04	-1.7E-07	2.8E-11	-27.28	49.41
PG	-4.2E+02	3.3E-01	2.8E-04	-1.9E-07	3.6E-11	-300.78	-120.39
Propanal	-1.8E+02	1.4E-01	1.5E-04	-9.8E-08	2.3E-11	-124.23	-39.58
Acetone	-2.1E+02	1.4E-01	1.7E-04	-1.1E-07	2.5E-11	-152.63	-63.64
Water	-2.4E+02	3.5E-02	2.0E-05	-9.3E-09	1.8E-12	-228.59	-210.3
acetic acid	-4.2E+02	1.0E-01	1.4E-04	9.5E-08	2.3E-11	-377.89	-257.18
allyl alcohol	-1.2E+02	1.3E-01	1.7E-04	-1.1E-07	2.6E-11	-71.23	12.45
PGDA	-7.9E+02	4.5E-01	3.0E-04	-2.1E-07	5.3E-11	-631.09	-398.28
PGMA ^a	-6.0E+02	3.9E-01	2.9E-04	-2.0E-07	4.5E-11	-465.93	-259.33
diPG	6.0E+02	5.7E-01	3.9E-04	-2.7E-07	6.6E-11	802.40	1097.05

a:Approximated with average for PG and PGDA

Table 5.16: Equilibrium constants estimated from Gibbs energy of reaction calculations at reaction temperature of 673 K

Reaction	Keq at 673 K
PG → PO +water	1.3×10 ³
PG → propanal + water	1.1×10 ¹⁰
PG → allyl alcohol +water	1.0×10 ⁶
PG → acetone +water	8.3×10 ¹¹
PO → propanal	8.2×10 ⁶
PO → acetone	6.0×10 ⁸
PO → allyl alcohol	740

Appendix L: Weisz Prater calculation

Mass transport limitations were calculated using the Weisz-Prater criterion. The observable modulus was first calculated by Eq. 5.7.

$$\phi_w = \frac{(r_{obs}^*)\rho_{CAT}}{D_{eff}C_{PGA}} \left(\frac{d_p}{6}\right)^2 \tag{5.7}$$

Here, $r*_{obs}$ is the observed rate of reaction per weight of catalyst calculated by moles reacted/time/weight of catalyst bed = 2.5×10^{-6} moles/g cat/s for a conversion of 40% at a WHSV of 1.7 h⁻¹. The bulk density of the catalyst was measured in the laboratory to be 774 kg/m³. Assuming a void volume of 0.5, the particle density, ρ_{CAT} , is then 1548 kg/m³. The particle diameter, d_p, of the silica gel catalysts was between 0.2 to 0.5 mm, with an average value of 0.35 mm. C_{PGA} is calculated as F_{PGA}/v , where F_{PGA} is the feed rate of propylene glycol and its acetates in vapor phase, and v is the vapor phase volumetric flowrate, including the inert carrier gas nitrogen. The value of C_{PGA} = 8.41 moles/m³.

The effective diffusivity D_{eff} of feed in nitrogen is estimated (Eq. 5.8), where pore tortuosity τ is assumed to be equal to the inverse of particle porosity ε , and D_{BA} is bulk diffusivity of feed in nitrogen.

$$D_{eff} = D_{PGA} \left(\frac{\varepsilon}{\tau}\right) = D_{BA} \varepsilon^2 \tag{5.8}$$

D_{PGA} is determined from the Chapman-Enskog relation expressed in Eq. 5.9:

$$D_{PGA} = \frac{1.86 \times 10^{-3} T^{3/2} \sqrt{\frac{1}{M_1} + \frac{1}{M_2}}}{P\Omega \sigma_{12}^2} cm^2 / s$$
 (5.9)

where 1 and 2 are the two molecules present in the gas mixture, in this case PGMA and nitrogen respectively, T is temperature in Kelvin (673 K), M_1 and M_2 are the molar masses of the components in g/mole (118 and 28 g/mole respectively), P is pressure in atm (1 atm), Ω is the temperature dependent collision integral (determined from NIST tables to be 1.3), σ^2_{12} is the average collision diameter (calculated from molecular volumes to be 3.11 Å).

Particle porosity, ε is the ratio of void volume in the catalyst particle over the total volume of the catalyst particle = 0.422.

The calculated value of D_{eff} is $9.6 \times 10^{-6} m^2/s$.

The observable modulus, $\phi_w = 1.1 \times 10^{-7}$.

The Thiele modulus (φ) and effectiveness factor (η) for PGA epoxidation are calculated from the observable modulus $\phi_w = \eta \varphi^2$ assuming the reaction is first order in PGA and thus $\eta = \frac{\tanh(\varphi)}{\varphi}$. Value of η calculated is 0.99, which is within the range of negligible intraparticle mass transport limitations, and the observed rate is close to the intrinsic value.

Appendix M: TGA curve calculations, atomic concentrations from XPS and EDS analyses

Calculations from TGA curves shown in Figure 5.6 show that potassium acetate ketonizes to form potassium carbonate at reaction conditions.

Neat potassium acetate weight before:22.05 mg

Neat potassium acetate weight after: 15.07 mg

Percentage weight loss = 29.51%

Percentage expected weight loss =
$$\frac{\text{(molar mass of acetone)(moles of KOAc)}}{2\text{(molar mass of KOAc)(moles of KOAc)}} = \frac{58.08}{2\times98.15} = 29.59\%$$

Supported potassium acetate before: 44.23 mg

Supported potassium acetate after: 41.3459 mg

Percentage weight loss observed = 6.5%

Percentage expected weight loss = (total weight) (loading of KOAc per gram of catalyst) *.2959/total weight = 7.25%

Sample XPS spectra are shown in Figure 5.21 and Figure 5.22.

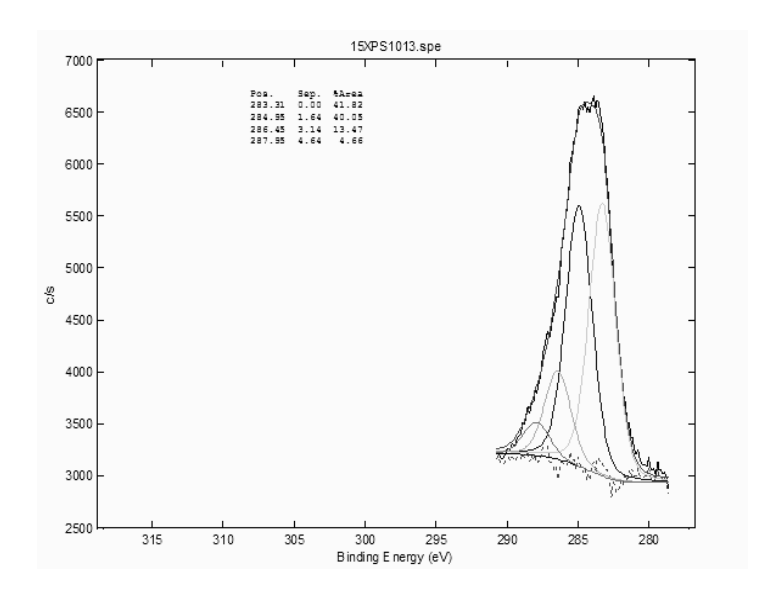


Figure 5.21: XPS C 1s spectra of 1.5 mmol/g KOH on silica gel post reaction

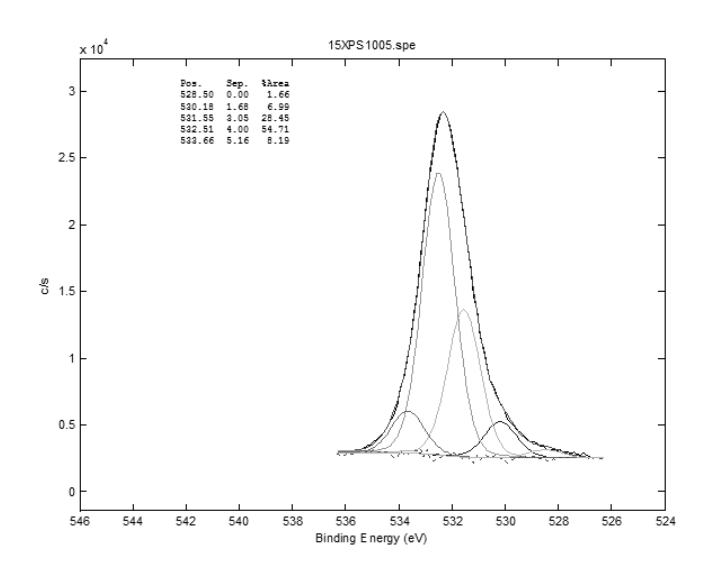


Figure 5.22: XPS O 1s spectra of 1.25 mmol/g K₂CO₃ on CPG post reaction

Atomic concentrations from XPS and EDS analyses are reported below in Table 5.17 through Table 5.19.

Table 5.17: Atomic concentrations from XPS spectra for 2.5 mmol K^+/g catalyst made from KOH, KOAC and K_2CO_3

	Silica gel calcined	2.5 mmol/g KOH on silica gel Post reaction	2.5 mmol/g KOAc on silica gel Post reaction	1.25 mmol/g K ₂ CO ₃ on silica gel Calcined, unused	1.25 mmol/g K ₂ CO ₃ on silica gel Post reaction
C	0	60.33	22.65	30.77	52.44
О	70.79	28.3	52.41	45.68	32.94
Si	29.21	4.67	17.05	14.78	10.51
K	0	6.34	7.89	5.75	3.92
O/Si	2.4	6.1	3.1	3.1	3.1

Table 5.18: XPS spectra for lower loadings of KOH on silica gel (0.5 and 1.5 mmol/g)

	0.5 mmol/g KOH on silica gel Calcined, unused	0.5 mmol/g KOH on silica gel Post reaction	1.5 mmol/g KOH on silica gel Post reaction
С	7.28	32.56	16.61
0	66.52	45.86	58.03
Si	24.50	17.48	23.72
K	1.7	4.10	1.64
O/Si	2.7	2.6	2.4

Table 5.19: Atomic concentrations from XPS spectra for K₂CO₃ on CPG before and after use

	1.25 mmol/g	1.25 mmol/g
	K_2CO_3 on	K_2CO_3 on
	CPG	CPG
	Calcined, unused	Post reaction
С	12.86	16.56
О	58.22	56.35
Si	25.04	24.22
K	3.88	2.88
O/Si	2.3	2.3

Atomic concentrations obtained from EDS analyses in 3-4 selected areas as highlighted in SEM images (Table 5.20). Figure 5.23 through Figure 5.25 show SEM images for post reaction catalyst samples.

Table 5.20: Atomic concentrations from EDS spectra for 2.5 mmol K^+/g catalyst made from KOH, KOAC and K_2CO_3 .

	2.5 mmol/g KOH on silica gel Calcined, unused	2.5 mmol/g KOH on silica gel Post reaction	2.5 mmol/g KOH on silica gel Calcined, unused	2.5 mmol/g KOH on silica gel Post reaction	1.25 mmol/g K ₂ CO ₃ on silica gel Calcined, unused	1.25 mmol/g K ₂ CO ₃ on silica gel Post reaction
С	4.5±4.5	22.9±5.9	22.9±10.3	24.0±5.4	17.2±18.8	19.6±5.7
О	61.4±0.04	53.2±3.3	52.4±7.1	53.4±2.8	53.1±8.2	51.0±3.2
Si	31.7±1.4	20.2±2.7	16.5±4.7	15.6±3.7	2.7±1.9	25.1±2.4
K	4.5±0.5	3.7±0.8	5.6±1.1	7.0±1.1	0.5 ± 0.7	4.9±1.2

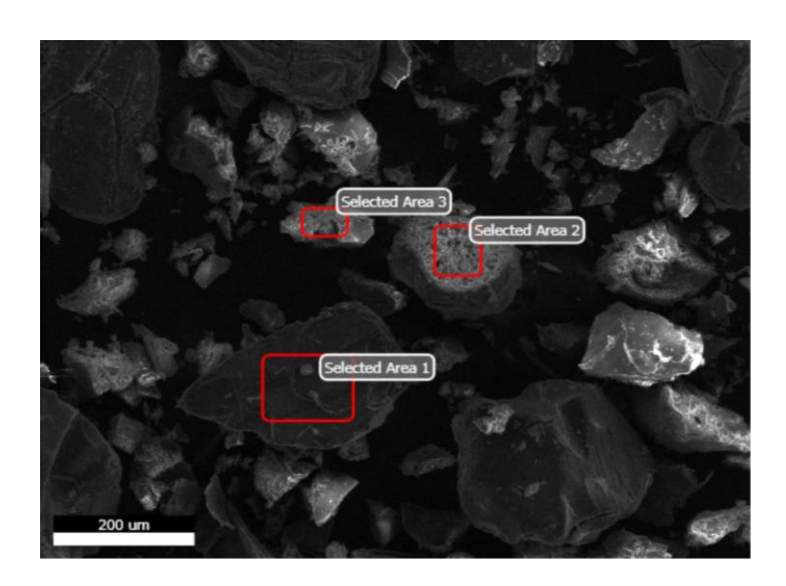


Figure 5.23: SEM image of post reaction 2.5 mmol/g KOH on silica gel

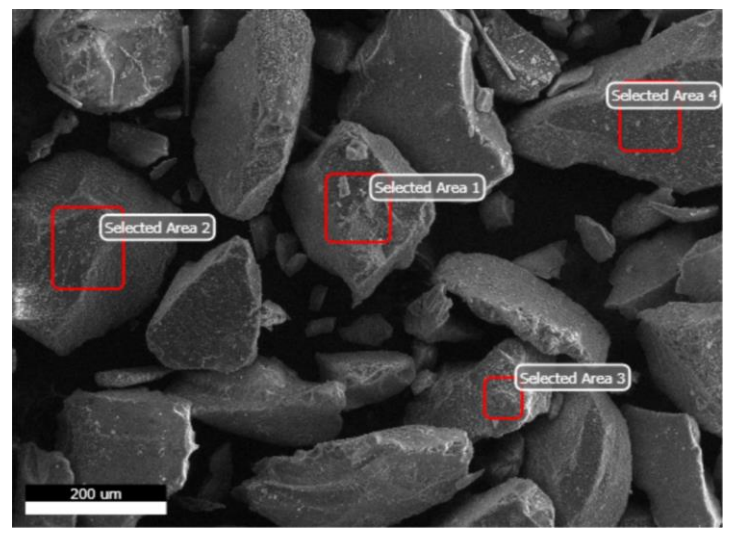


Figure 5.24: SEM image of post reaction 2.5 mmol/g KOAc on silica gel

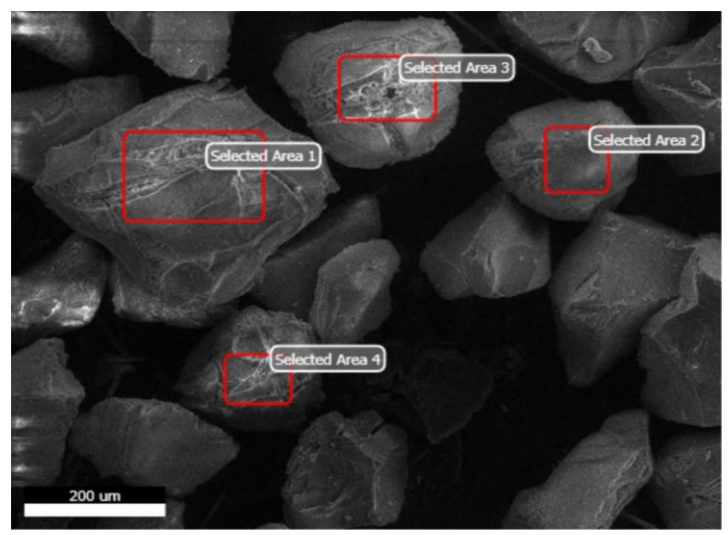


Figure 5.25: SEM image of post reaction 1.25 mmol/g K₂CO₃ on silica gel

REFERENCES

REFERENCES

- (1) Lab Breakthrough: ADM Leads to Petroleum-Free Glycol Production Facility http://energy.gov/articles/lab-breakthrough-adm-leads-petroleum-free-glycol-production-facility (accessed Mar 25, 2015).
- (2) Trent, D. L. In *Kirk-Othmer Encyclopedia of Chemical Technology*; John Wiley & Sons, Inc., 2000.
- (3) Barbelli, M. L.; Santori, G. F.; Nichio, N. N. Bioresour. Technol. 2012, 111, 500-503.
- (4) Sheldon, R. A. Green Chem. **2014**, 16 (3), 950–963.
- (5) Chen, G.-Q.; Patel, M. K. Chem. Rev. **2011**, 112 (4), 2082–2099.
- (6) Rodriguez, B. A.; Stowers, C. C.; Pham, V.; Cox, B. M. *Green Chem.* **2014**, *16* (3), 1066–1076.
- (7) Zuwei, X.; Ning, Z.; Yu, S.; Kunlan, L. Science **2001**, 292 (5519), 1139–1141.
- (8) Binning, R. C.; Null, H. R. Production and recovery of propylene oxide by plural stage distillation and caustic addition. US3350417 A, October 31, 1967.
- (9) Meiers, R.; Dingerdissen, U.; Hölderich, W. F. J. Catal. **1998**, 176 (2), 376–386.
- (10) Clerici, M. G.; Bellussi, G.; Romano, U. J. Catal. **1991**, 129 (1), 159–167.
- (11) Costantini, M.; Jouffret, M. Production of epoxides from lower alkane-1,2-diols. US4297287 A, October 27, 1981.
- (12) Yu, Z.; Xu, L.; Wei, Y.; Wang, Y.; He, Y.; Xia, Q.; Zhang, X.; Liu, Z. *Chem. Commun.* **2009**, No. 26, 3934–3936.
- (13) Ryu, J.-Y. Process for epoxidizing vicinal diols. EP0145447 A1, June 19, 1985.
- (14) Sherwin, M. B.; Frank, M. E. Process for preparing oxirane compounds. US4399295 A, August 16, 1983.
- (15) Sherwin, M. B.; Peress, J. Cracking of mixtures containing hydroxyesters. US4012424 A, March 15, 1977.
- (16) Weitz, H.-M.; Hartig, J.; Platz, R. Basic decarboxylation of propylene glycol esters in a high boiling solvent. US4158008 A, June 12, 1979.
- (17) Fouquet, G.; Merger, F.; Baer, K. From propylene glycol, catalyst, alkali metal carboxylate. US4226780 A, October 7, 1980.
- (18) Dubnikova, F.; Lifshitz, A. J. Phys. Chem. A **2000**, 104 (19), 4489–4496.

- (19) Namuangruk, S.; Khongpracha, P.; Pantu, P.; Limtrakul, J. *J. Phys. Chem. B* **2006**, *110* (51), 25950–25957.
- (20) Amberlite and Amberlyst Resins http://www.sigmaaldrich.com/chemistry/chemical-synthesis/learning-center/technical-bulletins/al-142/amberlite-amberlyst.html (accessed Mar 25, 2015).
- (21) Dent Glasser, L. S.; Kataoka, N. Cem. Concr. Res. 1981, 11 (1), 1–9.
- (22) Weisz, P. B.; Hicks, J. S. Chem. Eng. Sci. 1995, 50 (24), 3951–3958.
- (23) Lukić, I.; Krstić, J.; Jovanović, D.; Skala, D. *Bioresour. Technol.* **2009**, *100* (20), 4690–4696.
- (24) Rees, C. A.; Provis, J. L.; Lukey, G. C.; van Deventer, J. S. J. *Langmuir* **2007**, *23* (15), 8170–8179.
- (25) Rees, C. A.; Provis, J. L.; Lukey, G. C.; van Deventer, J. S. J. *Langmuir* **2007**, *23* (17), 9076–9082.
- (26) Simonsen, M. E.; Sønderby, C.; Li, Z.; Søgaard, E. G. *J. Mater. Sci.* **2009**, *44* (8), 2079–2088.
- (27) Bal, R.; Tope, B. B.; Das, T. K.; Hegde, S. G.; Sivasanker, S. *J. Catal.* **2001**, 204 (2), 358–363.
- (28) Nesbitt, H. W.; Bancroft, G. M.; Henderson, G. S.; Ho, R.; Dalby, K. N.; Huang, Y.; Yan, Z. *J. Non-Cryst. Solids* **2011**, *357* (1), 170–180.
- (29) Sawyer, R.; Nesbitt, H. W.; Secco, R. A. J. Non-Cryst. Solids **2012**, 358 (2), 290–302.
- (30) Shchukarev, A. V.; Korolkov, D. V. Cent. Eur. J. Chem. 2004, 2 (2), 347–362.
- (31) Zemek, J.; Jiricek, P.; Gedeon, O.; Lesiak, B.; Jozwik, A. J. Non-Cryst. Solids **2005**, 351 (19–20), 1665–1674.
- (32) Bailey, O. H.; Montag, R. A.; Yoo, J. S. Appl. Catal. Gen. 1992, 88 (2), 163–177.
- (33) Malinowski, S.; Basinski, S. J. Catal. 1963, 2 (3), 203–207.
- (34) Yaws, C. L. Yaws' Critical Property Data for Chemical Engineers and Chemists, 2012.